



**HAL**  
open science

# The Risk Assessment of Work-related Musculoskeletal Disorders based on OpenSim

Jing Chang

► **To cite this version:**

Jing Chang. The Risk Assessment of Work-related Musculoskeletal Disorders based on OpenSim. Robotics [cs.RO]. Ecole centrale de Nantes, 2018. English. NNT: . tel-01969371v1

**HAL Id: tel-01969371**

**<https://hal.science/tel-01969371v1>**

Submitted on 4 Jan 2019 (v1), last revised 5 Dec 2019 (v2)

**HAL** is a multi-disciplinary open access archive for the deposit and dissemination of scientific research documents, whether they are published or not. The documents may come from teaching and research institutions in France or abroad, or from public or private research centers.

L'archive ouverte pluridisciplinaire **HAL**, est destinée au dépôt et à la diffusion de documents scientifiques de niveau recherche, publiés ou non, émanant des établissements d'enseignement et de recherche français ou étrangers, des laboratoires publics ou privés.

# THESE DE DOCTORAT DE

L'ÉCOLE CENTRALE DE NANTES  
COMUE UNIVERSITE BRETAGNE LOIRE

ECOLE DOCTORALE N° 602  
*Sciences pour l'Ingénieur*  
Spécialité : « Robotique - Mécanique »

Par

**Jing CHANG**

**« Evaluation des risques de troubles musculo-squelettiques liés au travail basée sur OpenSim »**

Thèse présentée et soutenue à l'Ecole Centrale de Nantes, le 30 novembre 2018  
Unité de recherche : Laboratoire des Sciences du Numérique de Nantes

## **Rapporteurs avant soutenance :**

Georges DUMONT      Professeur, Ecole Normale Supérieure de Rennes  
Gérard POISSON      Professeur, Université d'Orléans, IUT de Bourges

## **Composition du Jury :**

Président :      Laurence CHEZE      Professeur, Université Claude Bernard Lyon 1  
Examineurs : Liang MA      Associate Professor, Tsinghua University

Dir. de thèse : Fouad BENNIS      Professeur, Ecole Centrale de Nantes  
Co-dir. de thèse : Damien CHABLAT      Directeur de Recherche, CNRS



# Contents

<b>Acknowledgements</b>	<b>1</b>
<b>Glossary</b>	<b>3</b>
<b>I General Introduction</b>	<b>5</b>
I.1 Motivations	5
I.2 Thesis structure	6
I.3 Contribution to the assessment of physical risks of Musculoskeletal disorders	7
<b>II Literature Research</b>	<b>17</b>
II.1 Abstract	17
II.2 Musculoskeletal disorders: an epidemiologic overview	19
II.2.1 Definition of MSDs	19
II.2.2 Contributing factors to MSDs	20
II.3 MSDs physical risk assessment in practice	22
II.3.1 Observational methods	22
II.3.2 Self-report methods	27
II.3.3 Summary	28
II.4 Work load analysis	28
II.4.1 Work load evaluation: ergonomic methods	29

---

II.4.2	Joint moment measurement	30
II.4.3	Muscle force assessment	32
II.4.4	Summary	38
II.5	<b>Fatigue: the accumulation effect of workloads</b>	<b>38</b>
II.5.1	Physical fatigue: central and peripheral	38
II.5.2	Determination of muscle fatigue	39
II.5.3	Biomechanical modeling of muscle fatigue	42
II.6	<b>Muscle fatigability</b>	<b>46</b>
II.6.1	Definition of muscle fatigability	46
II.6.2	Measurement of muscle fatigability	47
II.7	<b>Digital human modeling in MSDs physical risk assessment</b>	<b>49</b>
II.7.1	The development of digital human modeling	49
II.7.2	Digital human modeling in Ergonomics	52
II.7.3	Biomechanical digital human modeling	54
II.7.4	OpenSim	55
II.8	<b>General summary</b>	<b>58</b>
<b>III</b>	<b>The Indication of Muscle Fatigue with Surface EMG</b>	<b>61</b>
III.1	Abstract	61
III.2	Introduction	62
III.3	Methods	64
III.3.1	Subjects	64
III.3.2	Experiment protocol	64
III.3.3	Experiment setups	65
III.3.4	Data collection	65
III.3.5	Data analysis	66
III.4	Results	67
III.4.1	Simple contraction session	67
III.4.2	Fatigue sessions	67
III.4.3	RMS response exclusively to fatigue	68
III.5	Discussions	68
III.5.1	Force-RMS relationship in simple contraction	68
III.5.2	RMS during Fatigue Process	69
III.5.3	EMG response exclusively to fatigue	70
III.6	Conclusions	72

<b>IV Muscle Fatigue Analysis in OpenSim</b>	<b>73</b>
IV.1 Introduction	73
IV.1.1 Objectives	73
IV.2 Methodology: OpenSim human modeling and muscle fatigue analysis	<b>74</b>
IV.2.1 Muscle fatigue analysis	74
IV.3 Data and Simulation	<b>75</b>
IV.4 Results of simulation	<b>76</b>
IV.4.1 General muscle force decline	76
IV.4.2 Comparison among different muscles	77
IV.4.3 Influence of fatigability	77
IV.5 Discussions	<b>79</b>
IV.6 Conclusions	<b>81</b>
<b>V The Build-up of a Full-chain Musculoskeletal Human Model in Open-Sim</b>	<b>83</b>
V.1 Introduction	<b>83</b>
V.1.1 The existing OpenSim musculoskeletal models	83
V.1.2 The full-chain effect of human motion	83
V.1.3 Objective	85
V.2 Model development	<b>85</b>
V.3 The Full-chain model	<b>86</b>
V.3.1 BodySet	88
V.3.2 ConstraintSet	91
V.3.3 ForceSet	91
V.3.4 MarkerSet	94
V.4 The scaling method of OpenSim models	<b>95</b>
V.4.1 Methodology	96
V.4.2 Results	99
V.4.3 Discussions on the use of 3D scan in the estimation of body segment masses	102
V.4.4 Conclusions	106
<b>VI The Application of the Full-chain Model on Posture Analysis of an Overhead Drilling Task</b>	<b>107</b>
VI.1 Introduction	<b>107</b>
VI.2 Simulation setup	<b>108</b>

---

VI.3 Simulation results . . . . .	<b>110</b>
VI.3.1 Joint moments . . . . .	110
VI.3.2 Muscle activations . . . . .	111
VI.4 Discussions . . . . .	<b>113</b>
VI.4.1 The full chain effect . . . . .	113
VI.4.2 The full-chain model as a way of ergonomic posture analysis . . . . .	115
VI.4.3 Overhead working . . . . .	115
VI.5 Conclusions . . . . .	<b>118</b>
<b>VII Conclusions and Perspectives</b>	<b>119</b>
VII.1 Contributions . . . . .	<b>119</b>
VII.1.1 Muscle fatigue . . . . .	119
VII.1.2 Working posture analysis . . . . .	120
VII.1.3 The framework of the MSDs physical risk assessment . . . . .	122
VII.2 Further investigations and perspectives . . . . .	<b>122</b>
<b>VIII Jing CHANG's publications</b>	<b>125</b>
<b>Bibliography</b>	<b>127</b>

## List of Figures

I.1	An explanatory model of the contributing factors to Musculoskeletal disorders . . . . .	8
I.2	Diagram of the experiment. . . . .	10
I.3	Workflow of the muscle fatigue prediction process of OpenSim with the muscle fatigue analysis plug-in. . . . .	11
I.4	Load on the erector spinae muscle during 10s running. . . . .	11
I.5	Force capability trends of ten muscles during 10 min running. $k = 1.0min^{-1}$ . Force of each muscle is normalized by its maximum. . . . .	12
I.6	The Full-chain model on the OpenSim interface. . . . .	13
I.7	The geometrical model generated from 3D scan. . . . .	14
I.8	The simulated overhead drilling operation. . . . .	14
I.9	Six drilling postures for the drilling operation are analyzed. . . . .	15
II.1	An explanatory model of the contributing factors to MSDs . . . . .	21
II.2	Rapid Entire Body Assessment Checklist [15]. . . . .	23
II.3	A schema for shoulder joint moment calculation [42]. Posture configuration is determined by the length of upper arm $l_{SE}$ and lower arm $l_{EW}$ , as well as the upper arm incline angle $q_1$ and elbow angle $q_2$ . . . . .	30
II.4	Traditional ergonomic method determines the configuration of human posture by its projection on the sagittal plane ([44], p262). . . . .	31



II.5	The diagram of muscular-tendon structure [46]. Muscle fibers are oriented at an angle $\alpha$ with the tendon. Tendons moves only along its axis. As the muscle contracts, muscle fibers shorten and the angle $\alpha$ increases. . . . .	32
II.6	The diagram of motor unites [46]. Each motor unite is functionally disjoint with the others. Motor unite $i$ is excited by signal $u(i)$ , gets activated and produces fiber force $F_i^M$ . . . . .	33
II.7	The diagram of muscle force generation process [46]. The activation dynamics correspond to the calcium release, diffusion, and bonded to troponin. The contraction dynamics correspond to the energization of cross-bridges between thick and thin filaments, through which muscle forces are generated. . . . .	34
II.8	The muscle-tendon model [51]. $L_{MT}$ - the total length of the muscle and tendon ; $L_T$ - the length of the tendon; $L_M$ - the length of the branch of muscle fibers; $\alpha_M$ - the pennated angle. . . . .	34
II.9	The muscle force-length relation. . . . .	36
II.10	The muscle force-velocity relation at length $L_o^M$ . . . . .	37
II.11	The normalized tendon force - tendon strain relation. . . . .	37
II.12	MET diagram . . . . .	44
II.13	An EMG activity plot of bicep, triceps and trapezius in a push-pull cycle. [86] . . . . .	45
II.14	The variable anthropometry man model in SAMMIE. . . . .	50
II.15	The reach capability analysis with ERGOMAN. . . . .	51
II.16	The application examples of the RAMSIS. . . . .	52
II.17	Graphical rendering of digital human models in 3Dexperience . . . . .	52
II.18	The prediction of operator's visual accessibility in Delmia. . . . .	53
II.19	The prediction of the operation path of an object-moving task. . . . .	53
II.20	The joint load estimation and evaluation in 3DSSPP. . . . .	54
II.21	A musculoskeletal model in Anybody. . . . .	55
III.1	The sEMG-fatigue experiment posture. . . . .	66
III.2	The statistics of RMS in simple contraction test with respect to 5 muscle force levels. . . . .	67
III.3	The statistics of RMS in fatiguing test with respect to 5 muscle force levels. . . . .	68
III.4	The statistics of RMS in fatiguing test with respect to 5 muscle force levels. . . . .	69
IV.1	Full body running digital human modeling. Muscles are represented by red lines. . . . .	75
IV.2	Workload on erector spinae muscle during 10s arbitrary running at 3.96 m/s. . . . .	77
IV.3	Force capability lines of ten muscles during 10 min running. $k = 1.0 \text{ min}^{-1}$ . Force of each muscle is normalized by its maximum. . . . .	78

---

IV.4	Force capability lines of erector spinae with different preset $k$ values. Force is normalized by the maximum. . . . .	79
V.1	Raabe's full-body lumbar spine model [4]. . . . .	86
V.2	Topology views of two OpenSim models. . . . .	87
V.3	The Saul's 7 degree-of-freedom arm model [5]. . . . .	88
V.4	The topology view of the Full-chain OpenSim model. . . . .	89
V.5	A general view of the script of the Full-chain model. . . . .	90
V.6	The definition of the <b>Pelvis</b> body of the Full-chain model. . . . .	90
V.7	Diagram of a OpenSim joint. . . . .	90
V.8	Script of a OpenSim joint. . . . .	91
V.9	The location of biceps and its representation in the Full-chain model. . . . .	93
V.10	The definition of the right gluteus medius in the Full-chain model. . . . .	93
V.11	The Full-chain model on the OpenSim interface. . . . .	94
V.12	Body markers that indicate the location of joint plates. . . . .	96
V.13	The 3D geometric model of the subject generated by 3D scan. . . . .	97
V.14	The mesh of pelvis dismembered from the whole-body 3D model. . . . .	97
V.15	The OpenSim model used for error analysis. . . . .	98
V.16	Coordinate ( $q$ ), velocity ( $\omega$ ), acceleration ( $d\omega/dt$ ) of right hip flexion in the motion. . . . .	102
V.17	Right hip flexion moments calculated from the two models. . . . .	104
VI.1	Six working postures for a drilling task . . . . .	108
VI.2	Simulations of six drilling postures. From left to right: low close reach (L-C); low middle reach (L-M); low far reach (L-F); high close reach (H-C); high middle reach (H-M); high far reach (H-F). . . . .	109
VI.3	Shoulder moment according to the worker posture . . . . .	109
VI.4	The shoulder rotation moment is considerable beside of the elevation moment . . . . .	110
VI.5	The muscle activations in total for the six postures under studied . . . . .	112
VI.6	Locations of three muscle groups . . . . .	112
VI.7	Muscle activations of specific body parts . . . . .	114
VI.8	Backward drilling posture in current simulation (left) and in Anton's work(right) [43]. . . . .	116



## List of Tables

I.1	Normalized RMS values corresponding to five force levels during sMVC session. . . . .	10
I.2	Estimated average muscle activation of the six working postures. . . . .	15
II.1	Distribution of days away from work (DAFW) by the type of event [10].	20
II.2	The features of some observation-based tools for MSDs risks assessment [23]. . . . .	24
II.3	The classifications of shoulder posture of some observational tools(adapted from [24]). . . . .	26
II.4	The measurement of MVC in previous researches. . . . .	40
II.5	Parameters of the Force-load fatigue model. . . . .	43
II.6	Parameters of the dynamic Force-load joint fatigue model. . . . .	45
II.7	Fatigability values determined from different MET models [83]. . . . .	48
II.8	DHM software . . . . .	57
III.1	The physical characteristics of subjects in the EMG experiment. . . . .	64
III.2	Normalized RMS values corresponding to five force levels during sMVC session. . . . .	67
III.3	EMG amplitude changes during sustained maximal voluntary contraction. . . . .	70
IV.1	Basic characteristics of the analyzed muscles. . . . .	76
IV.2	General information of muscle force capabilities . . . . .	78
IV.3	Comparison of muscle force capabilities between different fatigabilities.	80

V.1	Existing OpenSim musculoskeletal models. . . . .	84
V.2	The degrees of freedom of the Full-chain model. . . . .	92
V.3	Volume, density and mass of the whole body and segments. . . . .	101
V.4	Errors of proportionally scaled segment masses with respect to the approximate masses. . . . .	101
V.5	Errors of the joint moments calculated from the scaled model, with respect to that from the approximate model . . . . .	103
VI.1	Model joint space settings. Unit: degree. . . . .	110
VI.2	Estimated joint moments of six simulations. Unit: $N.m$ . . . . .	111
VI.3	Estimated muscle activations . . . . .	113
VI.4	Estimated activations of individual muscles. . . . .	114

# Acknowledgements

I would like to give my sincere thanks to Mr Claude Jard and the fellows of the Laboratoire des Sciences du Numérique in Nantes for their kind supports during my thesis.

I would like to express my gratitude to Mr. Fouad Bennis and Mr. Damien Chablat, my thesis directors. I owe to them the liberal and strict atmosphere of our team. They raise me to be open, critical and humble. Both my life and my work benefit from their great kindness, their availability, their professional guidance and their scientific qualities.

I would like to give my thanks to the jury for their participation in my defence, to Mr. Georges Dumont and Mr. Gérard Poisson for their interest in my work; to Mr. Liang Ma for his patience and help and the valuable advice. I would always appreciate the chance to work with him.

Thank all my friends from Nantes and China for the homey atmosphere around me; thank my family for their patience, understanding and love that have always been there for me.

With these few lines, I would like to express to them how much their presence is necessary to me. Thank you very much.



# Glossary

- EMG: electromyography
- DAFW: distribution of days away from work
- MVC: maximal voluntary contraction
- MET: maximum endurance time
- sEMG: surface electromyography
- MUAP: motor unit action potential
- MSDs: musculoskeletal disorders
- RMS: root-mean-square
- CMC: computed muscle control
- DoF: degree of freedom
- NMT: neuromusculoskeletal tracking





# I

---

## General Introduction

### 1.1 Motivations

Despite the fact that industrial automation has been greatly developed in the last several decades, manual task is essential in many industries. Workers engaged into physical tasks are exposed to high risks of work-related musculoskeletal disorders, which bring about physical and mental afflictions, reduce work performance and cause great loss to the industries and the society. The work-related musculoskeletal disorders has been a global concern. Its risk assessment, if easily accessible and well-conducted, would benefit the ergonomic work design and occupational protections.

The biomechanics applies the laws of physics and engineering concepts to describe motion and forces, as stated in the book of Frankel and Nordin [1]. It is a multidisciplinary activity that combines engineering science with biological science. In this age, it is the belief of many biomechanists that the understanding of biomechanical principles should be further developed to promote its application in industry, especially for the identification and assessment of occupational risks.

This thesis seeks for improvements of the biomechanical methods with regard to the risk assessments of the work-related musculoskeletal disorders. Generally speaking, the occupational biomechanics mainly deal with two types of problems [2]: the impact trauma which caused by the sudden forces, and the overexertion trauma that caused by volitional activities. Musculoskeletal disorders, with whom the thesis attempts to deal, is one of the main overexertion traumas. Compared with the sudden force, impact of the volitional activities is highlighted by

their accumulating effect. Therefore, special attention here will be paid to the work-related fatigue, which is the result of work load accumulation. Other than withdraw some condition-specific conclusions from conventional ergonomic experiments, this thesis seeks for more understanding about the biologic features as well as the general mechanic regular patterns of muscle fatigue, for the purpose of fatigue determination and prediction.

It may be controversial whether fatigue is avoidable or not. But enormous researches of biomechanics and ergonomics in the last one hundred years have shown undoubtedly that work-related fatigue is amenable to the proper arrangement of the working posture. It has been commonly recognized that when conducting the same task, different working postures bring about gradable loads on particular body parts. However, the overall body load brought about by different postures is seldom examined. Given that human body is integral and systematic, there is a necessity to explore a general method to evaluate the posture load on whole-body in a comprehensive way.

The last two decades have witnessed the rapid development of biomechanical digital human modeling. The leading platforms include OpenSim and Anybody. Compared with the conventional digital human techniques, the biomechanical digital human modeling is characterized by the application of musculoskeletal models that rooted in both biologics and mechanics. The biomechanical analysis gives estimations of not only skeletal mechanics but also muscle activation statuses.

On this account, this thesis will then tend to the evaluation of the whole-body posture load using OpenSim. The possibility of optimizing the working posture for a given task in view of whole-body load is discussed.

## **I.2 Thesis structure**

This thesis explores the development of biomechanic methods for the risk assessment of work-related MSDs. On the whole, efforts are made from two aspects: the determination and prediction of muscle fatigue, the evaluation of whole-body posture loads.

The main part of this thesis consists of six chapters. The next chapter (chapter II) deals with the states of the art with regard to the risk assessment of work-related musculoskeletal disorders. Two primary problems are identified: the assessment of muscle fatigue as well as the measurement of workload, for which the surface EMG and the biomechanical digital human modeling techniques are highlighted respectively as the promising means. Chapter III and chapter IV focus on the muscle fatigue. In Chapter III, a new surface EMG-based muscle fatigue indicator is proposed and examined with an experiment involving 15 subjects. The new indicator is marked with good performance in tasks involving inconstant workload as well as with relative complex measurement process. In chapter IV, attempts are made to predict muscle fatigue by integrating a muscle fatigue mathematical model into OpenSim. Chapter V and chapter VI deal with the assessment of workload. As illustrated in Section I.1, there is a necessity to explore a general method to evaluate the posture load on the whole body, other than on a partial body part. Chapter V introduces the build-up of a full-chain OpenSim musculoskeletal model, then the errors brought about by the scaling method used by OpenSim for the subject-specification of body segment masses are analyzed. In chapter VI, the model is used for the assessment of whole-body posture loads of an overhead drilling task. The use of average muscle activation level as the indicator to posture loads is discussed. At last, conclusions and perspectives of the overall research work are presented in chapter VII.

### **I.3 Contribution to the assessment of physical risks of Musculoskeletal disorders**

This thesis contributes to the physical risk assessment of the work-related Musculoskeletal disorders in view of two ergonomic issues: muscle fatigue and posture load. For the muscle fatigue, efforts are made for its posterior indication (chapter III) as well as for its prior prediction (chapter IV). For the posture loads, efforts are made to appraise its physical influence on the whole body: a Full-chain biomechanical model is built up in chapter V, which is then applied to appraise the different postures of an overhead drilling task in chapter VI.

## Chapter II. Literature research

This chapter reviews the state of arts about the work-related musculoskeletal disorders and the related issues. Epidemiological studies about occupational Musculoskeletal disorders are firstly reviewed and an explanatory model of the contributing factors to Musculoskeletal disorders is summarized (see Figure I.1). As far as the objective of physical risk assessment, three primary problems are identified: the measurement of workloads, the assessment of the workload accumulation effect and the quantification of personal traits.

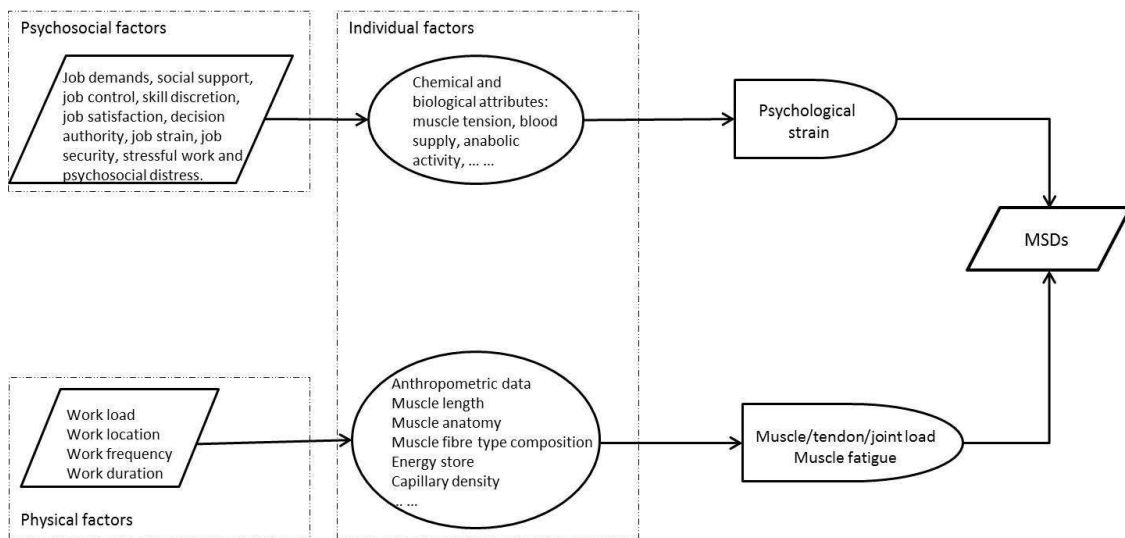


**Figure I.1** – An explanatory model of the contributing factors to Musculoskeletal disorders

The Musculoskeletal disorders physical risk assessment methods that are most-used in practical are reviewed, which emphasize the need of seeking for new comprehensive and practical methods. Then the ergonomic and biomechanical methods for the three identified problems are reviewed. For the measurement of workload, individual muscle anatomy are the more concrete indicators than other ergonomic indicators, which are feasible with the development of the biomechanical muscular models. For the workload accumulation effect, its main physical manifestation is muscle fatigue, which could be indicated by surface EMG and predicted by the biomechanical force-based muscle fatigue model. The individual physical characteristics, defined as the muscle fatigability, could be quantified by the tendency of the muscle strength to decline with respect to its maximal capacity as well as the external load.

Finally, the development of digital human modeling techniques is reviewed. OpenSim, a free-available software for musculoskeletal human modeling is highlighted as the promising tool for the integration of physical risk assessment of work-related Musculoskeletal disorders.

### Chapter III. The indication of muscle fatigue with surface EMG

This chapter concerns about the indication for muscle fatigue, which serves as the posterior assessment of the Musculoskeletal disorders physical risks. The surface EMG is one of the main choices.

Despite of the fact that the surface EMG has been widely used in ergonomics to indicate muscle fatigue, the EMG characteristic values are actually very limited as indicators: the spectral compression is often slight and insignificant statistically, and the amplitude is significantly affected by the exerting muscle force. In industries, when it comes to comparing different work designs in aspect of their fatiguing effect, these traditional indicators would be insufficient.

In this chapter, a new fatigue indicator is conceived based on the surface EMG amplitude. Two factors have been proven to influence the amplitude root-mean-square (*RMS*) of a fatiguing muscle: its fatigue level and its exerting force. The idea of the new indicator is to eliminate the force-induced *RMS* changes, as expressed by Equation I.1.

$$RMS_{fe} = RMS_f - RMS_s \quad (I.1)$$

The  $RMS_f$  and  $RMS_s$ , noted as the fatiguing *RMS* and simple-contracting *RMS*, are recorded in the fatiguing muscle and the fresh muscle respectively, with the same exerting force. Their difference, the  $RMS_{fe}$ , is the conceived indicator.

Then an experiment is designed to test the new indicator. The experiment includes the sustained static maximal voluntary contraction of the elbow flexors (see Figure I.2). The contraction lasts for 60 seconds, during which the muscle force declines from almost 100% MVC all the way along to about 50% MVC. The EMG signals of the biceps corresponding to when the force reaches 90% MVC, 80% MVC, 70% MVC, 60% MVC and 50% MVC were selected. At each of the five contraction levels, EMG signal of the fresh biceps were also recorded. The  $RMS_{fe}$  is calculated hereby. Result shows that the  $RMS_{fe}$  increases along with

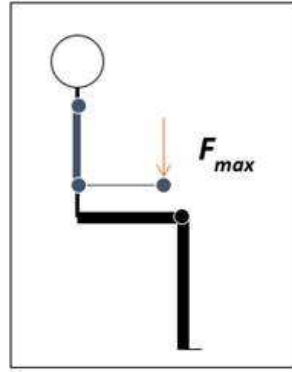


**Figure I.2** – Diagram of the experiment.

	90 % MVC	80 % MVC	70 % MVC	60 % MVC	50 % MVC
$RMS_f^*$ (%)	95.38(13.55)	96.37(19.58)	89.69(18.30)	80.06(14.37)	70.19(16.90)
$RMS_{fe}^*$ (%)	0.54(11.78)	2.24 (19.18)	14.70 (16.42)	14.67(18.88)	21.27(18.66)

\* Normalized by the RMS values corresponding to maximal force.

**Table I.1** – Normalized RMS values corresponding to five force levels during sMVC session.

the fatigue process to as much as 20% (see Table I.1), which implies that more and more extra effort is needed as muscle fatigue intensifies. The conceived indicator provides better indication to muscle fatigue than the traditional  $RMS_f$  in this condition. Conclusion is drawn that the new indicator could be used as a supplement of the traditional ones, especially for the comparison of the fatigue states of a muscle under different working loads.

#### Chapter IV. Muscle fatigue analysis in OpenSim

This chapter deals with the muscle fatigue prediction, which would serve as the prior assessment of the Musculoskeletal disorders physical risks. This work is based on the biomechanical digital modeling software OpenSim. The musculoskeletal models of OpenSim enable the muscle contraction dynamics, which allows optimizations algorithms such as the Compute Muscle Control to be applied to distribute joint load down to individual muscles.

A plug-in is written to OpenSim to estimate the accumulation effect of the real-time muscle loads onto the remaining force output ability of each muscle. The plug-in refers to the Force-load muscle fatigue model. Workflow of the muscle fa-

tigue prediction process is shown in Figure I.3. The prediction could be applied at any time to all the muscles for arbitrary tasks, with considerations of individual fatigability. Then the plug-in is tested on a set of data from the project of Hamner

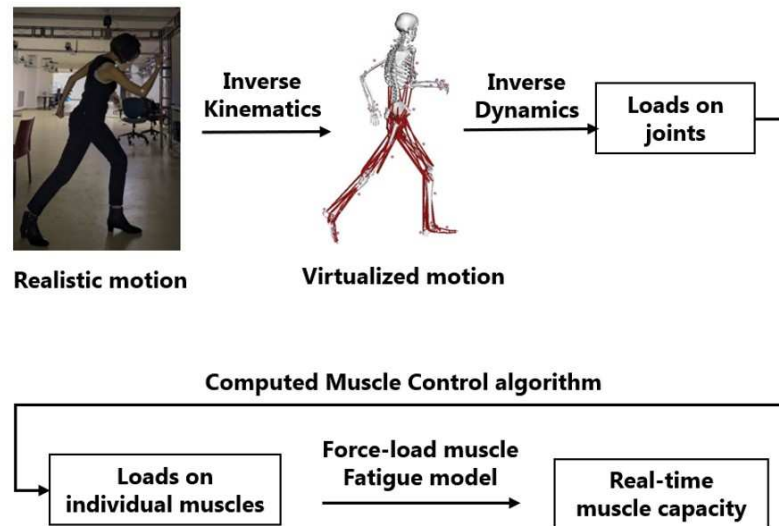


**Figure I.3** – Workflow of the muscle fatigue prediction process of OpenSim with the muscle fatigue analysis plug-in.

et al. [3]. It is recorded from the real motion of a male subject running at 3.96m/s. The computed load of the erector spinae muscle is shown in Figure I.4. The simu-

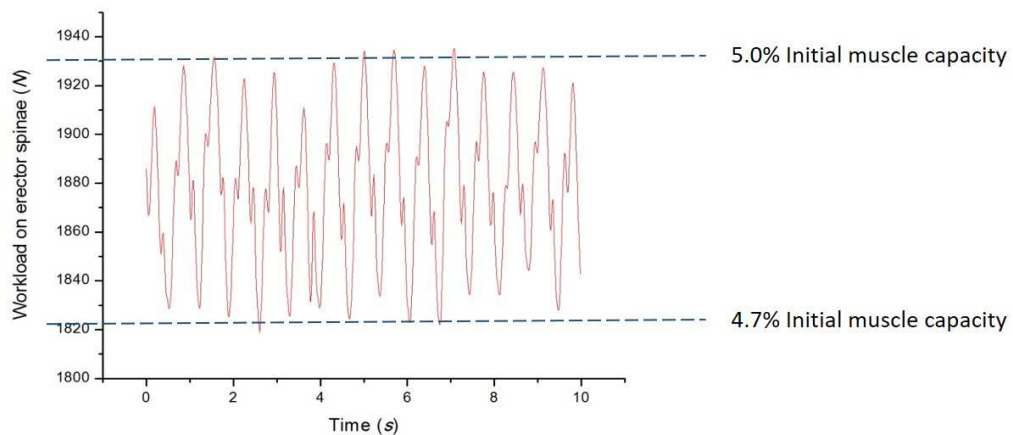


**Figure I.4** – Load on the erector spinae muscle during 10s running.

lation result shows that for a subject fatigue-resistant (fatigability  $k = 1.0\text{min}^{-1}$ ), the muscle capabilities would reduce to 60% to 70% of their maximum after run-



ning at  $3.96 \text{ m/s}$  for 10 min (shown in Figure I.5). While for someone fatigue-fragile (fatigability  $k = 1.0 \text{ min}^{-1}$ ), his muscles would lose 50% to 60% of their initial maximal capability. It can be concluded that the plug-in is easy to apply

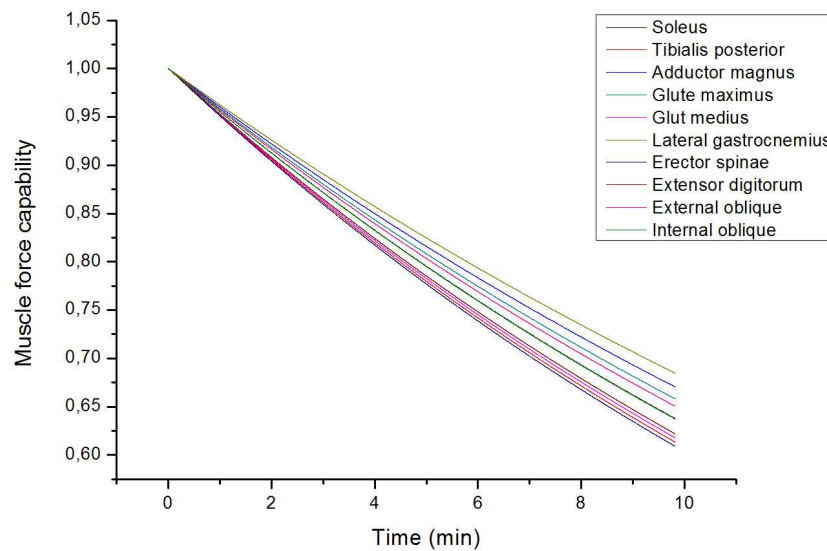


**Figure I.5** – Force capability trends of ten muscles during 10 min running,  $k = 1.0 \text{ min}^{-1}$ . Force of each muscle is normalized by its maximum.

for comprehensive prediction of muscle fatigue. Experimental verification is supposed to be acted on. The plug-in could serve as a functional tool for the prior musculoskeletal disorders risk assessment.

## Chapter V. The build-up of a full-chain musculoskeletal human model in OpenSim

The development of muscle fatigue is amendable to proper working postures. Enormous biomechanical researches have emphasized the necessity to analyze human dynamics in view of the full dynamic chain. In this chapter, a full-chain musculoskeletal human model is built up in OpenSim for the whole-body posture load analysis.

The Full-chain model is developed based on Raabe's FBLs model [4] and Saul's arm model [5]. It consists of 46 body parts, 424 muscles and 37 DoFs, shown in Figure I.6.

Then the scaling methods that used for the subject-specification of body iner-

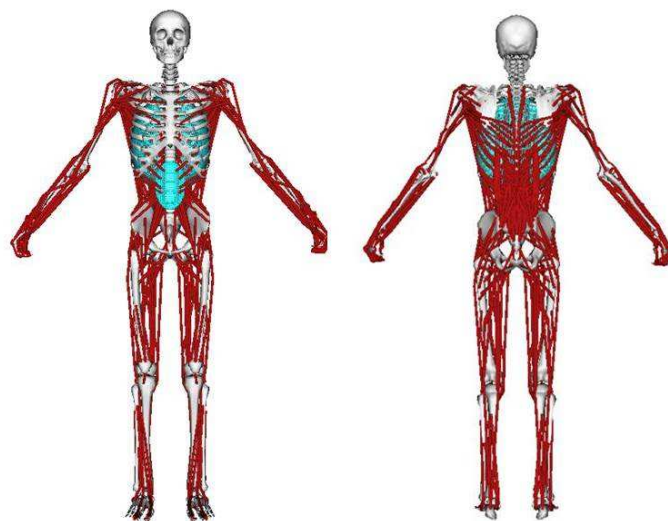


**Figure I.6** – The Full-chain model on the OpenSim interface.

tial parameters in OpenSim is studied. Traditionally, to specify a general OpenSim model to a new worker, the mass of each segment is scaled with the weight ratio of the worker to the model. Errors of this scaling method as well as the influence brought about by the errors on dynamics analysis is assessed.

A 3D scan is applied on a male subject to construct his 3D geometric model (see Figure I.7), according to which segment volumes are calculated and masses are determined. The determined segment masses data is taken as the yardstick to assess OpenSim proportionately scaled model. As a result, the error of segment mass reaches up to 5.31% of the overall body weight (torso). Influence on the dynamic analysis was examined with kinematic data of a two-step ordinary walking. The calculated joint moments were found to have an average difference from 3.65% to 12.68% between models with the two sets of data.

### **Chapter VI. The Application of the Full-chain model on posture analysis of an overhead drilling task**

In this chapter, the Full-chain model developed in chapter V is used for whole-body posture analysis. The simulated task is an overhead drilling operations (see Figure I.8). Six postures with two reach height levels and three reach length levels are analyzed (see Figure I.9).

Instead of drawing empirical conclusions that fit for this specific case, this the-

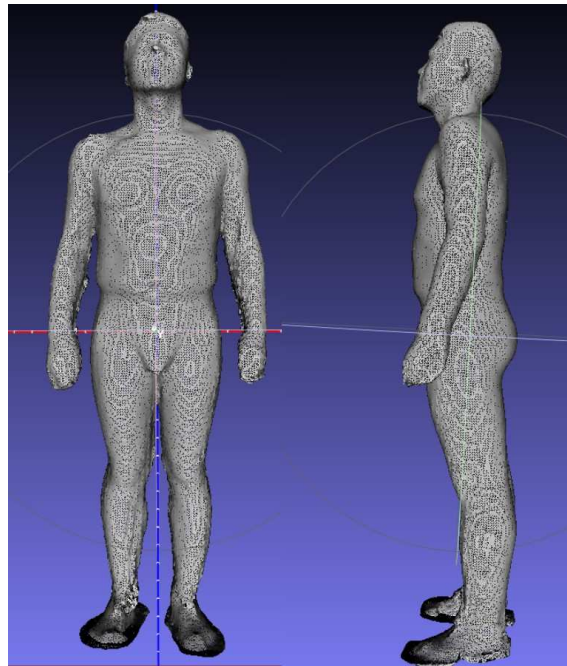


**Figure I.7** – The geometrical model generated from 3D scan.

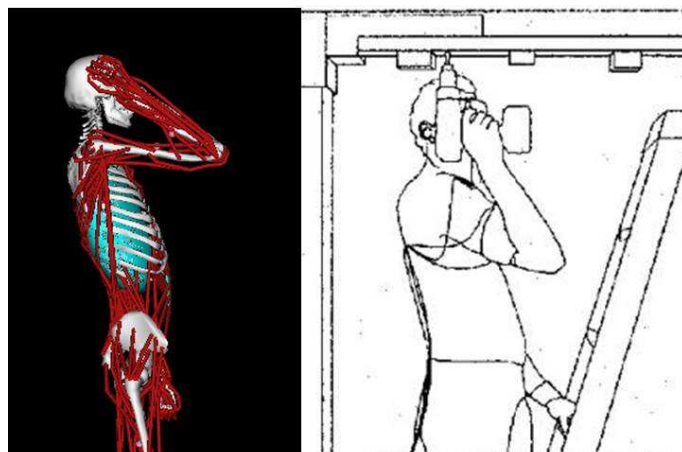


**Figure I.8** – The simulated overhead drilling operation.

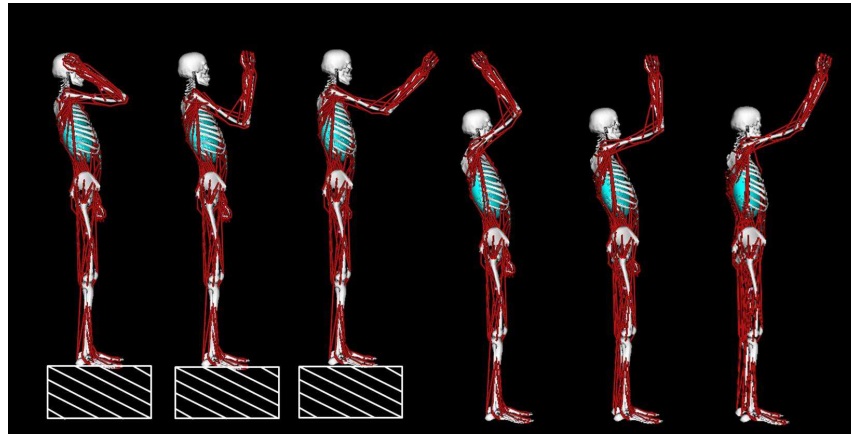


**Figure I.9** – Six drilling postures for the drilling operation are analyzed.

**Table I.2** – Estimated average muscle activation of the six working postures.

Muscle groups	No. of muscles	Mean muscle activation					
		L-C	L-M	L-F	H-C	H-M	H-F
Right lower arm	18	6.88%	3.96%	1.20%	8.60%	3.18%	1.42%
Right upper arm-shoulder	22	2.18%	4.92%	8.18%	8.31%	6.38%	8.59%
Right Latissimus dorsi	14	82.29%	0.39%	81.64%	40.95%	0.43%	78.97%
Left Latissimus dorsi	14	0.09%	0.06%	0.84%	0.10%	0.06%	0.65%
Right hip abductor	10	0.34%	0.32%	0.41%	0.38%	0.32%	0.37%
Left hip abductor	10	16.77%	16.77%	16.77%	16.77%	16.77%	16.77%
Whole-body	424	5.81%	2.80%	6.43%	5.29%	3.62%	6.92%

sis put more emphases on exploring the general method for the assessment of the posture loads on whole body. The average muscle activation level (varies from 0 to 100%) is proposed as the indicator of whole-body posture load other than the muscle force. The estimated average muscle activation level of the six simulated postures are shown in Table I.2.

Results shows that the average muscle activation of the six postures varies from 2.8% (low-middle reach) to 6.9% (high-far reach). Conclusion could be drawn that the average muscle activation can be an effective indicator to the posture loads on the whole body. Besides, the Full-chain OpenSim model facilities the posture load assessment in that it enables the comprehensive estimation of multi-degree-of-freedom joints' moments, as well as in that understanding how the

muscles across body cooperate as a full dynamic chain. The possibility of optimizing working posture in view of total muscle efforts is discussed.

# II

---

## Literature Research

### II.1 Abstract

This chapter reviews the state of arts about the work-related musculoskeletal disorders and the related issues. Firstly, the epidemiologic studies are reviewed, which underlines three primary points for the physical risk assessment of work-related musculoskeletal disorders: the measurement of workload, the evaluation of the accumulating effect of workload, and the quantification of individual physical characteristics. Then the methods that are currently used for the risk assessment are reviewed, which emphasizes the necessity of seeking for more accurate methods.

From Section II.4, studies about the three primary points are reviewed respectively. For the measurement of workload, individual muscle forces are the more concrete indicators, which are feasible with the development of the biomechanical muscular models. For the workload accumulation effect, its main physical manifestation is muscle fatigue, which could be indicated by surface EMG and predicted by biomechanical force-based muscle fatigue model. The individual physical characteristics, defined as the muscle fatigability, could be quantified by the tendency of the muscle strength to decline with respect to its maximal capacity as well as the external load. The measurement methods of fatigability are reviewed. It is suggested that more measurement be conducted with different populations, so that the database of a populational muscle fatigability would be enlarged as with the other anthropometric measures.

Finally, the development of digital human modeling techniques is reviewed.

OpenSim, a free-available software for musculoskeletal human modeling is highlighted as the promising tool for the integration of physical risk assessment of work-related MSDs.

In conclusion, there is a necessity to improve the practical methods of the physical risk assessment of work-related musculoskeletal disorders. Biomechanical digital human modeling technique is promising to contribute to the improvements. Efforts are needed for the measurement of workload on the overall body, for the predication of muscle fatigue in a task, and for the objective indication of fatigue.

## II.2 Musculoskeletal disorders: an epidemiologic overview

### II.2.1 Definition of MSDs

Despite of the rapid development of automation techniques, manual work is still irreplaceable in many cases due to its flexibility and adaptability. Manual tasks like drilling, sanding, and material handling are inevitable in many industries, which demand higher level and longer-lasting physical loads. Workers engaged in these tasks are exposed with high risks of Musculoskeletal disorders (MSDs).

As reported by the Health, Safety and Executive in UK [6], the average rate of MSDs of all industries in Britain is about 1,500 per 100,000 workers (average date from 2014 to 2017). Industries of construction, agriculture, transportation and storage, human health and social work activities are highlighted by the highest MSDs risks. In France, MSDs take up more than 75% of the occupational diseases in 2015 [7], which underlies a huge population involved.

MSDs are defined as the injuries and disorders to muscles, nerves, tendons, ligaments, joints, cartilage and spinal discs and do not include injuries resulting from slips, trips, falls or similar accidents [8]. Body parts most commonly involved are the low back, neck, shoulder, forearm, and hand [9], while the lower extremity gains also lots of attentions.

MSDs results in high rate of employee turnover and sick leave as well as a huge amount of health compensation. The record of 2016 occupational injury and illness of Massachusetts, Unite States shows that working days loss due to over-extension and bodily reaction, with a proportion of 36.4%, is ranked as the first cause factor of sick leave [10] (Table II.1). Data of the Britain shows that 8.9 million working days are lost due to MSDs; In European Union, it was estimated that the MSDs bring about 0.2% to 5% GDP loss [11].

One of the main task of occupational biomechanics is to apply biomechanical principles in the control of work-related MSDs risks from aspects of work design and worker management. This should be based on a solid understanding of MSDs-related knowledge and pragmatic techniques. The task is promising in protecting the welfare of workers and the benefits of industries and the society.



**Table II.1** – Distribution of days away from work (DAFW) by the type of event [10].

Number of Cases and Percent Distribution of DAFW Cases by Event, Massachusetts, Private industry, 2016, [Total Cases = 31,140]		
Event Category	Number	Percentage
Overexertion and Bodily Reaction	11,340	36.4%
Contact with Object, Equipment	7,630	24.5%
Falls, Slip, Trips	7,260	23.3%
Violence and Other Injuries by Person or Animal	1,790	5.7%
Exposure to Harmful Substances or Environment	1,680	5.4%
Transportation Incidents	1,350	4.3%
Fires and Explosions	*	*

\*Data was unpublishable

## II.2.2 Contributing factors to MSDs

As is always the case, work-related MSDs, common and prevalent phenomena in actual life, are found to have complex relationships with numerous factors. Occupational epidemiology has revealed three categories of related factors: physical factors, psychosocial factors and individual factors.

Physical factor is always mentioned as the "exposure to risk" factor for MSDs. It denotes the influence of work design and working conditions on human physique. As Burdorf [12] has reviewed, heavy physical work, static work posture, frequent bending and twisting, lifting and forceful movements, repetitive movements and whole-body vibration were the most commonly listed occupational risk factors for disorders of the back in epidemiology. For the MSDs of the neck and upper-limb, evident exposure includes: work with hands at or above shoulder level, localized shoulder muscle fatigue, work tasks strenuous to the muscle tendon structures of the upper limb, repetitive arm work, constrained head and arm posture, and the use of vibrating handtools [13].

These physical exposure factors were summarized by Armstrong et al. [13] down to four variables: work load, work location, work frequency and work duration. In the view of biomechanics, these factors (except for the vibration factor) make influence on human body by two means: body loads (muscle/joint/tendon loads) and the accumulation effects of body loads along time.

The psychosocial factors denote the risk factors that contribute to MSDs through

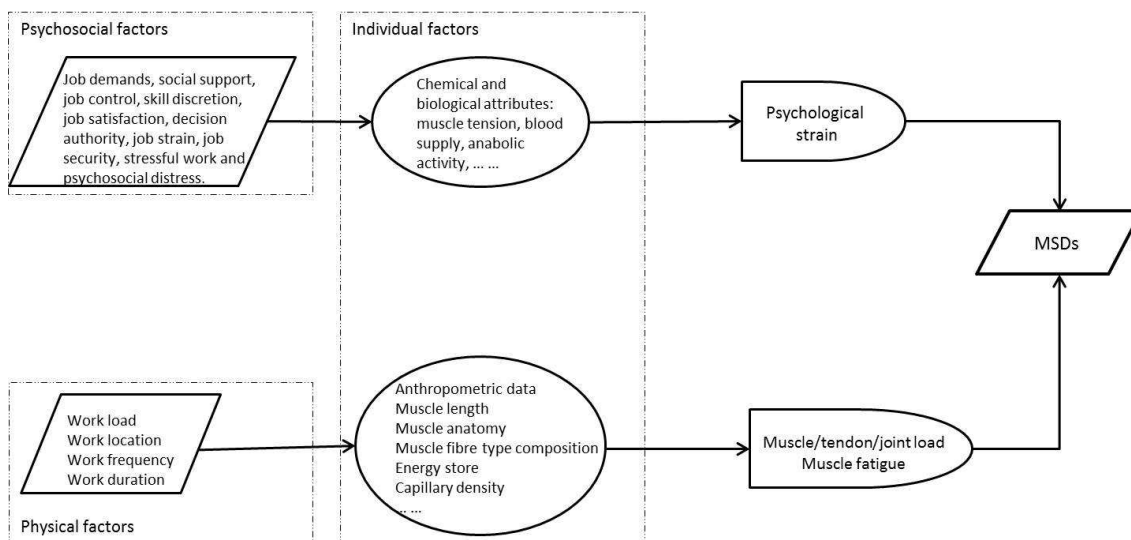


**Figure II.1** – An explanatory model of the contributing factors to MSDs

impacts on workers' mental health status. Psychosocial stressors at work have been found to be associated with risk of MSDs by enormous studies. Haukea et al. [14] summarized the results of 54 longitudinal related studies and concluded 10 factors that are mostly investigated: job demands, social support, job control, skill discretion, job satisfaction, decision authority, job strain, job security, stressful work and psychosocial distress. It has been concluded that psychosocial factors should be considered as independent predictors of MSDs.

The individual factors refer to the physical and mental attributes specific to the subject which determine how the subject reacts to the physical factors and psychosocial factors. Those in regard to the physical factors include the anthropometric data of the subject (body size and shape), the muscle anatomy, the muscle fiber type composition, energy store, capillary density and so on [13]. These factors determine how the work load is distributed to each part of the body, as well as how the load is accumulated and fatigues the body. The individual attributes concerning the psychological factors affect the transform from psychosocial stressors to psychological strains chemically and biologically. The explanatory model is shown in Figure II.1.

This thesis focuses on the physical risks for MSDs of individuals, which is the second pathology path in Figure II.1. The primary questions that concern biomechanical researches in this field are:

- how to evaluate the muscle/tendon/joint load given a specific work situation;
- how to evaluate the fatigue effect of the muscle/tendon/joint load given a specific work frequency and/or work duration;
- how the individual factors influence the muscle/tendon/joint load and its fatigue effect.

It is of great importance to assess the physical risk of MSDs in view of worker protection. The assessment is supposed to involve consideration of the above three aspects. In the next section, assessment methods that are currently used is to be reviewed.

### **II.3 MSDs physical risk assessment in practice**

In this section, ergonomics tools that are most commonly used in practice to assess the physical risks for MSDs are reviewed and discussed. These assessment tools are based on either the observation of work processes or self-reports, noted as the observational methods and self-reported methods.

#### **II.3.1 Observational methods**

Conventional observational method is usually based on pens and papers. Practitioners observe the working process being assessed, recognize the listed traits of the work, and grade these traits according to the instructions of the tool. A score or a code is then assigned to each of the traits, which represents the risk level of that trait. Then the scores or codes are processed together according to the predefined method by each specific tool, which generates an overall value. The value is the assessed indicator of the physical risk level of MSDs. The Figure II.2 is an example.

Some tools of this method assess the MSDs risks of whole-body, while some others focus on specific body parts such as the low back, the neck and shoulder. Tools of the former type commonly used in ergonomics include the Posturegram [16], the Ovako Working Posture Analyzing System (OWAS) [17], the Posture Targeting [18] and Quick Exposure Check (QEC) [19], Rapid Entire Body Assessment

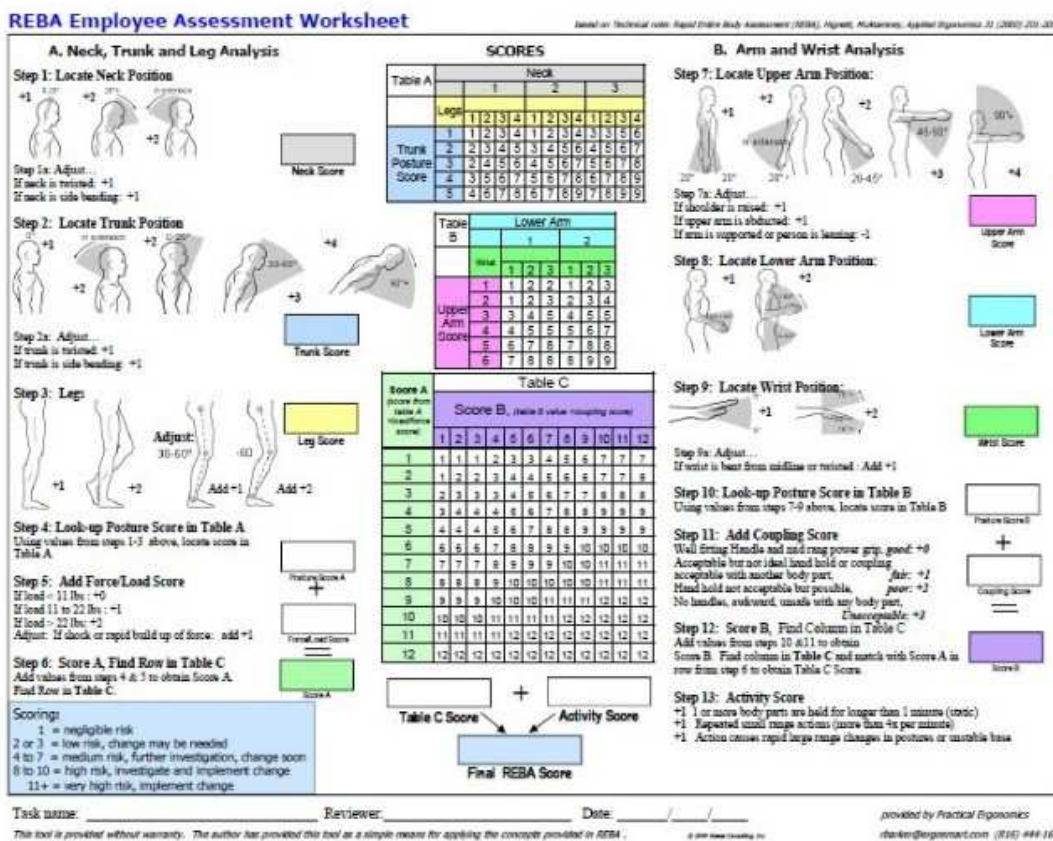


Figure II.2 – Rapid Entire Body Assessment Checklist [15].

(REBA, see Figure II.2) [15]; tools of the latter type include the Rapid Upper Limb Assessment (RULA) [20], the Hand-Arm-Movement Analysis (HAMA) [21] and the PLIBEL (Method for the identification of musculoskeletal stress factors that may have injurious effects) [22]. The features of these tools are concluded by Li and Buckle [23], as shown in Table II.2.

Generally, traits to be observed and taken as input data include the working posture, the external force and the time sequence of the task (task frequency and duration).

**Working posture as the input data**

Generally, working posture is the trait valued most in these observational tools. Descriptions such as ‘head turned partly to side or slightly forward’ and ‘head turned to side or head forward about 20°’ are used to classify the postures. An

**Table II.2** – The features of some observation-based tools for MSDs risks assessment [23].

Tools	Features and applications
Posturegram	<p>Body postures are categorized and recorded by time sampling on to cards as digital numbers.</p> <p>Whole body posture evaluation for static tasks.</p>
OWAS	<p>Categorized body postures in digital numbers, including force; time sampling, has action categories.</p> <p>Whole body posture analysis.</p>
Posture Targeting	<p>Postures are marked as angles and directions together with work activities by time sampling.</p> <p>Whole body posture recording for static tasks.</p>
QEC	<p>Estimate exposure levels for body postures, repetition of movement, force / load and task duration for different body regions, with a hypothesized score table for their interactions. Assessing the change in exposure for both static and dynamic tasks.</p>
RULA	<p>Categorized body posture as coded numbers, including force and muscle activities; time sampling, with action categories.</p> <p>Upper limb assessment.</p>
HAMA	<p>Record the types of motion, grasps, hand position and features of load handled; the data is linked to work activities.</p> <p>Upper limb assessment.</p>
PLIBEL	<p>Checklist with questions answered for different body regions. Identification of risk factors</p>
REBA	<p>Score the body posture, estimate the load, with action levels.</p> <p>Risk assessment of the entire body for non-sedentary tasks.</p>

example of the classification of shoulder posture in several tools are shown in Table II.3.

### **External force as the input data**

Most tools of this method consider external forces as absolute values exerted during work, such as OWAS, RULA, REBA. OWAS classifies force into three level: under 10 kg, 10 to 20 kg and over 20 kg. REBA classifies force as under 5 kg, 5 to 10 kg and over 10 kg. For RULA, the criteria is 2 kg or less, 2 to 10 kg or over 10 kg. The exerted forces that are repetitive, or static, or exerted rapidly are considered specially.

### **Time sequence as the input data**

The MSDs risk brought about by the load accumulation effect is mainly assessed by the duration and frequency of tasks. For example, the RULA and REBA classify the task into static (duration longer than 1 min) and repetitive; The most comprehensive consideration of the time sequence is defined by the LUBA [25], where tasks with various numbers of phases and various duration of those phases is accepted. It also allows the changes of external load between phrases. In spite of this, the observational methods takes poor consideration about arbitrary motion and multi-tasks.

### **Discussions**

Generally speaking, the observational methods are easy to apply, inexpensive, and without disruption to the work. However, the defects are also evident. As discussed in section II.2.2, the physical risk of MSDs for an individual is depending on three aspects: the load on body parts (muscles/tendons/joints), the cumulative effect of the body load, and the individual traits. The observation-based method reviewed in this section involves considerations about the first and the second aspects, while neglecting the individual traits.

The observational tools are posture-based. Problems arise here in that they function poorly in dynamic tasks and multi-tasks. It is very complex to decompose a dynamic task into postures, external forces and task durations when the

**Table II.3** – The classifications of shoulder posture of some observational tools(adapted from [24]).

Posture	LUBA*	RULA	REBA	EN1005-4**
Arm flexion	0°- 45°	0°- 20°	0°- 20°	0°- 20°
	45°- 90°	20°- 45°	20°- 45°	20°- 60°
	90°- 150°	45°- 90°	45°- 90°	> 60°
	> 150°	> 90°	> 90°	
Arm extension	0°- 20°	0°- 20°	0°- 20°	> 0°
	20°- 45°	< 20°	< 20°	
	45°- 60°			
	> 60°			
Arm adduction	0°- 10°	-	-	0°- 20 °
	10°- 30°			20°- 60°
	>30°			>60°
Arm abduction	0°- 30°	0°	0 °	< 0°
	30°- 90°	>0°	>0 °	
	>90°			
Arm medial rotation	0°- 30°	0°	0°	-
	30°- 90°	> 0°	> 0°	
	> 90°			
Arm lateral rotation	0°- 10°	0°	0°	-
	10°- 30°	> 0°	> 0°	
	> 30°			

\* LUBA: postural loading on the upper body assessment [25].

\*\* EN 1005-4: Evaluation of working postures in relation to machinery [26].

posture and external force change from instance to instance, and duration of each phrase is very short.

Even in the assessment of posture load on body parts, where the primary emphasis is laid, the observational method has a long way to go. The first effort should be made in the clear and complete description and definition of postures. For instance, the shoulder joint is a ball joint that permit the humerus to rotate in three dimensions. The description of shoulder posture requires at least three parameters in the Cartesian coordinate: arm adduction, arm elevation and arm rotation. As we can see in Table II.3, even of the upper-limb-focused tools, many do not have complete shoulder posture descriptions: arm rotation is ignored in most case. The second effort is expected in the consideration of the combination effect of risky postures. Since the human body is systematic and body parts are intra-supported and connected as a chain. The ignorance of the full-chain effect would also inhibit the unequivocal evaluation of body loads.

### II.3.2 Self-report methods

Theoretical basis of this method is the association between the perceived physical demand and MSDs that has been reported by previous researches [27, 28, 29, 30]. The objective of the self-report is to evaluate the perceived physical demand. In ergonomics, some scales and questionnaires with examined validity and reliability are available in this aspect, such as the the Job Content Questionnaire (JCQ) (physical part) [31], the Body-map [32], Borg's perceived exertion scale [33], the Swedish Occupational Fatigue Inventory (SOFI) [34].

The concept of 'industrial comfort' was raised [32], the measure of which is the level of discomfort. Based on this concept, the Body-map ask for ratings on the perceived discomfort level, which is the worker's subjective feeling. The JCQ emphasizes more on worker's impression about the working situation. Items like 'in my job I am Often moving/lifting very heavy loads', 'in my job I am working for long periods with my head or arms in awkward positions' are asked. The Borg's perceived exertion scale [33] estimates the worker's effort, breathlessness and fatigue. The SOFI focuses more on the fatigue. Five aspects are included:



lack of motivation, sleepiness, physical discomfort, lack of energy and physical exertion, which involve both peripheral and central fatigue.

The assessment given by the self-report method has been shown to be a good indicator to MSDs by many researches. The assessment of the risk of MSDs in the self-report method could be seen as a synthetic measure of the cumulative body loads and the individual traits. In the explanatory model about the development of MSDs in Section II.2.1 (Figure II.1), it goes near to the third phrase, the 'muscle/tendon/joint load and local muscle fatigue'. Differences between the two are that: 1. the measure of the self-report method is the part of 'the muscle/tendon/joint load and local muscle fatigue' reflected subjectively by the worker, and 2. the measure may be influenced by the worker's physiological condition also.

### II.3.3 Summary

As discussed in Section II.2.2, three aspects should be considered in terms of physical risks of MSDs assessment of individuals: the work load on body parts, the cumulative effect of the body load, and personal traits. Observational method involves the consideration of the work load and the cumulative effect, but with a lack of accuracy. The self-report method touches upon all the three aspects synthetically. But given that the objective of the physical risk assessment is to get a clear idea about the source of risks and hereby to control the risk, the use of the self-report method would be limited by the synthesis as well as the interference of the worker's physiological condition.

From the next section, we are going to review the biomechanical techniques of the three aspects concerning MSDs physical risk: the work load analysis, the cumulative effect of body loads (fatigue), and personal traits with the purpose of seeking for new method of MSDs physical risk assessment.

## II.4 Work load analysis

As concluded in the last chapter, the assessment of physical risks of MSDs should be founded on three aspects: the measurement of instant work load, the evaluation of the accumulation effect of the instance work load, and the proper

involvement of subject-specific characteristics. In this section, existing ergonomic methods of the first aspect, i.e., the measurement of instance work load on human body will be reviewed and discussed.

#### II.4.1 Work load evaluation: ergonomic methods

In ergonomics, it is very often desirable to evaluate the loads on human body of a work. Measures that are commonly used include the surface electromyography (sEMG), the work pulse, the acceleration of body parts, the joint moment, ect..

The sEMG is the indicator of muscle activities. For the assessment of work loads, the sEMG offers two types of measures: the muscle activating time and the intensity. The first measure is practical especially in the prolonged low-level-load works [35]. For example, the studies of Hägg & Åström [36] and Veiersted et al. [37] have shown that the lack of rest time, demonstrated by the continuous measurable sEMG of the trapezius muscle, is one of the most important determinant of the neck MSDs. The second measure, usually calculated by the 50th or 90th percentile of the sEMG activity, is used to indicate the intensity of work load [38]. For example, in the study about the authentic work of dental hygienists, the load on the forearm extensor muscles was found to be high, with the 90th percentile sEMG activity as much as 23% of its maximal [39].

Work pulse was defined as the difference between working heart rate and resting heart rate [40]. Large work pulse indicates strenuous work and heavy work load [38]; The body acceleration measured by accelerometers placed on certain parts of body provides information about the movement demand of the work, which was also used as an indicator to work load [41, 38]. Problem of these two measures as indicators of workloads is that they are indirect and affected by many other factors. The measurement validity is questionable.

Joint moment is a direct indicator of workloads, the measurement of which should be based on mechanical analysis. The mechanical analysis requires the clear knowledge about joint posture, velocity, acceleration and external force. The measurement method and main challenges are discussed in the next section.

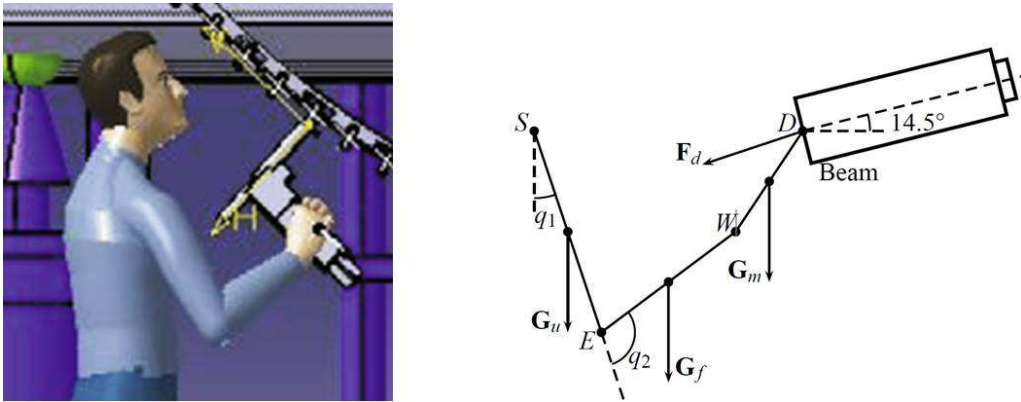


**Figure II.3** – A schema for shoulder joint moment calculation [42]. Posture configuration is determined by the length of upper arm  $l_{SE}$  and lower arm  $l_{EW}$ , as well as the upper arm incline angle  $q_1$  and elbow angle  $q_2$ .

#### II.4.2 Joint moment measurement

As illustrated above, the calculation of joint moment is based on the knowledge of joint kinematics and external forces. The accuracy of estimated joint moment is limited mainly by the measurement of joint kinematics: joint posture, velocity and acceleration.

In ergonomic practice, the joint posture is very often determined from the worker's two-dimensional motion projection on the sagittal plane. Figure II.3 shows the schema used by Ma et al. [42] to calculate the shoulder joint load of a static drilling task. The same method has been used by Anton et al. [43] in the estimation of subjects' shoulder joint moment during a static overhead drilling.

The sagittal plane-projection has been very commonly used to determine the joint postures. Posture configuration based on the sagittal plane-projection (shown in Figure II.4) has long been used to predict the maximal moment of joint's flexion-extension movement, with numerous prediction equations, as has been summarized by Chaffin in his book ([44], p263).

This method is simple and practical for static joint moment estimation, and works well in single-degree-of-freedom joint such as the elbow. The shortages are also evident. Firstly, the lack of information about joint velocity and acceleration limits its usage in dynamic cases. Furthermore, even in static case, the measurement is incomplete for multi-degree-of-freedom joint. For example, the

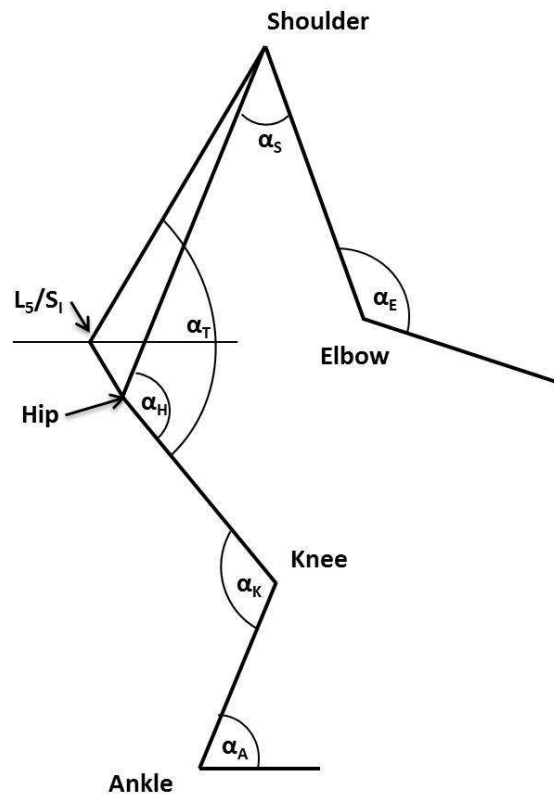


**Figure II.4** – Traditional ergonomic method determines the configuration of human posture by its projection on the sagittal plane ([44], p262).

shoulder joint is a ball-in-socket joint with three degrees of freedom. With the sagittal plane-projection method, only the shoulder elevation moment can be determined. Movement on the other planes, such as shoulder rotation and shoulder adduction moment, are ignored. Yet as stated by An et al. [45], the arm configuration of the frontal plane makes significant difference in joint loads as well.

Future development in joint moment measurement would turn more and more to the digital human modeling techniques. Those who involve biomechanical musculoskeletal model could provide complete description of joint movement. With the help of digital techniques, the time sequence of posture configuration can be generated, as well as that of joint velocity and acceleration. The digital human modeling techniques are reviewed in Section II.7.

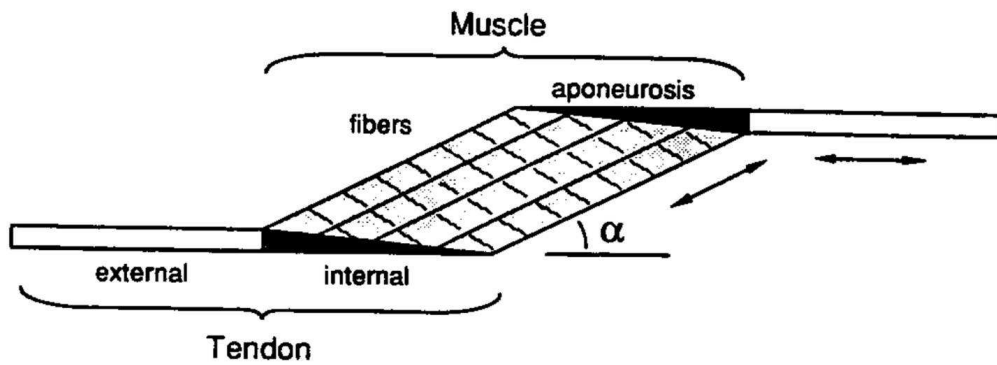


**Figure II.5** – The diagram of muscular-tendon structure [46]. Muscle fibers are oriented at an angle  $\alpha$  with the tendon. Tendons moves only along its axis. As the muscle contracts, muscle fibers shorten and the angle  $\alpha$  increases.

### II.4.3 Muscle force assessment

Human motion starts from the exciting signal sent by the central nervous system to muscles, which brings about muscle contractions. Then the contracted muscle forces are transmitted by tendons to joints, hence movements happen subsequently. Muscle is the only apparatus that contracts voluntarily in the musculoskeletal system. Since it is very difficult to measure the force of individual muscles, most ergonomic practitioners would stop by joint moments when estimating workloads. But if we want to take a close look at the work load, muscle force is something of great interest.

This section will review and synthesize the knowledges of muscle-tendon properties, as well as the biomechanical models that have been developed in the last century with enormous efforts of the biomedical and biomechanical scientists.

#### Muscle-tendon architectures

A muscle can be considered as a branch of muscle fibers with equal length, aligned in parallel, with an acute angle  $\alpha \geq 0$  to the tendon, as shown in Figure II.5. The branches of muscle fibers are attached to the aponeurosis, the internal part of the tendon (the dark region in Figure II.5) on its two ends.

The smallest contraction unit of the muscle is called a motor unit. It is defined as a nerve axon and the set of muscle fibers innervated by this nerve axon and its branches [47]. A muscle can be viewed as a collection of  $n$  motor units, each with

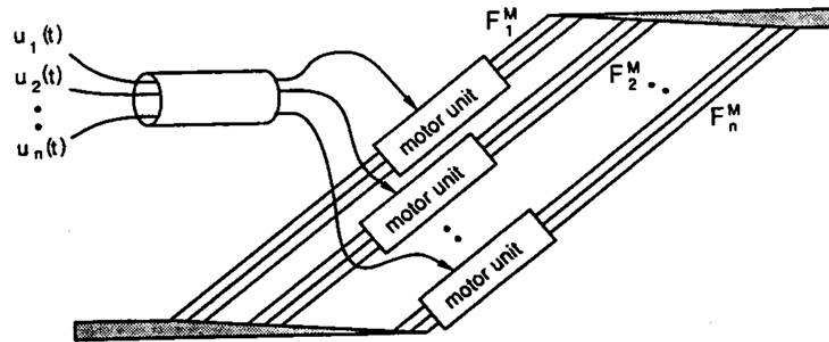


**Figure II.6** – The diagram of motor unites [46]. Each motor unite is functionally disjoint with the others. Motor unite  $i$  is excited by signal  $u(i)$ , gets activated and produces fiber force  $F_i^M$ .

its control sequence  $u_i(t)$  from the central nerve system, as shown in Figure II.6. The summation of all motor units forces ( $F_i^M$ ) is the generated force of the muscle  $F^M$ . The motor units are always classified into the 'slow contracting' and 'fasting contracting', with different energy metabolic and fatigue properties.

The muscle force generation process starts from the excitation of the central nervous system. The command signal is transmitted to the muscle fiber. The innervated motor unit would discharge in synchrony with one another. This neural and muscular excitation process is always referred to as the 'neuromuscular excitation', or 'neural excitation' in this thesis. Then the surface action potential is transmitted to the interior of the muscle by means of the transverse tubular system. Calcium ions enter the muscle cell, triggering the release of calcium from the sarcoplasmic reticulum. Calcium diffuses to the myofilaments and combines with the troponin-tropomyosin system, which allows actin and myosin to interact. This interaction in the presence of ATP results in cross-bridge cycling, which produces forces. The calcium dynamics that mediate the neural excitation-muscle contraction coupling is always mentioned as the 'muscle activation' process [46].

The muscle force generation dynamics can be divided into two phrases: muscle activation dynamics and muscle contraction dynamics, as shown in Figure II.7. The former refers to the process from central nerve system excitation signals ( $u(t)$ ) being input to the motor unit to the muscle being activated (muscle activation level  $a(t)$ ); the latter corresponds to the process of activated muscle fibers contraction, hereby muscle force ( $F^M(t)$ ) is generated.

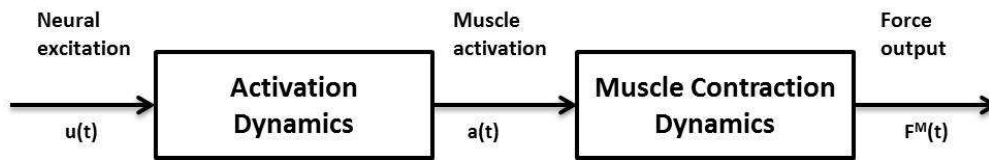


**Figure II.7** – The diagram of muscle force generation process [46]. The activation dynamics correspond to the calcium release, diffusion, and bonded to troponin. The contraction dynamics correspond to the energization of cross-bridges between thick and thin filaments, through which muscle forces are generated.

### Musculo-tendon contraction mechanics modeling

As stated by Zajac [46], all the researches investigating the musculo-tendon contraction use are based on the mechanical model developed by Hill [48], Wilki [49], Ritchie and Wilkie [50] at around 1950s. This model is known as the Hill-type model (see Figure II.8). It consists of a muscle in series with a tendon. The tendon is modeled by an elastic element whereas the muscle is modeled by a contractile element (CE) in parallel with an elastic element. The CE generates an 'active force' ( $F^{CE}$ ). By comparison, the elastic element is also called a passive element (PE) and generates a 'passive force' ( $F^{PE}$ ). For the muscle, both PE and CE contribute to the muscle force ( $F^M$ ). The force  $F^{CE}$  depends in the muscle fiber length  $L^M$ , the contraction velocity  $v^M$ , and the muscle activation level  $a(t)$ .

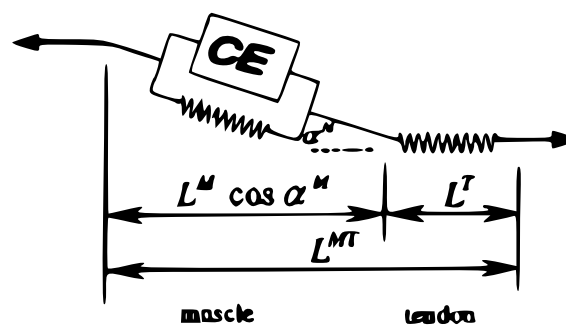


**Figure II.8** – The muscle-tendon model [51].  $L^{MT}$  - the total length of the muscle and tendon ;  $L^T$  - the length of the tendon;  $L^M$  - the length of the branch of muscle fibers;  $\alpha_M$  - the pennated angle.

### Muscle activation dynamics

The muscle activation dynamics concern about how the muscle reacts to the excitation signal sent by the central nervous system and transfers the neural exci-

tation to muscle activation. It is related to the dynamic process of calcium being released from the sarcoplasmic reticulum, diffused and bonded with the troponin. Some researchers define it as the relative amount of calcium bond to troponin [52]. With the same level of neural excitation, calcium release and diffusion would be less efficient as the amount of available calcium decreases, which is expressed as the sluggishness of muscle activation as the current activation level increases.

Given the dimensionless input  $u(t)$  (the excitation level, from 0 to 1), the muscle activation level could be modeled by a non-linear first order differential equation [51, 53]:

$$\frac{da}{dt} = \frac{u - a}{\tau_a(a, u)} \quad (\text{II.1})$$

where  $\tau_a(a, u)$  is a time constant that varies with activation level:

$$\tau_a(a, u) = \begin{cases} \tau_{act}(0.5 + 1.5a); & u > a \\ \tau_{deact}/(0.5 + 1.5a); & u \leq a \end{cases} \quad (\text{II.2})$$

where  $\tau_{act}$  is the activation time constant and  $\tau_{deact}$  is the deactivation time constant. Typical values for  $\tau_{act}$  and  $\tau_{deact}$  time constants are 10 ms and 40 ms, respectively.

The full activation (i.e.,  $a(t) = 1$ ) occurs when the muscle has been maximally excited (i.e.,  $u(t) = 1$ ) for a long time. Conversely, the muscle which has not been excited for a long time is inactivated (i.e.,  $u(t) = a(t) = 0$ ).

### Musculo-tendon contraction dynamics

Musculo-tendon contraction dynamics coorespond to the transformation of muscle activation to force generation, which depend on the activation-force-length-velocity properties of muscle and the elastic properties of tendon.

When the muscle is in steady state (in comparison with the state of being shortening or lengthening) , the isometric force is developed. The developed force depends on the muscle's force - length property and activation level. At stated above, both the CE and the PE contributes to the developed muscle force. The active force is generated when muscle length is between  $0.5L_0^M$  and  $1.5L_0^M$ . The  $L_0^M$  is called the optimal muscle fiber length, the length at which  $F^{CE}$  peaks and from which  $F^{PE}$  develops. A Gaussian curve could be used to describe the  $F^{CE} - L$



relationship of muscles. The active force is scaled by the activation level, and the passive force is assumed to be independent with it, as shown in Figure II.9.

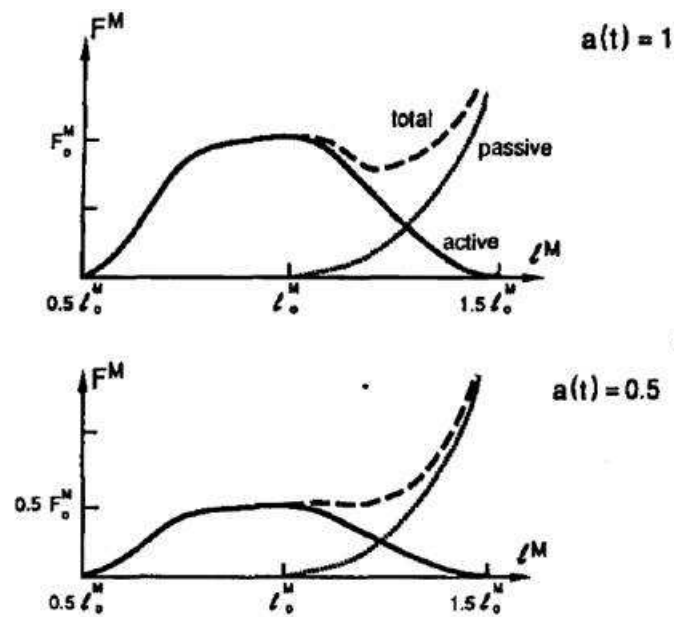


**Figure II.9** – The muscle force-length relation.

When a muscle is subjected to a constant external force, it shortens and then terminates at a length at which the external force can be held steadily (specified by the muscle force-length relation). Given the length trajectories and external forces, the empirical muscle force - contraction velocity relation could be constructed for any muscle length between  $0.5L_0^M$  and  $1.5L_0^M$ . The  $F - v$  relation curve at the optimal muscle length  $L_0^M$  is shown in Figure II.10. At the optimal muscle length  $L_0^M$ , a maximal shortening velocity  $v_m$  is defined, at which the muscle cannot sustain any force, whatever the activation level is.

Tendon force was assumed to increase exponentially with strain during an initial toe region, and linearly with strain thereafter, shown in Figure II.11. The tendon strain at maximum isometric force is defined as parameter  $\varepsilon_0^T$ .

### **The properties and parameters to simulate the dynamics of a specific muscle-tendon unit**

As discussed above, to formulate a muscle-tendon contraction model, the following properties are in need:

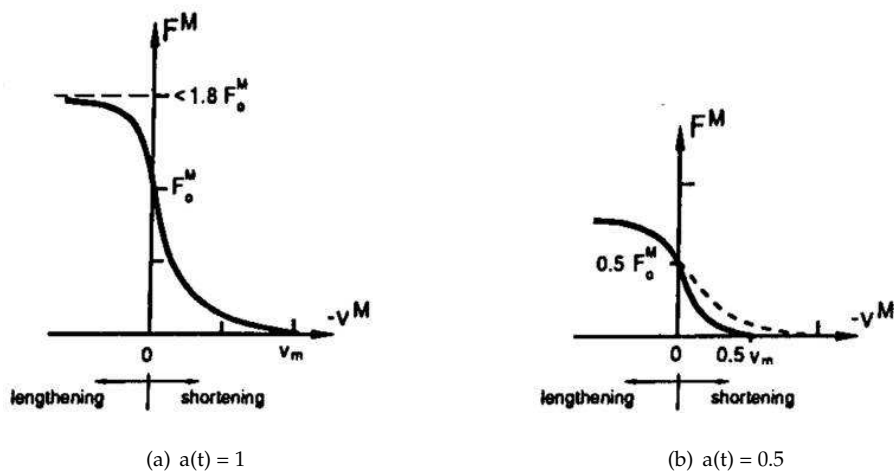


Figure II.10 – The muscle force-velocity relation at length  $L_0^M$

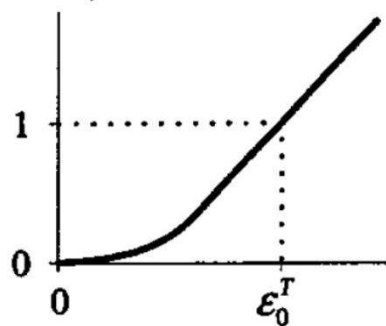


Figure II.11 – The normalized tendon force - tendon strain relation.

- A dimensionless force-length curve of PE;
- A dimensionless force-length curve of CE;
- A dimensionless force-velocity curve;
- A dimensionless activation dynamics equation.

And the parameters needed to specify a muscle-tendon unit are:

- Peak isometric active force  $F_0^M$ ;
- Optimal muscle fiber force  $L_0^M$ ;
- Optimal muscle pennation angle  $\alpha_0$ ;
- Maximal shortening velocity  $v_m$ ;
- The tendon strain at maximal isometric force  $\epsilon_0^T$ .

With proper definition of the above properties and specification of the parameters, it is achievable to simulate the muscle-tendon dynamics. Hence the understanding about work load onto specific muscles is expectable. Nowadays this work has been realized with the help of digital human modeling techniques, which is about to be introduced in Section II.7.

#### **II.4.4 Summary**

In this section, the ergonomic methods as well as the biomechanical methods to measure the work load on human body are reviewed and discussed, as the first step to assess the physical risks of MSDs comprehensively. The measurement of joint moments and estimation of muscle forces are highlighted as the more precise and promising methods, in comparison with traditional ergonomic methods. The next section would discuss about the second step of the physical risks assessment: the accumulation effect of the measured workloads.

### **II.5 Fatigue: the accumulation effect of workloads**

The accumulation effect of workloads is mentioned as “fatigue” in this thesis. Workloads influence both the physical and psychological conditions, therefore fatigue would happen in both physics and psychologies. This thesis focuses on the physical part.

#### **II.5.1 Physical fatigue: central and peripheral**

Physical fatigue is supposed to manifest as the decline of physical performance. In the whole human physical motion system, skeletal muscle is the only component that can be controlled voluntarily by the nervous system. Therefore it would not be too assertive to consider muscle fatigue as the representation of physical fatigue.

Muscle fatigue is referred as the decline of muscular ability of using biological energy to generate force or power. It was defined as ‘any reduction in the ability to exert force in response to voluntary effort’ ([44], p43). This reduction can be caused by failures at one or more sites along the path from central nervous system to contractile apparatus. For example, it is generally agreed that biochem-

ical changes that happened within muscle fibers, such as the lactate concentration, the breakdown of the phosphagens and glycogen are related with force loss [54, 55]. Also, considerable researches report declines in surface electromyogram (EMG) activity during voluntary fatiguing contractions [56, 57, 58], which suggests that inadequate neuromuscular activation resulted from either a decline of central nerve system motivation or a failure of peripheral electrical transmission, is also related with force loss.

### II.5.2 Determination of muscle fatigue

For ergonomic researchers and practitioners, it is often desirable to have means for muscle fatigue measurement. In ergonomics, fatigue is usually measured in three means: the reduction of maximal voluntary contraction (MVC), the self-rating discomfort, as well as the surface myoelectric activity change. Self-rating discomfort was reported to be a valid estimator [59], but its usage is limited by the subjectivity. Here we overview the other two measures.

#### The decline of maximal voluntary contraction

It is the most commonly used fatigue measure in ergonomic fatigue-related researches. The MVC is defined as the capacity to produce torque or force by a maximal voluntary isometric muscular exertion [60]. Table II.4 summarizes the traits of protocols used to measure the MVC in previous studies.

As summarized in Table II.4, the MVC is mostly measured as the largest value during a static contraction or across several contractions. A contraction usually lasts for 2 to 6 seconds. The subject was simply asked to exert his maximal force, or to exert his maximal force as rapid as possible. The largest output force is taken as the MVC value in all these protocols.

As far as the definition of muscle fatigue, the decline of MVC would be its most validate measure. The only problem of this measure is that it requires interruptions of the tasks or experiments. Besides, in some situations we need to determine the fatigue level in the middle of a fatiguing process, then the measurement of MVC would bring about extra fatigue and influence the following task.

**Table II.4** – The measurement of MVC in previous researches.

First author	Muscles	No. of trials	Duration of each trial	Determination of MVC
Petrofsky [56]	Handgrip, biceps, adductor pollicis and quadriceps	3	< 3 s	The largest force of all trials
Nussbaum [61]	Torso extensor muscles	3		The largest torque of all trials
Iridiastadi [62]	Upper arm muscles	4 to 5	6 s	The largest force of all
Nussbaum [63]	Shoulder and arm muscles		5 s.	Follow a ramp-up, hold, and ramp-down process. The largest force of all trials
HÄkkinen [64]	Thigh muscles		2.5 s	The subjects respond to an auditory signal by exerting their maximal force as rapidly as possible and to maintain that force.
Maïsetti [65]	The vastus medialis and vastus lateralis	2		The highest torque produced during three successive contractions
West [66]	The hand and wrist flexor muscles	3	3.5 s	The largest of the three trials
Krogh-Lund [67]	Arms	At least 3		The largest 1-s average value reached within any single force recording
Sood [68]	Shoulder muscles	Trials continued until the maximal force was lower than that exerted in a previous trial.		The largest force of all.

### Determination muscle fatigue with EMG

Surface electromyography (sEMG) uses the surface electrodes to record the myoelectric (ME) activity. The ME activity manifests the neuromuscular activation of a contracting muscle. As De Luca [69] has put it, ME signal is exceedingly complicated. It is influenced by the anatomical and physiological properties of muscles, the control scheme of the peripheral nervous system, and the characteristics of the detecting instruments. In the past half century, enormous efforts have been made to raise the level of awareness of the cause and effect of the influential factors mentioned above and EMG signal. However, to consider all these process and phenomena in a quantitative manner is still beyond our reach.

Yet the use of the EMG signal to evaluate the level of muscle fatigue is considerably appealing, in that the signal displays the in-situ, time dependent changes of muscle states [70].

Overall, sEMG signal is the synthesis of myoelectric and anatomic properties: the shape of motor unit action potential (MUAP) waveform [71], the firing rate of MUAP trains, the recruitment of new motor units [69] as well as the subcutaneous tissues which act as a volume conductor and cause a spatial low-pass filtering effect when conducting myoelectric signals [72]. In the process of fatigue, metabolites such as lactic acid concentrate, for which the muscle fibre conduction velocity (CV) decreases. The decrease of CV directly changes the shape of the MUAP waveform and leads to the compression of EMG spectrum towards its lower part [73]. As a result, more energy passes through the tissues which act as a low pass filter, and is detected by the surface electrodes, leading to an increase of sEMG amplitude.

The sEMG-based indicators of muscle fatigue that are currently used can be divided into two types: i. the decrease of frequency domain eigenvalue, such as the median power frequency (MDF); ii. the increase of time domain eigenvalue, such as the root-mean-square (RMS) [74, 75]. But it should be noted that these sEMG indicators are not always applicable. Firstly, sEMG spectral compressions which bring about the decrease of frequency domain eigenvalue are sometimes slight and insignificant statistically, especially during low force level tasks [59, 63].

As De Luca [76] puts it, the usage of spectral variables should be limited to isometric, constant-load tasks greater than 30% of maximal force. And the sEMG amplitude, which manifests by the time domain eigenvalues, is significantly affected by muscle force: greater force leads to larger amplitude [57, 77]. Therefore its usage is limited to the constant-force fatigue process. There is a demand to develop and check more fatigue-indicator based on sEMG.

### II.5.3 Biomechanical modeling of muscle fatigue

Several models have been developed to characterize the fatigue progress. They could be categorized into two groups: biochemical models and mechanical models.

Biochemical models are based on physiological or chemical mechanisms that happened within muscles during force-generation procedures. Such as the  $Ca^{2+}$  cross-bridge model [78] which is based on the cross-bridge mechanism that happened within muscle fiber; the force-pH model [79], which is based on the pH value variation during muscle activation, fatigue and recovery. These models involve many physiological variables. For example, by the  $Ca^{2+}$  cross-bridge model, there are more than 20 variables to describe the muscle fatigue mechanism only for quadriceps, which makes it impractical for ergonomic use.

Mechanical model is based on the mechanical properties of muscle groups. For example, the half-joint endurance model [80] is used to calculate the fatigue at joint level. Fatigue level is expressed as the actual holding time normalized by maximum holding time of the half-joint; the motor units pattern model [81], in which three phenomenological parameters are introduced to describe the activation, fatigue and recovery process.

#### Force-load fatigue model

Specifically, Ma et al. [82] proposed a 'Force-load fatigue model' based on mechanical parameters. According to this model, during a fatiguing process, muscle strength changes depend on 1. Muscle capacity, calculated by maximal voluntary muscle strength; 2. External load; 3. Intrinsic muscle fatigability. The model was described as a differential function, as shown by Equation II.3. Basically, the de-

crease rate of the current exertable muscle force ( $dF_{cem}(t)/dt$ ) is associated with the current exertable muscle force ( $F_{cem}(t)$ ), the percentage of current workload ( $F_{load}(t)/MVC$ ). The ratio  $k$  reflects the subject's sensitivity to fatigue. Explanations of the parameters are shown in Table II.5 [83].

$$\frac{dF_{cem}(t)}{dt} = -k \frac{F_{cem}(t)}{MVC} F_{load}(t) \quad (\text{II.3})$$

In the ergonomic studies of muscle fatigue, the Maximum endurance time (MET)

Item	Unit	Description
MVC	N	Maximum voluntary contraction, maximum capacity of muscle
$F_{cem}(t)$	N	Current exertable maximum force, current capacity of muscle
$F_{load}(t)$	N	External load of muscle, the force which the muscle needs to generate
$k$	$\text{min}^{-1}$	Intrinsic value, fatigability
$f_{MVC}$		$f_{load}/MVC$ (in static cases)

**Table II.5** – Parameters of the Force-load fatigue model.

is always mentioned. It denotes the duration in which the muscle force ability ( $F_{cem}$ ) declines down to the current external muscle load ( $F_{load}$ ) (Figure II.12). Enormous ergonomists have come up with different MET prediction models empirically, such as the most well-known Rohmert's MET curve [84]. In static case where  $F_{load}(t)$  is constant, a general MET model can be deprived from the Load-force fatigue model, as shown by Equation II.4.

$$MET = -\frac{\ln(f_{mvc})}{k f_{mvc}} \quad (\text{II.4})$$

In this MET model, there is only one variable parameter ( $k$ ). This parameter quantifies the muscle's tendency of force decline in the fatiguing process. It is defined as the fatigability. This parameter explains the difference found in previous empirical MET models [83]. More related studies are reviewed in Section II.6.

#### Further development of the Force-load fatigue model

The original Force-load fatigue model is mainly used for single muscles in static cases. Some researchers have developed it further for dynamic cases with multi-muscles and joints. Ma et al. [83, 85] introduced the effect of joint angle, speed,



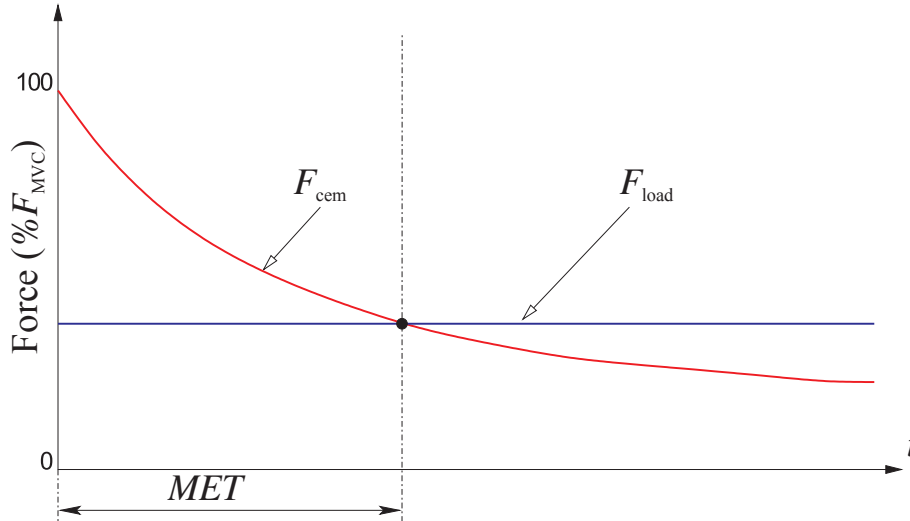


Figure II.12 – MET diagram

and acceleration as well as that of the inertia of body parts, by which the dynamic fatigue process at joint level is modeled. The proposed model is shown in Equation II.5. Parameters are explained in Table II.6.

$$\frac{d\Gamma_{cem}(t)}{dt} = -k \frac{\Gamma_{cem}(t)}{\Gamma_{MVC}} \Gamma_{load}(t) \quad (\text{II.5})$$

The joint load ( $\Gamma_{load}(t)$ ) could be modeled by a variable depending on the angle, the velocity, the acceleration and the external load (see Equation II.6).

$$\Gamma_{load}(t) = \Gamma(t, \theta, \dot{\theta}, \ddot{\theta}) \quad (\text{II.6})$$

Seth et al., (2016) [86] included considerations about the co-contraction effect into the dynamic joint fatigue model. The co-contraction happens when both the agonist and antagonist muscle around a joint contract simultaneously in a movement. For example, in a arm push-pull movement, the biceps and the triceps work as the agonist and antagonist muscles respectively. EMG measurement shows that in a push-pull cycle, there is a certain period that both the two muscles contract with contrary functions (see Figure II.13).

The extended model include a co-contraction factor  $n$  (see Equation II.7). The value of  $n$  was determined by the relative EMG activities of the agonist and antagonist muscles. Experiment showed that the co-contraction factor of the elbow flexion muscle group was between 0.5 and 0.7 [86].

$$\frac{d\Gamma_{cem}(t)}{dt} = -k \cdot n \cdot \frac{\Gamma_{cem}(t)}{\Gamma_{MVC}} \Gamma_{load}(t) \quad (\text{II.7})$$

Item	Unit	Description
$\Gamma_{MVC}$	N.m	Maximum voluntary contraction of joint torque
$\Gamma_{cem}(t)$	N.m	Current exertable maximum joint torque
$\Gamma_{joint}(t)$	N.m	External load of muscle, the torque which the joint needs to generate
k	$\text{min}^{-1}$	Intrinsic value, fatigability
$\tau_{MVC}$		$\tau_{MVC} = \Gamma_{joint}^{max} / \Gamma_{MVC}$
$\theta$	rad	Joint angle
$\dot{\theta}$	$\text{rad.s}^{-1}$	Joint speed
$\ddot{\theta}$	$\text{rad.s}^{-2}$	Joint acceleration

**Table II.6** – Parameters of the dynamic Force-load joint fatigue model.

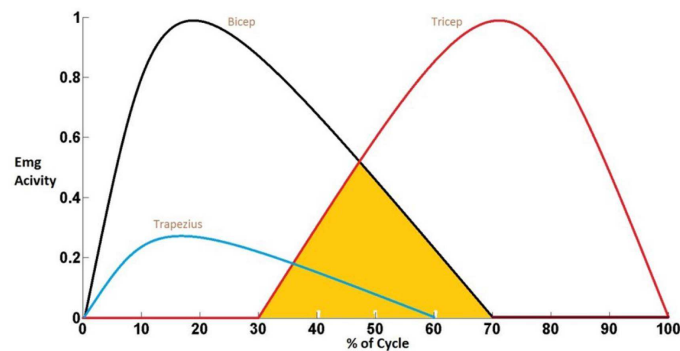


**Figure II.13** – An EMG activity plot of bicep, triceps and trapezius in a push-pull cycle. [86]

## II.6 Muscle fatigability

By now we have reviewed the evaluation of both workload and its accumulation effect regarding the physical risk assessment of MSDs. As pointed out in Section II.2, the third primary question in this area is the evaluation of fatigue-related individual factors, which will be discussed in this section.

### II.6.1 Definition of muscle fatigability

The fatigue-related individual factors include the fatigue rate and recovery rate. They are inherent and determined by intrinsic physical characteristics and may be differentiated from person to person. The fatigue rate, or the fatigability, is defined as below [87]:

"Muscle fatigability describes a tendency of a muscle from a given subject to get tired or exhausted, and it should only be determined by the physical and psychological properties of the individual subject."

Ideally, fatigability has the following features:

- The fatigability is a term describing the intrinsic physical capacity to resist fatigue;
- The fatigability is determined by individual internal factors, such as muscle composition, neuromuscular activation pattern, etc.;
- The fatigability of a muscle should have a weak dependency on external factors;
- The fatigability should keep stable for a given subject for a certain period.

Fatigability takes a significant proportion in the development of muscle fatigue. A study shows that in a dynamic elbow flexor operation, time to failure was about 40% prolonged for women than men ( $9.7 \pm 5.5$  vs.  $6.1 \pm 2.1$  min, respectively;  $p = 0.02$ ) [88]. According to Kent-Braun et al. [89], the older group shows significantly much less force loss than the younger group after a series of exercises (post exercise MVC / pre exercise MVC: 0.84 vs. 0.73 respectively;  $p < 0.01$ ). The difference may lie in the variation of the fatigue mechanisms with age and

gender. Therefore, it would be favorable to consider the variation of fatigability when predicting muscle fatigue.

Anthropometric data is essential in ergonomic practice [44]. For example, to design a work space, we will refer to the percentile length of body parts in order to predict the worker's spatial reach. Similarly, the involvement of the percentile fatigability would benefit the prediction of work-related muscle fatigue to a large extent. This should be based on the proper measurement of fatigability.

### II.6.2 Measurement of muscle fatigability

In previous researches, the subject's fatigability has been indicated by the MET under a certain level of workload [88], and the decline rate of MVC after a certain period of time [89]. The two methods generate relative references to the subject's fatigability, which vary with the external workloads.

The Force-load muscle fatigue model that introduced in Section II.5 involves a parameter  $k$ , which quantifies the force decline tendency of the muscle strength. It is an absolute value, detached with both external workload and current force-output ability. Therefore, the measurement results of  $k$  could be applied uniformly to other cases.

#### Determining fatigability from MET models

For several decades, muscle fatigue has always been studied with the empirical MET models of joints. These MET models predict the time for a muscle group to get exhausted under a certain workload. The most famous MET model is Rohmert's curve [84], based on which numerous MET has been developed. These models are very useful in determining work-rest allowances.

As discussed in Section II.5, during static tasks when the external load is constant, a general MET model (Equation II.5) could be derived from the Force-load fatigue model. The derived MET model has high linear relationships with almost all the static empirical MET models ( $r > 0.95$ ) [83].

A method is developed to determine the fatigability of each empirical MET equation [83]. Here the  $k$  is determined by minimizing the summarized linear

Segment	$k_1$	$k_2$	$k_3$	$k_4$	$k_5$	$k_6$	Mean	SD
General	1.201	1.051	1.463	1.247	0.872	2.152	1.331	0.409
Shoulder	2.340	2.340	1.433	0.718			1.708	0.681
Elbow	0.877	0.901	0.743	3.519	1.313	1.911	1.544	0.965
Hip	0.626	1.428	0.628	0.309	0.737	0.300	0.671	0.376

**Table II.7** – Fatigability values determined from different MET models [83].

difference between the empirical MET model and the model-derived MET model. The determined fatigability values are shown in Table II.7.

Table II.7 shows that fatigability varies from joint to joint. This could be explained by the variation of proportions taken by Type I and Type II muscle fibers in different muscle groups. Hip joints are more fatigue-resistant than the shoulder and the elbow.

### Determining fatigability by experiments

There are two experimental methods to measure the fatigability based on the Force-load fatigue model. One includes static submaximal contraction operations and the other includes a static maximal voluntary contraction task.

#### In submaximal contraction condition

This experiment is conducted by Ma et al., [90]. Considering the Force-load fatigue model, in a static operation in which workload ( $F_{load}$ ) keeps constant, the reduction of the muscular strength can be predicted by Equation II.8. This equation describes the muscle fatigue progression in the form of an exponential function. The relative workload  $f_{MVC}$  is determined by the task design, and it can be calculated via force analysis. MVC and  $F_{cem}$  could be measured. Therefore, fatigability  $k$  can be determined by linear regression.

$$\frac{\ln(F_{cem}(t_i)/MVC)}{f_{MVC}} = -kt_i \quad (\text{II.8})$$

A typical overhead drilling operation under laboratory conditions was used to measure muscle fatigue progression at shoulder joint level. There were nine fatiguing sessions during each of which subjects were asked to hold the constant external load (about 33% MVC ). After each session, the muscle strength time

$F_{cem}(t_i)$  was measured by asking the subject to exert maximal voluntary strength with a peak force for 3 to 5 s. Muscle fatigue progression of each subject was fitted with Equation II.8. Thirty-five out of 40 subjects had a high coefficient of determination over 0.8 in joint moment regression. Determined fatigability  $k$  is  $1.02 \pm 0.49$ .

#### **In maximal contraction condition**

If the task is conducted under sustained maximal voluntary contraction (sMVC) condition, an operator would try to maintain the maximum voluntary contraction in his/her best. Under this condition,  $F_{load}(t)$  always equals to  $F_{cem}(t)$  theoretically. Therefore, the force decline under sMVC could be derived as Equation II.9. By measuring the force decline process ( $F_{cem}(t)$ ), parameter  $k$  can be determined with curve fit.

$$F_{cem}(t) = \frac{MVC}{kt + 1} \quad (\text{II.9})$$

## **II.7 Digital human modeling in MSDs physical risk assessment**

### **II.7.1 The development of digital human modeling**

The field of ergonomics has been considerably developed to the point where the role of ergonomist has migrated more and more into the design process, rather than the producing or post-producing process [91]. This is largely due to the development of computed-aided ergonomics which enables computer-generated virtual environments as well as the digital human modeling. This permits analysis and calculation of ergonomical issues before physical implementations. The adoption of the digital human modeling is getting prevalent in the field of military as well as the manufacturing industries such as the automotive, clothing, and aviation sectors [91].

Digital human modeling (DHM) is a digital representation of the human that could be inserted into a virtual environment to facilitate prediction of safety and performance. The development of the DHM would date back to the later 1960s, when Ryan and Springer at Boeing Aircraft developed a digital human model that could be used to assess pilot reach requirements for people of varied anthropometry [92]. In 1970, Chaffin, Kilpatrick, and Hancock developed a seated model for

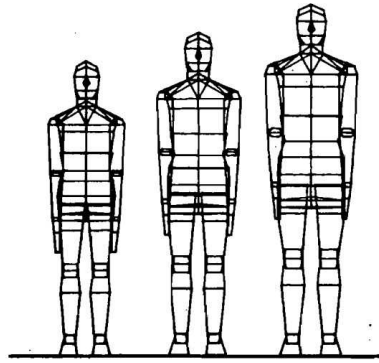


**Figure II.14** – The variable anthropometry man model in SAMMIE.

manual work design which demonstrated a 3D graphical mannequin that enables inverse kinematics for postures and reach zone predictions [93]. At the same time, in Europe, the System for Aiding Man-Machine Interaction Evaluation (SAMMIE) was developed [94]. Digital human model in this system is composed of 3D polygons. The 5th, 50th, and 95th percentile male model was available (see Figure II.14) [95]. The system was reported to be applicable especially to the evaluation of workplace geometry and vision assessments in materials handling.

In later 1970s and 1980s, the 3D Static Strength Prediction Program (3DSSPP) was developed which included a 3D mannequin that could be adjusted anthropometrically according to subject population. Then the workspace and task information was integrated to perform more ergonomic assessments [96].

In 1980s, in France, the ERGOMAN was created by the Laboratoire d'Anthropologie Appliquée et d'École Humaine in Paris. The model is based on a 20-links architecture with 22 joints and 46 degrees of freedom. Model dimensions were calculated from a set of 22 anthropometric measurements. The model runs with a EUCLID-IS CAD software, as shown in Figure II.15. The application was used to analyze the operators' working posture, reach capability, the minimal activity volume, visibility, and workspace control layouts [97].

In the later 1980s and 1990s, the mannequin JACK was created [98]. The main application of JACK is animation and visualization in vehicle design and architecture. The model consists of 39 body elements; visualization takes place using area segment imagery with textures. The anthropometric database is derived mainly

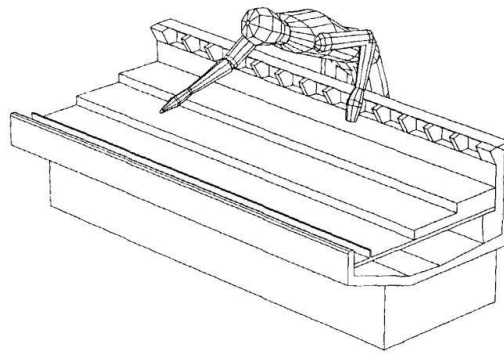


**Figure II.15** – The reach capability analysis with ERGOMAN.

from the Human Solutions Library and NASA data. JACK has been widely used in aerospace and automotive as well as manufacturing companies such as the British Aerospace, Volvo, Caterpillar and John Deere [99].

During the 1980s, the computer man model SAFEWORK was developed at the Ecole Polytechnique in Montreal. It covers three modules: anthropometry, movement, and analysis. The posture and movement simulation enables the movement of short chains in the model's arms, legs, and torso by means of inverse kinematics. Vision simulation, fixed accessibility areas, a joint-dependent comfort evaluation, maximum force calculation, and a center of gravity analysis are available as analysis tools. SAFEWORK is available solely in the form of an integration unit with CATIA by Dassault Systems.

From the 1990s, the field of digital human modeling entered into a stage of rapid development. Numerous tools has been developed with different emphases. One of them is the RAMSIS (Realistic Anthropological Mathematical System for Interior Comfort Simulation), which was rated as 'the most extensive industrial project ever done for the development of a mannequin' [99]. It was developed to facilitate the design of ergonomic interiors of vehicles for the German automotive industry. The anthropometric data could be generated from the body measurement relationships, desired percentile as well as from an international anthropometric database. Posture and movement prediction is available. Additionally, there are more than 80 functions for the ergonomic analysis of vehicles and vehicle interiors, such as the vision and mirror simulation, seat simulation, accessi-



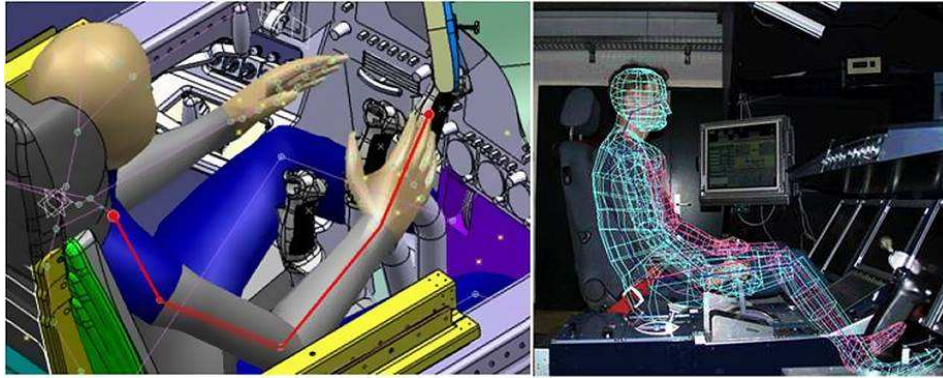


**Figure II.16** – The application examples of the RAMSIS.



**Figure II.17** – Graphical rendering of digital human models in 3Dexperience

bility limits, comfort, belt analyses, etc.(see Figure II.16). The system is available as a stand-alone version for UNIX and Windows, as a CAD integration unit with CATIA, and as a programming library for independent applications.

In 3Dexperience, the graphical rendering of digital human models has improved but their features remain limited (Figure II.17). It is mainly an evolution of V5 CATIA/DELMIA with new anthropometric databases.

### **II.7.2 Digital human modeling in Ergonomics**

Digital human modeling is a powerful tool to augment ergonomic practice. Benefits come in several ways. For example, it permits the designers to check the visual accessibility of the workers before the workbench is fixed. Figure II.18 shows the visual zone prediction of drivers in a certain configuration, presented in the software Delmia.

The second important application of DHM is to predict operation postures and

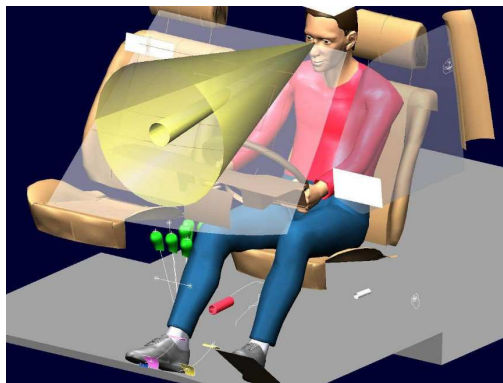


**Figure II.18** – The prediction of operator’s visual accessibility in Delmia.

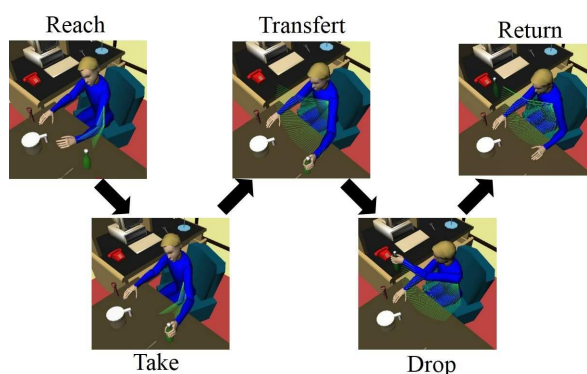


**Figure II.19** – The prediction of the operation path of an object-moving task.

paths. This is always based on the DHM integrated with the simulation of working environments. Figure II.19 shows an example of the path prediction of an object-moving operation. This operation path prediction enables the ergonomists to check the operator’s reach zone as well as the possible collisions with tools or environment, which facilitates work design. The prediction of operation posture makes it promising to optimize the working posture from the aspect of reducing work loads.

The concern about work loads and physical discomfort is the other main theme of the DHM. Traditionally, the digital mannequin is viewed as a rigid-body manipulator with multiple degree of freedoms. By applying the mechanical kinematic and dynamic analysis, it is possible to have a view about the joint configurations and joint loads. Figure II.20 shows an example of joint load estimation with the 3DSSPP. Physical risk evaluation is given from the view of populational joint capacity data. Nowadays with the development of biomechanics, the digital

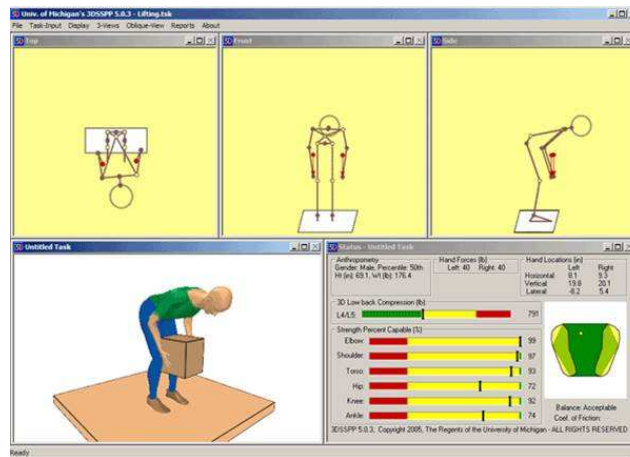


Figure II.20 – The joint load estimation and evaluation in 3DSSPP.

model is not only constraint with rigid-body constitution, but involves more and more the physiological attributes. Musculoskeletal model is replacing the traditional rigid-body model. More development in this area is reviewed in the next section.

### II.7.3 Biomechanical digital human modeling

Biomechanical digital human modeling is an unified field of computational mechanics, biomechanics, and ergonomics. The leading platforms in this area are Anybody [100, 101] and OpenSim [102].

The human body is modeled by an mechanism of rigid segments connected by joints and actuated by muscles, known as a musculoskeletal model (see Figure II.21). The musculoskeletal models differ from the traditional rigid-body model not primarily in the appearance, but in the modeling of muscles. In both Anybody and OpenSim, the muscle actuators are based on the Hill-Type model (see section II.4 for details about a Hill-type muscle). Advantages of the musculoskeletal models lie in their great potential in muscle force estimation, for which the extension algorithm of inverse dynamics is expected.

When the motion kinematics and external forces are already known, the inverse dynamics can be applied to compute the internal forces. This procedure could be simply to solve linear equilibrium equations when the 'internal forces' are merely joint moments. For the computing individual muscle forces, the redundancy problem arises: no enough equilibrium equations are available to de-



Figure II.21 – A musculoskeletal model in Anybody.

termine all the muscle forces, for we have more muscles than necessary to drive most motions. The idea is to construct algorithms which simulate the choose of central nervous system from the infinite possible sets of muscle forces. Since human is able to repeat motions very preciously, it is believed that the control strategy of muscle activation has some rational criterion.

It is usually assumed that the control strategy is an optimal strategy. Therefore the uniform mathematical description of the extension algorithm is to minimize an objective function while the cooperation of muscle forces subject to the given joint moments and reaction forces.

**Minimize**  $G(F_M)$

**when**  $F$

**subject to**  $CF = F_{External}$

where  $G$  is the objective function of the muscle activation strategy  $F_M$ , and  $F = [F_M^T F_R^T]^T$  ( $F_M$  muscle forces, and  $F_R$  joint moments).

Between the two mainstream platform, the OpenSim is freely available for modeling and simulation of movement. Details about it is reviewed in the next section.

#### II.7.4 OpenSim

As mentioned above, OpenSim is a digital human modeling platform. It allows users to build and analyze different musculoskeletal models. A model consists of a set of rigid segments connected by joints. Muscles and ligaments span the

joints, develop force, and generate movements of the joints. After the build-up of a musculoskeletal model, OpenSim takes experimentally-measured kinematics, reaction forces and moments as input data. This is usually obtained by motion capture system from a subject. The experimental kinematics (*i.e.*, trajectories of markers, joint centers, and joint angles) are used to adjust and scale the musculoskeletal model to match the dimensions of the subject [103].

For dynamic simulation, an inverse kinematics problem is solved to find the model joint angles that best reproduce the experimental kinematics. Then a residual reduction algorithm is used to adjust the kinematics so that they are more dynamically consistent with the experimental reaction forces and moments. Finally, a computed muscle control algorithm is used to find a set of muscle excitations and distribute forces across synergistic muscles to generate a forward dynamic simulation that closely tracks the motion [103]. In this way, the workload of each muscle is accessible along an arbitrary motion, which would pave way for the fatigue analysis.

Muscle contraction dynamics deals with the force-length-velocity relationships and the elastic properties of muscles and tendons. In OpenSim, it is modeled by a lumped-parameter model [103]:

$$\frac{dl_m}{dt} = f_v^{-1}(l_m, l_{mt}, a) \quad (\text{II.10})$$

where  $l_m$  is the muscle length,  $l_{mt}$  is the muscle-tendon actuator length, and  $f_v$  is the force velocity relation for muscle.

The main functions of virtual human simulation tools are posture analysis and posture prediction. Posture analysis techniques have been used in fields of automotive, military, and aerospace. These human modeling tools rely mainly on visualization to provide information about body posture, reach ability and field of view [104]. These tools are capable of determining the workspace of virtual human [105], assessing the visibility and accessibility of an operation [106], evaluating postures [107].

Although the joint reaction force and muscle load are accessible in OpenSim and Anybody, the accumulation effect has not been taken into account; and no accurate fatigue analysis is available. In Table II.8, we can compare the differ-

Table II.8 – DHM software

	Jack	CATIA/Delmia	3DSSPP	Anybody	OpenSim
Model constitution	Rigid body	Rigid body	Rigid body	Bone & muscle	Bone & muscle
Model anthropometric data	Database	Database	Database	Subject-specific	Subject-specific
Complex motion	X	X	X	V	V
Joint load	V	V	V	V	V
Muscle load	X	X	X	V	V
Muscle model analysis	V	X	X	X	X

ent software present according to five properties: Model constitution, model anthropometric data, complex motion, joint load, muscle load and muscle model analysis. In the next chapter we will choose the OpenSim software because it is possible to add plugins by programming and that all other criteria are validated. In addition, it can be easily connected to a motion capture system.

## II.8 General summary

Musculoskeletal disorders have prevailed and brought about great loss to industries and the society. The risk assessment of the physical contributing factors will benefit work design and worker protections. Traditional physical risk assessment methods includes the posture-based observational methods and the self-report methods, which are criticized by either a lack of accuracy or the interference of the worker's physiological condition. There is a necessity to improve the risk assessment method, for which three primary problems is supposed to be tend to: the measurement of work load, the prediction and indication of muscle fatigue, and the quantification of individual factors.

For the measurement of workloads, the measurement of joint moments and estimation of individual muscle forces are highlighted as the more precise and promising methods, in comparison with traditional ergonomic methods. As the accumulation effect of physical workloads, muscle fatigue can be predicted by applying the Force-load muscle fatigue model and indicated by the surface EMG. The fatigue-related individual factors, defined as the muscle fatigability, can be determined from either the previous empirical MET model or by experiments. Both of the two determination methods are based on the Force-load muscle fatigue model. The involvement of the percentile fatigability would benefit the prediction of work-related muscle fatigue to a large extent.

The digital human modeling technique has a history of more than 50 years. It facilitates the ergonomic considerations in the early stage of work design. Benefits include the check of visual accessibility, the prediction of operation postures and working paths, as well as the evaluation of physical work loads. The biomechanical digital human modeling technique is equipped with musculoskeletal human model. Compared with the traditional ones, it excels in the ability of estimating the muscle activation statuses and forces. The biomechanical DHM is promising to benefit for the development of physical risk assessment methods of MSDs.

In accordance with the above reviews, for those who pursue to improve the MSDs physical risk assessment, prior efforts should be made to integrate the

biomechanical muscle fatigue model into the biomechanical DHM to enable fatigue prediction. In this thesis, efforts are also made to develop the surface EMG indicators of muscle fatigue, which could be an objective index for appraising the developed fatigue predicting tool.





# III

---

## The Indication of Muscle Fatigue with Surface EMG

### III.1 Abstract

The thesis works on the improvement of physical risk assessment of MSDs, for which main efforts will be made to enable muscle fatigue prediction in the biomechanical DHM. But apart from prior prediction, we need also the posterior indication for muscle fatigue, for which the surface EMG is one of the main choices.

The compression of EMG spectrum and increase of the EMG amplitude are most commonly used to indicate muscle fatigue. But both of the two indicators have their limitation. In this chapter, a new indicator is proposed based on the EMG root-mean-square value. The new indicator targets at excluding the influences of muscle output force, and is supposed to be applicable for process involving inconstant muscle loads. The indicator is tested in an maximal static voluntary contraction session. Data from 15 subjects shows that the proposed indicator increase with the intensity of fatigue. It is concluded that the proposed indicator could be used to indicate muscle fatigue as a supplement of the traditional ones. The main limitation of this indicator would be the multi-step procedure demanded for its determination.

### III.2 Introduction

This chapter focuses on the indication of muscle fatigue. In ergonomics, muscle fatigue is usually indicated from three aspects: the reduction of force output capability, the self-rating discomfort, as well as the myoelectric activity change. The reduction of force output capability has been well modeled [82], and been used to describe fatigue and calculate fatigue resistance [83, 90]; the self-rating discomfort was reported to be a valid estimator but its usage might be limited due to the subjectivity. The myoelectric activity monitored by surface EMG (sEMG) shows the in situ and real-time changes of the muscles [70]. Therefore, it has been frequently used to determine fatigue [76].

Overall, sEMG signal is the synthesis of myoelectric and anatomic properties: the shape of motor unit action potential (MUAP) waveform [71], the firing rate of MUAP trains, the recruitment of new motor units [69] as well as the subcutaneous tissues which act as a volume conductor and cause a spatial low-pass filtering effect when conducting myoelectric signals [72]. In the process of fatigue, metabolites such as lactic acid concentrate, for which the muscle fiber conduction velocity (CV) decreases. The decrease of CV directly changes the shape of the MUAP waveform and leads to the compression of EMG spectrum towards its lower part [73]. As a result, more energy passes through the tissues which act as a low pass filter, and is detected by the surface electrodes, leading to an increase of sEMG amplitude.

The changes of sEMG characteristic values, such as decrease of the median power frequency (MDF) and increase of the root-mean-square (RMS), are very often used to estimate fatigue [62, 74, 75]. But it should be noted that these sEMG indicators are not always applicable. Firstly, sEMG spectral compressions are sometimes slight and insignificant statistically, especially during low force level tasks [59, 63]. As De Luca [76] puts it, the usage of spectral variables should be limited to isometric, constant-load tasks greater than 30% maximal force. In addition, the sEMG amplitude is significantly affected by muscle force: greater force leads to

larger amplitude [57, 77]. It seems the RMS should only be used in constant-force fatigue process.

However, the tasks that are cared most are dynamic, inconstant-force ones. These tasks are characterized by time-varying changes in forces exerted variations as well as in working postures [62]. Both of the two factors lead to EMG changes despite of fatigue.

To indicate fatigue with sEMG in real operations, it is logistic to start from tasks with fixed posture and inconstant force, such as sustained static maximal exertions. Voluntary sustained static maximal exertions, or sustained maximum voluntary contractions (sMVC), are characterized by rapid muscle fatigue and continuous force decline [108]. In this process, the impact of intensifying fatigue on sEMG amplitude is overwhelmed by the impact of decreasing muscle force. As a result, the RMS turns to decline along with fatiguing progress [109].

### III.3 Methods

#### III.3.1 Subjects

A number of 15 subjects (7 males, 8 females) took part in the experiment. They were healthy, aged between 20 and 35 and free from any upper limb pain during the previous 12 months. All of them are right-handed. Other criteria include moderate (non-extreme) level of self-reported daily physical activity. After being fully informed of the nature of the experiment, they signed an informed consent. Anthropometry data were measured upon their arrival at the laboratory.

Characteristic	Mean	SD
Age (year)	28.3	4.7
Height (cm)	167.1	9.1
Weight (kg)	67.1	14.0
BMI	23.8	3.5
Maximum Voluntary Contraction (N)	137.8	47.8

**Table III.1** – The physical characteristics of subjects in the EMG experiment.

#### III.3.2 Experiment protocol

Before experiment, subjects were trained to sustain sub-maximal muscle force without joint movements.

The experiment includes three sessions. First there was the initial Maximum Voluntary Contraction (iMVC) session. Subject's iMVC was obtained in the position described above. At least three short-time MVC trials (each lasting for 3s) were performed, with 10 min rest in between. The iMVC trials were continued until there were three measures whose Coefficient of Variation (CV) was less than 5%. The average value of the three measures was taken as iMVC.

After a recovery break of 10 minutes, there came the simple contraction sessions, where subjects perform a series of five short-time sub-maximal exertions, from 50% MVC to 90% MVC, in steps of 10% MVC. The sequence of the five exertions was generated by computer randomly for every subject. Each exertion

lasted for only 3s to avoid fatigue. After each exertion, at least 5 minutes rest was taken until a complete recovery was reported by the subject. In this session, the interactive monitor that displayed the real-time force was set in front of the subjects and the target force level was clearly labeled on the screen.

Finally it was the sMVC fatigue session. After a total recovery of at least 15 min, the subject was asked to exert his maximum strength to lift the lever handle of the dynamometer and to sustain the maximum effort for 60 seconds. The force decline was recorded by the dynamometer automatically. Subjects received non-threatening verbal encouragement throughout the procedure.

### III.3.3 Experiment setups

The experiment platform consisted of a dynamometer (*BET*<sup>®</sup> Primus RS), a customized chair without armrest, an electromyography recorder (TeleMyo 2400T V2<sup>®</sup>) and an interactive monitor. The muscle force and the surface EMG were recorded by the dynamometer and EMG recorder at frequency of 20 Hz and 1500 Hz respectively. Real-time muscle force was recorded by and displayed on the monitor.

In the experiment, each subject was told to be seated on the chair with torso and upper arms perpendicular to the ground. The elbow joint angle of the dominant arm was kept at 90 degree with forearm supine and horizontal. Subject's output strength was transmitted to the dynamometer by a lever that is hold in hand (see Figure III.1). Body movement was mechanically restrained by belts restraining legs, trunk and shoulder to the chair. During the whole experiment, subjects were closely monitored to maintain the posture as still as possible. In all the experiments, bar arms were used and the room temperature was maintained around 22°C by air-conditioning if necessary.

### III.3.4 Data collection

Surface EMG data was collected from the biceps brachii muscles by a pair of disposable Ag-AgCl electrodes. The electrodes were 1cm in diameter each, placed on the belly of the biceps brachii, with a 2.0 cm space in between. The skin was carefully shaved, cleared by alcohol and slightly abraded. Intra-electrodes resis-



**Figure III.1** – The sEMG-fatigue experiment posture.

tance was kept below  $10K\Omega$ . A ground electrode was placed over the end of the humerus in the elbow flexor joint.

EMG signals were recorded continuously throughout the three test sessions. Raw signals were sampled at 1500 Hz. RMS was calculated using MATLAB.

### III.3.5 Data analysis

For each 3 s exertion of the simple contraction session, the RMS was calculated from the 1 s - long EMG signals fragment in the central of the 3 s - long signals (from 1 s to 2 s), noted as  $RMS_s$ .

During the sMVC, the muscle force declines from almost 100% MVC all the way along. For each subject, the time points when the force reaches 90% MVC, 80% MVC, 70% MVC, 60% MVC and 50% MVC were determined and the nearby EMG signals (1 s - long) corresponding to these time points were selected.  $RMS_s$  were calculated from these EMG signals fragments, noted as  $RMS_f$ .

By comparing the  $RMS_f$  with  $RMS_s$ , one may figure out the EMG amplitude changes caused by fatigue, precluding the effect of muscle force. For each subject, all RMS values were normalized by the RMS of EMG signals when he or she reached the peak force during the sMVC fatigue session.

$$RMS_{fe} = RMS_f - RMS_s \quad (III.1)$$

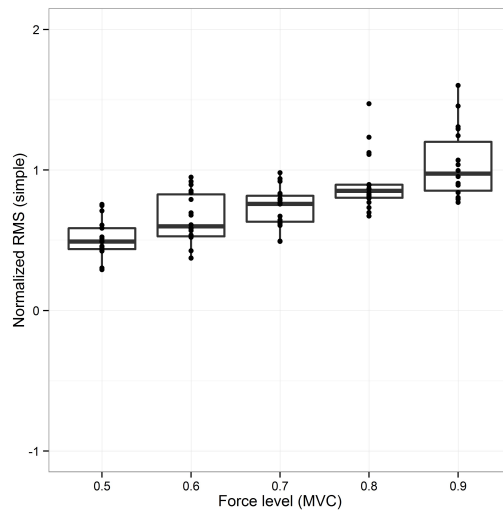


**Figure III.2** – The statistics of RMS in simple contraction test with respect to 5 muscle force levels.

	90 % MVC	80 % MVC	70 % MVC	60 % MVC	50 % MVC
$RMS_f^*$ (%)	95.38(13.55)	96.37(19.58)	89.69(18.30)	80.06(14.37)	70.19(16.90)
$RMS_{fe}^*$ (%)	0.54(11.78)	2.24 (19.18)	14.70 (16.42)	14.67(18.88)	21.27(18.66)

\* Normalized by the RMS values corresponding to maximal force.

**Table III.2** – Normalized RMS values corresponding to five force levels during sMVC session.

## III.4 Results

### III.4.1 Simple contraction session

Monotonous and significantly linear relationship (Pearson test:  $r = 0.74$ ;  $p < 0.001$ ) was found between muscle force and RMS values in the simple contraction session (shown in Figure III.2). Larger muscle force corresponds stronger EMG signals.

### III.4.2 Fatigue sessions

Under the influence of both muscle force declines and the fatigue increases, the amplitude of EMG decreases along the fatigue process. As shown in Figure III.3, from 90% MVC to 50% MVC, the  $RMS_f$  goes from 95.4% to 70.2% (normalized by RMS corresponding to maximal force).



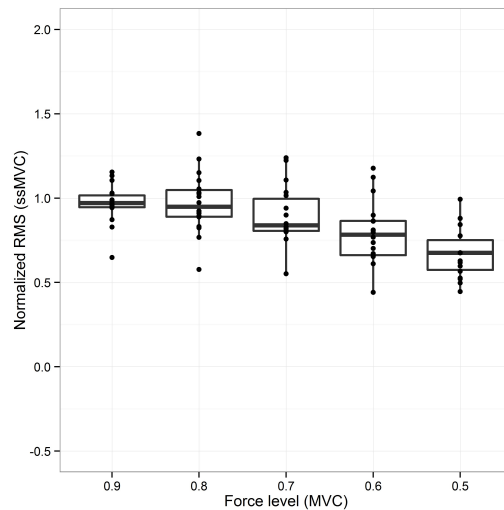


**Figure III.3** – The statistics of RMS in fatiguing test with respect to 5 muscle force levels.

### III.4.3 RMS response exclusively to fatigue

After precluding the influence of muscle force by Equation III.1, sEMG RMS response exclusively to fatigue was determined. Result shows that it increases with fatigue strengthening:  $RMS_{fe}$  goes from 0.54% up to 21.27% while muscle force reduces from 90% MVC to 50% MVC (see Table III.2). Boxplot is shown in Figure III.4.

## III.5 Discussions

### III.5.1 Force-RMS relationship in simple contraction

In this experiment, linear relationship was found between muscle forces and RMS values during the simple contraction session. This clear relationship between mechanical and the electrical responses of human muscle is well documented in previous researches [110, 111, 112] under voluntary isometric contractions. As mentioned above, the RMS value of the sEMG signals is decided by: (1). the percentage of MUAP trains wave that filtered by the tissue and reach the electrodes, designated as  $p$ ; (2). the average length of the MUAP trains, designated as  $\bar{l}$ ; (3). the firing rate of the MUAP trains, designated as  $f$ ; (4). the mean amplitude of filtered MUAP trains, designated as  $\bar{A}$ . Then RMS could be indicated by Equ-

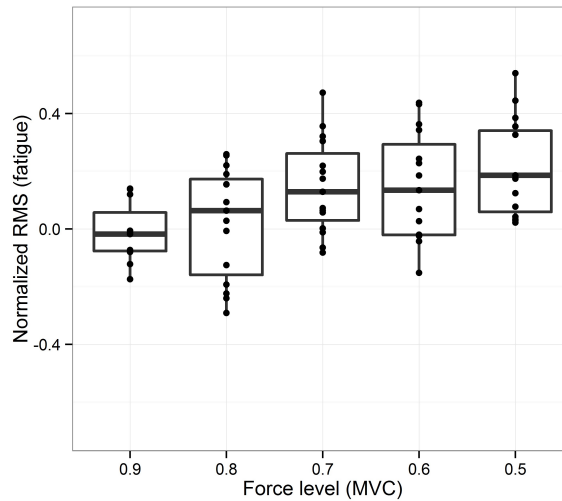


**Figure III.4** – The statistics of RMS in fatiguing test with respect to 5 muscle force levels.

tion III.2 ( $\tau_0$  is the Constant coefficient).

$$RMS = \tau_0 \cdot \bar{l} \cdot p \cdot f \cdot \bar{A} \quad (\text{III.2})$$

During the simple contractions when the muscles are fresh, the shape of MUAP waveform and the filtering threshold of the tissue remain unchanged. Therefore  $p$  is constant. With the increase of muscle force, MUs with higher firing rate of their amplitude potential trains are recruited and the firing rates of initial MUAP trains increase. These factors lead to the increases of  $\bar{A}$  and  $f$ , and furthermore an increase of total RMS.

### III.5.2 RMS during Fatigue Process

During the sMVC fatigue progress, the RMS reduces to about 70% when muscle force reaches 50% MVC. Similar results have been reported in previous researches, as listed in Table III.3. Generally, EMG amplitude reduced by 30% to 70% during a maximal voluntary contraction sustained for 60 s, depending on different muscles and protocols.

As mentioned above, the RMS of sEMG has been found to increase in the process of constant-force fatiguing tasks [56, 62, 74]. When the body tries to maintain the target forces, a progressive increase of MUAP trains firing rate take place and MUs with larger amplitude are recruited [116], which increase the  $f$  and  $\bar{A}$  in

Authors	Muscle	Indicator	Tendency	Magnitude
Stephens&Taylor [113]	First dorsal interosseous	srEMG*	Decrease	To 53% ± 7%
Bigland-Ritchie [114]	Adductor pollicis	srEMG*	Decrease	By 50% to 70%
Kent-Braun [77]	Ankle dorsiflexor	iEMG**	Decrease	To 72.6% ± 9.1%
Bigland-Ritchie [115]	Adductor pollicis	srEMG*	Decrease	About 50%

\* srEMG - Smoothed rectified EMG.

\*\* iEMG - Integreted EMG.

**Table III.3** – EMG amplitude changes during sustained maximal voluntary contraction.

Equation III.2. At the same time, the percentage of filtered MUAP trains  $p$  grows due to fatigue. As a result, the total RMS increases.

Whereas in the procedure of sustained maximal exertions, both acute muscle fatigue and rapid force decline are identified. The MUAP trains are pushed to change in two directions: on the one hand, in every moment of sMVC, the muscle is trying hard to maintain its original force, which leads to increases of  $f$  and  $\bar{A}$ ; on the other hand, as the muscle fails to maintain its original force, muscle force continue to decline, which brings about the decreases of  $f$  and  $\bar{A}$ . As a consequence, the impact of force decline prevails over that of fatigue and decreases of  $f$  and  $\bar{A}$  are observed [116]. Despite of the increase of the percentage of filtered MUAP trains  $p$ , the total RMS declines with time.

### III.5.3 EMG response exclusively to fatigue

After precluding the impact of muscle force changes, the sEMG RMS response to fatigue is found to increase from 0.54% to 21.27%, along with muscle force decreasing from 90% MVC to 50% MVC. The underlying implication is that in this process, although the firing rate of and average amplitude of MUAP trains decline significantly, increasingly extra effort is made compared with that when

the fresh muscle exerts same forces. The more severe the muscle fatigue is, the more extra effort it is needed.

It is notable from Table III.2 that no extra RMS increase is detected when force declines from 70% MVC to 60% MVC. This should be explained by the different percentage held by MU deactivation and firing rate slowing in force reduction at different force output level. As the muscle force increases, MUs are recruited in the order of their firing rate and twitch tension from low to high [69, 117] along with the average firing rate speeding up [118]. The recruitment of new MU was reported to terminate by 60% MVC [119] or 75% MVC [117] in biceps brachii. Conversely, during sMVC session, before the muscle force reaches about 70%MVC, the slowing of MU firing rate contributes the largest part to force loss. From 70% MVC to 60% MVC, the deactivation of MU takes part in. MUs with the largest twitch tension are deactivate, which makes a great contribution to force loss. Hereby, the firing rate slowing and RMS changes are not significant.

### III.6 Conclusions

In this chapter, a simple way to identify the sEMG RMS response to fatigue was tested on biceps brachii muscles during sMVC process. The impact of muscle force changes on RMS is precluded by simply subtracting the RMS of the fresh muscle when exerting corresponding force from the total RMS. Result shows that the sEMG RMS response to fatigue increases along with the fatigue process to as much as 20%, which implies that more and more extra effort is needed as muscle fatigue intensifies. It would be promising to use the RMS response exclusively to fatigue as an indicator of muscle fatigue. However, these results do not allow us to know the degree of muscle activation and it is difficult to find their two essential parameters, the MVC and the  $k$  fatigue index. This work can be used to correlate work predicting the effects of a task on muscle fatigue but does not easily characterize all the muscles of the human body. In Chapter V, we will present another method to adapt a model to the properties of a given operator.

# IV

---

## Muscle Fatigue Analysis in OpenSim

### IV.1 Introduction

As discussed in Chapter I, a comprehensive physical risk assessment of work-related MSDs for a subject should include the evaluation of workload and fatigue while considering his individual traits. The virtual human modeling is the most promising technique. Furthermore, the development of biomechanical muscle-tendon dynamic model makes it possible to investigate the force-generation dynamics of individual muscles. DHM integrated with muscle-tendon dynamics muscle models, such as the OpenSim, could estimate the workload onto individual muscles.

In the effort to involve muscle fatigue analysis into work design, there are two key problems that bother us. First, in actual working scene, the motion adopted by workers to finish a task would be arbitrary rather than routine and repeated. This makes it difficult to evaluate the exact workload carried by a certain muscle. Fatigue analysis, without the exact information about muscle workload, would be inaccurate. Second, muscle fatigue process varies a lot among human groups. The utilization of fatigue analysis would be limited without proper consideration about demographical human attribute.

#### IV.1.1 Objectives

In this chapter, a plug-in to OpenSim is written to involve the muscle fatigue analysis to an arbitrary task. Concrete muscle force capability change is specified

and the influence of demographic human attributes is considered. This work is promising to offer a virtual work design platform that helps to predict muscle fatigue.

## IV.2 Methodology: OpenSim human modeling and muscle fatigue analysis

### IV.2.1 Muscle fatigue analysis

The Force-load fatigue model depicts how muscle force declines with time with consideration of relative workload and intrinsic human attribute. The model was described as a differential function (Eq. II.3). According to this model, during a fatiguing process, muscle force capability ( $F_{cem}(t)$ ) changes depending on a) Maximal (or initial) muscle force capability,  $F_{max}$ ; b) External load on the muscle,  $F_{Load}(t)$  and c) Intrinsic muscle fatigability,  $k$ .

The object of this research is a concrete analysis of muscle fatigue. In another word, how force capability of each muscle declines during an arbitrary motion. According to the Force-load muscle fatigue model, this objective can be achieved on condition of two values: workload on each muscle along the motion and the maximal muscle capability.

#### The Maximal muscle force capability of each muscle

Muscle activation depends on the neural excitation level. In the case of a certain muscle contraction speed and muscle length, muscle force increases with muscle activation. Full activation (i.e.,  $a(t) = 1$ ) happens when a muscle contractile component has been maximally excited (i.e.,  $u(t) = 1$ ) for a long time [46]. During an arbitrary motion, muscle kinematics changes from time to time. We calculate the maximal muscle force  $F_{max}$  based on the CMC algorithm, in addition that the activation level of each muscle is preset to full level ( $a(t) = 1$ ).

As the final step, a Plug-in is written based on the Force-load muscle fatigue model, with the required inputs obtained by the above methods.

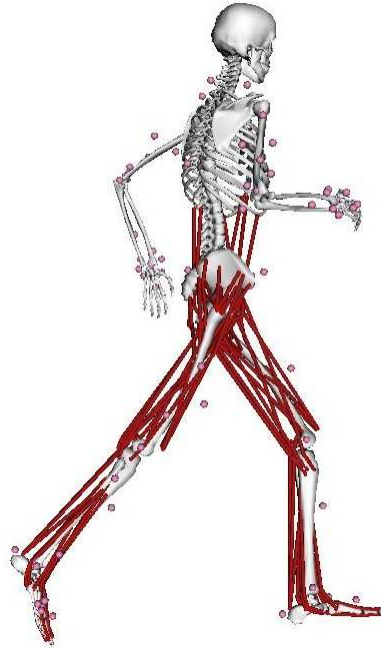


**Figure IV.1** – Full body running digital human modeling. Muscles are represented by red lines.

### IV.3 Data and Simulation

The plug-in is tested on a three-dimensional, 29 degree-of-freedom human model developed by Hamner from Stanford University [120]. The model, as the other OpenSim musculoskeletal models, is made up of bodies, joints, and muscle-tendon actuators. Specifically, this model consists of 20 body segments, 19 joints and 92 muscle actuators, as shown in Figure IV.1. The inertial parameters for the body segments in the model are based on average anthropometric data obtained from five subjects (age  $26 \pm 3$  years, height  $177 \pm 3$  cm, and weight  $70.1 \pm 7.8$  kg).

This model is developed to study the muscles' contribution to the acceleration of the body during running. It covers the muscles that needed for arbitrary running motions. These muscles could be classified into three groups: torso-core muscle group, pelvis-femur muscle group, and lower knee extremities muscle group.

The simulation data is also from the project of Hamner et al. [120]. It is recorded from a healthy male subject (height 1.83 m, mass 65.9 kg) running on a treadmill at 3.96 m/s. A total of 41 reflective markers are placed on the subject's anatomical landmarks during the experiment to scale the model to the subject's anthropom-



etry. Ground reaction forces and markers' trajectories are recorded. The recorded motion lasts for 10 s.

In our study, 10 muscles are selected from the three muscle groups to conduct muscle fatigue analysis. The basic characteristics of these muscles are listed in Table IV.1.

**Table IV.1** – Basic characteristics of the analyzed muscles.

Muscle name	Appertained group	Optimal fiber length ( $m$ )	Maximal isometric force ( $N$ )
Erector spinae	Torso-core	0.120	2500.0
External oblique	Torso-core	0.120	900.0
Internal oblique	Torso-core	0.100	900.0
Adductor magnus	Pelvis-femur	0.131	488.0
Glute maximus	Pelvis-femur	0.142	573.0
Glute medius	Pelvis-femur	0.065	653.0
Tibialis posterior	Lower knee	0.031	1588.0
Lateral gastrocnemius	Lower knee	0.064	683.0
Extensor digitorum	Lower knee	0.102	512.0
Soleus	Lower knee	0.050	3549.0

## IV.4 Results of simulation

During the arbitrary running, workloads on muscles vary from moment to moment. A typical muscle workload change is shown in Figure IV.2.

### IV.4.1 General muscle force decline

In order to investigate the fatigue process, the motion data is duplicated to 10 min. During the running process, muscle force capabilities decline with time. After input the fatigability ( $k$ ) of the subject, the detail information about force capability changes is accessible. A general view of force capability changes of the selected muscles are shown in Figure IV.3. Here the fatigability is set to  $1.0 \text{ min}^{-1}$ . Generally, the muscles' capabilities reduce to 60% to 70% of their maximum after running for 10 min.

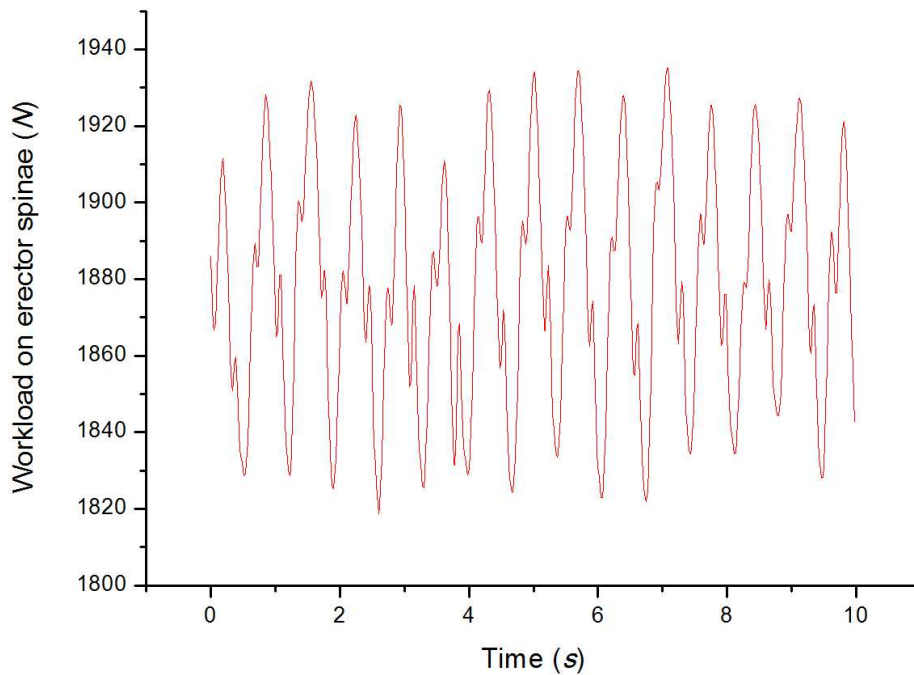


**Figure IV.2** – Workload on erector spinae muscle during 10s arbitrary running at 3.96 m/s.

#### IV.4.2 Comparison among different muscles

The initial and ending force capabilities of the selected muscles are shown in Table IV.2.

The proportion of force capability reduction is between 30% to 40% for each of the ten muscles. Erector spinae loses the maximal proportion of force. As far as the selected muscles, torso-core muscle group fatigues no less than the pelvis-femur or the lower knee group (average fatigue level:  $(36.8 \pm 2.1)\%$ ,  $(35.1 \pm 2.7)\%$ ,  $(36.1 \pm 3.2)\%$ , respectively).

#### IV.4.3 Influence of fatigability

Fatigability is a subject-specific parameter that might also varies between muscle groups. As mentioned in Section II.6, the determined value of  $k$  varies from  $0.87 \text{ min}^{-1}$  to  $2.15 \text{ min}^{-1}$  for general muscle groups. In the current study, we examine the influence of fatigability by comparing the fatigue level when  $k = 1.0 \text{ min}^{-1}$  with that when  $k = 2.0 \text{ min}^{-1}$ . A typical comparison is shown in Figure IV.4.

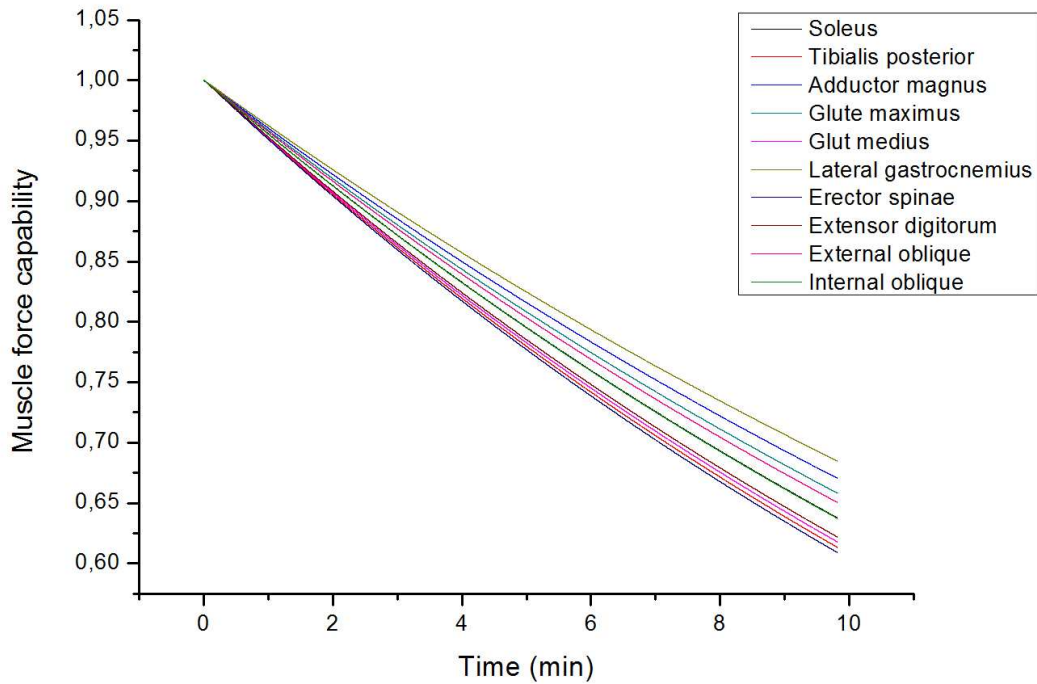


**Figure IV.3** – Force capability lines of ten muscles during 10 min running.  $k = 1.0 \text{ min}^{-1}$ . Force of each muscle is normalized by its maximum.

**Table IV.2** – General information of muscle force capabilities

Muscle name	Appertained group	Initial capabilities (N)	Final capabilities (N)	Proportion of reduction
Erector spinae	Torso-core	38703.5	23563.3	39.1%
External oblique	Torso-core	19876.2	12926.2	35.0%
Internal oblique	Torso-core	18374.8	11705.9	36.3%
Adductor magnus	Pelvis-femur	10923.7	7322.3	33.0%
Glute maximus	Pelvis-femur	12304.1	8096.3	34.2%
Glute medius	Pelvis-femur	19134.0	11817.8	38.2%
Tibialis posterior	Lower knee	36901.9	22624.1	38.7%
Lateral gastrocnemius	Lower knee	18231.9	12481.3	31.5%
Extensor digitorum	Lower knee	8940.7	5558.1	37.8%
Soleus	Lower knee	95221.7	60708.3	36.3%

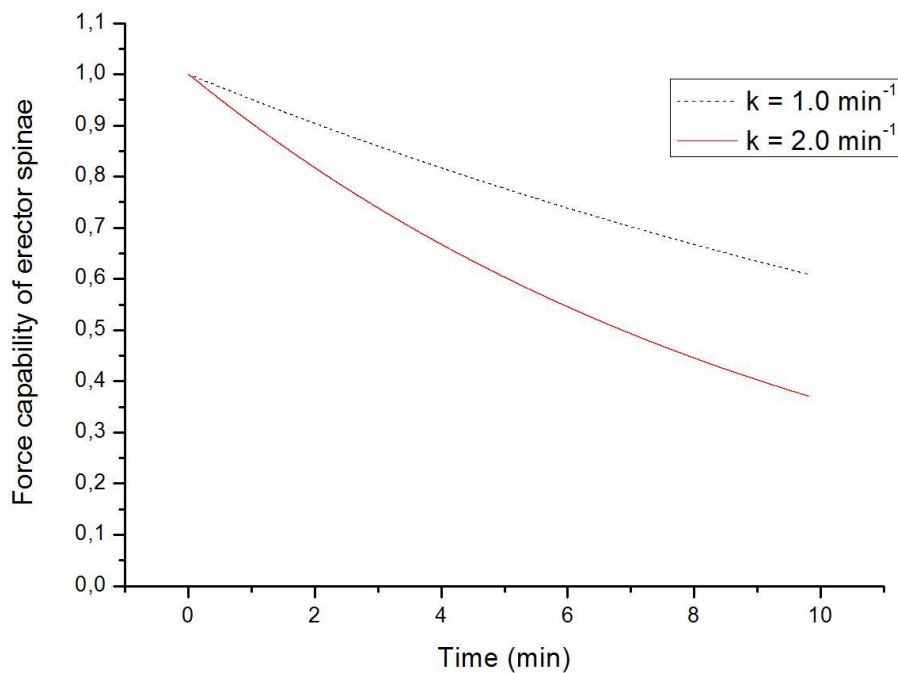


**Figure IV.4** – Force capability lines of erector spinae with different preset  $k$  values. Force is normalized by the maximum.

Table IV.3 manifests the fatigue level comparisons of all the ten muscles. Generally, the muscle reduces to 40% to 50% of its initial maximal capability. The relative sort of muscles' fatigue level remains unchanged.

## IV.5 Discussions

According to the simulation data, after 10 minutes' running at the speed of 3.96  $m/s$ , a healthy male subject is likely to lose 30% to 40% of his maximal muscle capability. The requirement of the running task at the current posture is about 5% of his maximal muscle capability. If the task continues, there would be a time in future when the subject's muscle capability reduces to near to the required workload. Muscles will enter into a risk zone [121, 42]. Damage will occur to muscles, which increases the risk of MSDs. The subject would change his posture unconsciously [122]. It is important to predict the exhausting time in the early process of work design.

In Hammer's research [120], the quadriceps (pelvis-femur muscle group) and

**Table IV.3** – Comparison of muscle force capabilities between different fatigabilities.

Muscle name	Appertained group	Proportion of capability loss	
		$k = 1.0 \text{ min}^{-1}$	$k = 2.0 \text{ min}^{-1}$
Erector spinae	Torso-core	39.1%	62.9%
External oblique	Torso-core	35.0%	57.7%
Internal oblique	Torso-core	36.3%	59.4%
Adductor magnus	Pelvis-femur	33.0%	55.1%
Glute maximus	Pelvis-femur	34.2%	56.7%
Glute medius	Pelvis-femur	38.2%	61.9%
Tibialis posterior	Lower knee	38.7%	62.4%
Lateral gastrocnemius	Lower knee	31.5%	53.1%
Extensor digitorum	Lower knee	37.8%	61.4%
Soleus	Lower knee	36.3%	59.4%

plantar flexors (lower knee muscle group) are the major contributors to acceleration of the body mass center during running, compared with the torso-core muscle group (erector spinae and iliopsoas). While in the current study, erector spinae, who loses 39.2% of its maximal capability, is found to be more fatigue-exposed than the others. Also, torso-core muscle group fatigues no less than the other two muscle groups. This phenomenon indicates that torso-core muscles undertake other supportive functions than contributing to body accelerating, such as counterbalancing the vertical angular momentum of the legs.

A subject with a higher fatigability value ( $k = 2.0 \text{ min}^{-1}$ ) losses about 20% of his maximal capability more than the subject with a lower fatigability value ( $k = 1.0 \text{ min}^{-1}$ ). The influence of fatigability is evident. It is essential to study the fatigability among different human groups.

It should be noticed that the current study considers no effect of fatigue recovery. Future study should integrate the muscle recovery for more accurate calculation.

## IV.6 Conclusions

In this chapter, a plug-in to OpenSim is written on the base of the Force-load muscle fatigue model and muscle force generation dynamics to obtain the concrete information about how force-output capability of each muscle declines along time.

Simulation on a three-dimensional, 29 degree-of-freedom human model shows that the force-output capability of ten selected muscles reduced to 60% - 70% after 10 minutes' running at the speed of  $3.96 \text{ m/s}$ , with a fatigability value of  $1.0 \text{ min}^{-1}$ . Torso-core muscle group, which has been found to contribute less to the body's acceleration in previous research, shows no less proportion of force loss than the other two groups. The difference in fatigue level caused by the change of fatigability is evident, which emphasizes the necessity of the study and determination of fatigability among different human groups.



# V

---

## The Build-up of a Full-chain Musculoskeletal Human Model in OpenSim

### V.1 Introduction

In biomechanics, the human body is always modeled as a open-chain multi-link system. The complexity of this system depends on the number of links that are considered. For efficiency reasons, the common way to study human motions is via the partial models that include the body parts on whom the loads are the mostly concerned, or those who carry the workload directly.

#### V.1.1 The existing OpenSim musculoskeletal models

In OpenSim, enormous efforts have been made to develop musculoskeletal models for motion analysis. As summarized in Table V.1. Generally, these models focus on specific body parts, which simplifies the biomechanical analysis and facilitates the study of a certain type of motion.

#### V.1.2 The full-chain effect of human motion

Biomechanical analysis of human positions and motions enables investigations on the neuromusculoskeletal system even beyond experiments. As far as the physical risk assessment of work-related MSDs, the workload as well as the development of muscle fatigue could be well estimated in OpenSim with the system developed in Chapter III.



**Table V.1** – Existing OpenSim musculoskeletal models.

Model	Author(s)	Description
gait2392_simbody	Ajay Seth, Darryl Thelen, Frank C. Anderson, Scott L. Delp	Primarily lower extremity model with two legs and a lumped torso segment. Includes 23 degrees of freedom and 92 muscle-tendon actuators.
gait10dof18musc	Ajay Seth, Darryl Thelen, Frank C. Anderson, Scott L. Delp	Trunk, pelvis and leg segments. 10 degrees of freedom, 18 muscles.
leg6dof9musc	Ajay Seth, Darryl Thelen, Frank C. Anderson, Scott L. Delp	Single leg, pelvis, femur, tibia, foot. 6 Degrees of Freedom, 9 muscles.
Arm26	Jeff Reinbolt, Ajay Seth, Sam Hamner, Ayman Habib	A right upper extremity model with 2 degrees of freedom and 6 muscles.
wrist	Robert Gonzalez, Thomas Buchanan, Scott Delp	A 10 degree of freedom, 23 muscle actuators, model of the lower arm.
SeperateLegs	Scott L. Delp	Two legs. 17 Degrees of freedom, 24 muscles.
Upper Extremity Dynamic Model	Katherine Saul, Xiao Hu, Craig Goehler Meghan Vidt, Melissa Daly, Anca Velisar, Wendy Murray	A right upper extremity dynamic model representing the anthropometry and force-generating capacity of the 50th percentile male.
Full Body Running Model	Sam Hamner, Ajay Seth, Scott Delp	Legs, trunk and arm segments (with inertial properties). 37 degrees of freedom, 30 muscles of the lower body, torque actuated arms.
Thoracolumbar spine and rib cage	Alexander Bruno, Dennis Anderson, Mary Boussein, Hossein Mokhtarzadeh, Katelyn Burkhart.	Male and female versions of fully articulated thoracolumbar spine (T1 through L5) and rib cage, plus pelvis, lumped head and neck, and upper extremities, includes 93 degrees of freedom, and 552 muscle-tendon actuators.
Lumbar Spine Model	Miguel Christophy, Nur Adila Faruk Senan, Moe Curtin	Lumbar bodies and torso containing 3 Dof and 238 muscle fascicles.
Full-body lumbar spine model	Margaret E. Raabe, Ajit M.W. Chaudhari	Consists of 21 Bodies, 29 Dof, and 324 musculotendon tendon actuators.

The accuracy of the risk assessment depends on the biomechanical analysis of joint and muscle workloads. When conducting biomechanical analyses, it should be noticed that the human body is systematic: body parts support each other directly and indirectly, in kinematics and dynamics. The state of one body part may influence another without physical contact.

For example, in the running sport where upper body movement is primarily powered by lower body movement [123], the swing of arms has been shown to make a significant contribution to the vertical propulsive impulses (about 5% to 10%) [124], which would also affect the running load on the lower limbs. The study of Arellano & Kram [125] revealed that the swing of arms actually reduces the metabolic energy demand (by 8%). Another example is that in a task of self-balance, the arm motions would influence the transversal pelvis-thorax moment up to 30% [126].

These researches remind us the necessity to analyze human motion in view of the full-chain effect. However, in all the existing OpenSim models, none involves the full human locomotor chain.

### V.1.3 Objective

The aim of this study is to develop a OpenSim musculoskeletal human model that includes segments and muscles of trunk and all the limbs, with which human motion could be analyzed in view of the full locomotor chain.

## V.2 Model development

To build up a full-chain OpenSim model, firstly we look into the existing full-body models. By now the most completed model is Raabe's full-body lumbar spine (FBLs) model [4] (see Figure V.1). It was developed by combining three previously built OpenSim models: Hamner's full-body model [120] for the base model, Christophy's lumbar spine model for the torso [127], and Arnold's model [128] of the patella. The FBLs model is comprised of 21 segments, 30 degrees-of-freedom, and 324 muscles. This model is characterized by its detailed description of trunk musculature [4]: The five lumbar vertebrae are modeled as individual bodies, each connected by a 6 degree-of-freedom joint. With 27 coupling

constraints, the net lumbar movement is described as three rotational degrees-of-freedom: flexion-extension, lateral bending, and axial rotation. Topology view of this model is shown in Figure V.2(a).

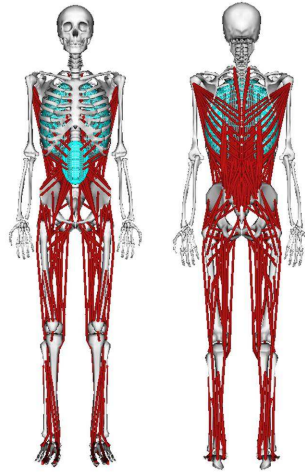


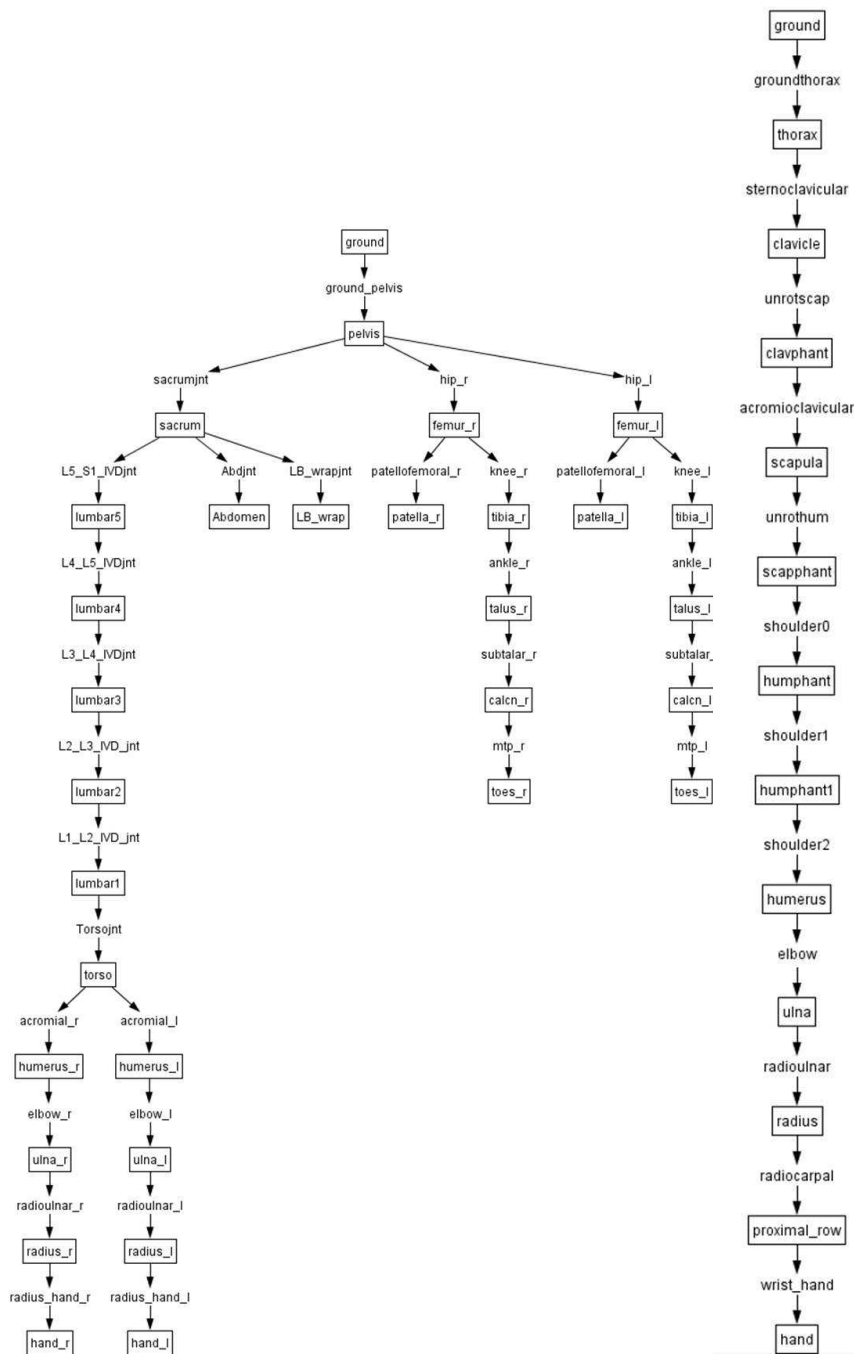
**Figure V.1** – Raabe’s full-body lumbar spine model [4].

Shortage of the FBL model lies in the lack of the musculotendon actuators of the upper limbs. For the modeling of the arm, we look into Saul’s model. It incorporates 7 degree-of-freedom and 50 musculotendon actuators (see Figure V.3) [5]. The 7 degree-of-freedom are: the shoulder rotation, elevation and abduction, the elbow flexion, the forearm rotation, and the wrist flexion and deviation. Topology view of this model is shown in Figure V.2(b).

The full-chain model is developed based on Raabe’s FBL model and Saul’s arm model. Structures of the lower limbs, pelvis and torso of the FBL model are reserved, while its humeri, ulnae, radii and hands are removed. A ‘welding joint’ is defined on the **torso**, by which the child body - **thorax** is defined. The structure of Saul’s arm model are connected to the **thorax**. Then the structure of the left arm are built symmetrically to the right one. Topology view of the full-chain model is shown in Figure V.4.

### V.3 The Full-chain model

The constructed Full-chain model consists of 46 body parts, 424 muscles and 37 DoFs. The model is defined from four aspects: the **BodySet**, which includes the definitions of the body parts and joints; the **ConstraintSet**, which includes the def-



(a) Raabe's full-body lumbar spine model

(b) Saul's arm model

Figure V.2 – Topology views of two OpenSim models.

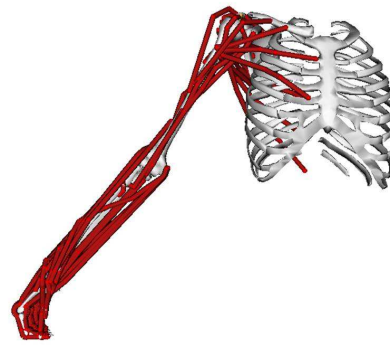


**Figure V.3** – The Saul's 7 degree-of-freedom arm model [5].

initions of relationships between joint movements; the **ForceSet**, which includes the definitions of muscles and tendons; and the **MarkerSet**, which includes the definitions of the locations of the reflection markers (see Figure V.5 for a general view of model codes).

### V.3.1 BodySet

In the **BodySet** section, we define a group of 46 bodies. For each body, property information (name, mass, location of mass center, inertia) as well as **Joint** and body geometry information (**VisibleObjects** and **WrapObjectSet**) are specialized (see Figure V.6).

The **Joint** define the relationship between bodies. As in Figure V.7, a joint (in red) defines the kinematic relationship between two frames ( $P$  and  $C$ ), each affixed to a body (the parent,  $P_o$ , the child body,  $C_o$ ) parameterized by joint coordinates.

A body is a moving reference frame ( $C_0$ ) in which its center-of-mass and inertia are defined, and the location of a joint frame ( $C$ ) fixed to the body can be specified. Similarly, the joint frame ( $P$ ) in the parent body frame ( $P_0$ ) can also be specified.

A **CustomJoint** permits the specification of 1 to 6 coordinates and user definition of the spatial transform to locate  $C$  with respect to  $P$  (see Figure V.8). Specially, a **WeldJoint** is defined on the body **torso**, fusing it with child body **thorax**. The joint introduce no coordinates. With each body, a geometry file can be associated by the **VisibleObject** property for visualization. The **WrapObjectSet** defines

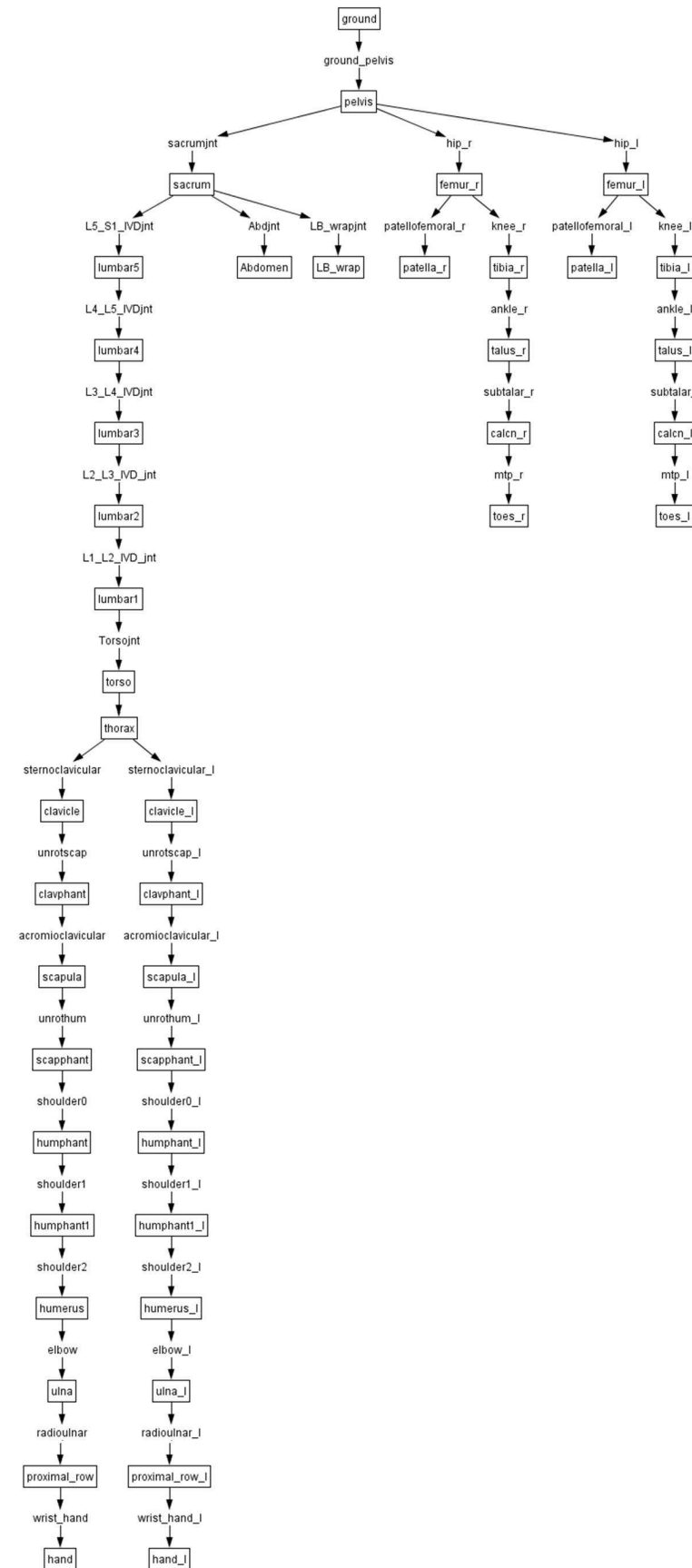


Figure V.4 – The topology view of the Full-chain OpenSim model.

```

1 <<?xml version="1.0" encoding="UTF-8" ?>
2 <OpenSimDocument Version="30000">
3   <Model name="Full-chain Model">
4     <length_units>meters</length_units>
5     <force_units>N</force_units>
6     <!--Acceleration due to gravity.-->
7     <gravity> 0 -9.80665 0</gravity>
8     <!--Bodies in the model.-->
9     <BodySet>
10      <objects>
13179      <groups />
13180    </BodySet>
13181    <!--Constraints in the model.-->
13182    <ConstraintSet>
13183      <objects>
13946      <groups />
13947    </ConstraintSet>
13948    <!--Forces in the model.-->
13949    <ForceSet>
13950      <objects>
42826      <groups />
42978    </ForceSet>
42979    <MarkerSet>
42980      <objects>
43110      <groups />
43111    </MarkerSet>
43112    <!--ContactGeometries in the model.-->
43113    <ContactGeometrySet>
43114      <objects />
43115      <groups />
43116    </ContactGeometrySet>
43117  </Model>
43118 </OpenSimDocument>
  
```

Figure V.5 – A general view of the script of the Full-chain model.

```

35 <Body name="pelvis">
36   <mass>11.777</mass>
37   <mass_center> -0.0707 0 0</mass_center>
38   <inertia_xx>0.1028</inertia_xx>
39   <inertia_yy>0.0871</inertia_yy>
40   <inertia_zz>0.0879</inertia_zz>
41   <inertia_xy>0</inertia_xy>
42   <inertia_xz>0</inertia_xz>
43   <inertia_yz>0</inertia_yz>
44   <!--Joint that connects this body with the parent body.-->
45   <Joint>
252   <VisibleObject>
298   <WrapObjectSet>
302 </Body>
  
```

Figure V.6 – The definition of the Pelvis body of the Full-chain model.

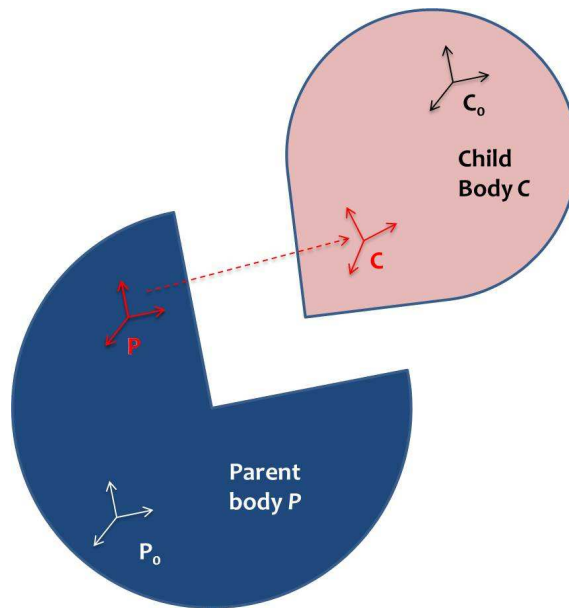


Figure V.7 – Diagram of an OpenSim joint.

```

<Joint>
  <CustomJoint name="ground_pelvis">
    <!--Name of the parent body to which this joint connects it
    <!--Location of the joint in the parent body specified in t
    <location_in_parent>0 0 0</location_in_parent>
    <!--Orientation of the joint in the parent body specified i
    <orientation_in_parent>0 0 0</orientation_in_parent>
    <!--Location of the joint in the child body specified in th
    <location>0 0 0</location>
    <!--Orientation of the joint in the owing body specified in
    <orientation>0 0 0</orientation>
    <!--Set holding the generalized coordinates (q's) that parm
    <CoordinateSet>
      <objects>
        <Coordinate name="pelvis tilt">
        <Coordinate name="pelvis list">
        <Coordinate name="pelvis rotation">
        <Coordinate name="pelvis tx">
        <Coordinate name="pelvis ty">
        <Coordinate name="pelvis tz">
      </objects>
    </CoordinateSet>
    <!--Whether the joint transform defines parent->child or ch
    <reverse>>false</reverse>
    <!--Defines how the child body moves with respect to the pa
    <SpatialTransform>
      <!--3 Axes for rotations are listed first.-->
      <TransformAxis name="rotation1">
      <TransformAxis name="rotation2">
      <TransformAxis name="rotation3">
      <!--3 Axes for translations are listed next.-->
      <TransformAxis name="translation1">
      <TransformAxis name="translation2">

```

Figure V.8 – Script of a OpenSim joint.

the locations and positions of virtual objects on which the muscles is going to be wrapped.

### V.3.2 ConstraintSet

The **ConstraintSet** defines the kinematic constraints between coordinates. A coordinate coupler relates the generalized coordinate of a given joint (the dependent coordinate) to any other coordinates in the model (independent coordinates).

In the Full-chain model, the joint **sternoclavicular** is defined on the **clavicle**, with the **thorax** as the parent body. The joint has two rotational coordinates: **sternoclavicular\_r2** and **sternoclavicular\_r3**. In the **ConstraintSet**, with two Coordinate Coupler Constraint, both the two coordinates are defined as the 'independent coordinate', with a kinematic relationships with the 'dependent coordinate' (shoulder elevation in this case). Therefore, the amount of the DoF of the model is reduced. The total DoFs are listed in Table V.2.

### V.3.3 ForceSet

In **ForceSet**, two types of force are defined: active forces such as the muscles and passive forces such as the ligaments and dampers.

In the OpenSim interface, the muscles are represented by red lines over body parts. Each muscle has a **GeometrySet** that specifies the muscle path by the **Path-PointSet** which defines the connection points on the body parts and the **Path-WrapSet** that defines the geometrical wrapping path over the body parts. Figure V.9 shows the display of the biceps muscles in the Full-chain model. The geom-



**Table V.2** – The degrees of freedom of the Full-chain model.

Body of motion	Joint	Coordinate name	Description
Hand	Wrist	Flexion	Hand flexion
Hand	Wrist	Deviation	Hand deviation in the palm plane
Hand	Wrist	Pro_sup	Hand rotation about the forearm
Arm	Elbow	Elbow_flexion	Elbow flexion
Arm	Shoulder	Shoulder_elv	Change of the thoraco-humeral angle
Arm	Shoulder	Shoulder_rot	Rotation of the upper arm about the humerus
Arm	Shoulder	Elv_angle	Rotation of the upper arm in the horizontal plane
Trunk	Waist	Flex_extension	Torso flexion in sagittal plane
Trunk	Waist	Lat_bending	Torso deviation in frontal plane
Trunk	Waist	Axial_rotation	Torso rotation about vertical axis
Thigh	Hip	Hip_flexion	Thigh flexion in sagittal plane
Thigh	Hip	Hip_adduction	Thigh adduction in frontal plane
Thigh	Hip	Hip_rotation	Thigh rotation about femur
Lower leg	knee	Knee_angle	Knee flexion
Foot	Ankle	Ankle_angle	Ankle flexion
Foot	Ankle	Subtalar_angle	Ankle deviation in frontal plane
Foot	Toe joint	Mtp_angle	Toe flexion
Whole body		Pelvis_tilt	Body tilt
Whole body		Pelvis_list	Body list
Whole body		Pelvis_rotation	Body rotation
Whole body		Pelvis_tx	Body transition front/back
Whole body		Pelvis_tz	Body transition left/right
Whole body		Pelvis_ty	Body vertical transition

entry setting is used not only for display purpose, but also for the calculation of

muscle lengths and velocities, which act as parameters in the muscle contraction dynamics.

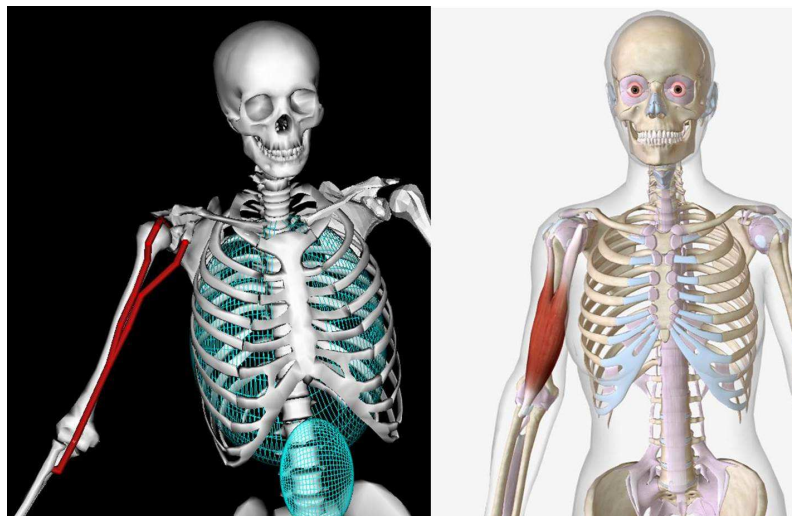


**Figure V.9** – The location of biceps and its representation in the Full-chain model.

Other parameters of the muscle contraction dynamics, such as the maximal isometric force, the optimal fiber length, the pennation angle at optimal are also specified, as well as those of the muscle activation dynamics such as the activation and deactivation time constant (see Figure V.10 for an example).

```

1  <<?xml version="1.0" encoding="UTF-8" ?>
2  <OpenSimDocument Version="30000">
3  <Model name="Full-chain Model">
4  <length_units>meters</length_units>
5  <force_units>N</force_units>
6  <!--Acceleration due to gravity.-->
7  <gravity> 0 -9.80665 0</gravity>
8  <!--Bodies in the model.-->
9  <BodySet>
10 <objects>
13179 <groups />
13180 </BodySet>
13181 <!--Constraints in the model.-->
13182 <ConstraintSet>
13183 <objects>
13946 <groups />
13947 </ConstraintSet>
13948 <!--Forces in the model.-->
13949 <ForceSet>
13950 <objects>
42926 <groups />
42978 </ForceSet>
42979 <MarkerSet>
42980 <objects>
43110 <groups />
43111 </MarkerSet>
43112 <!--ContactGeometries in the model.-->
43113 <ContactGeometrySet>
43114 <objects>
43115 <groups />
43116 </ContactGeometrySet>
43117 </Model>
43118 </OpenSimDocument>

```

**Figure V.10** – The definition of the right gluteus medius in the Full-chain model.

With the definition of the bodies, joint constraints and muscles, the Full-chain model is formed, as shown in Figure V.11. Then we seek to simulate the real motion with the model.

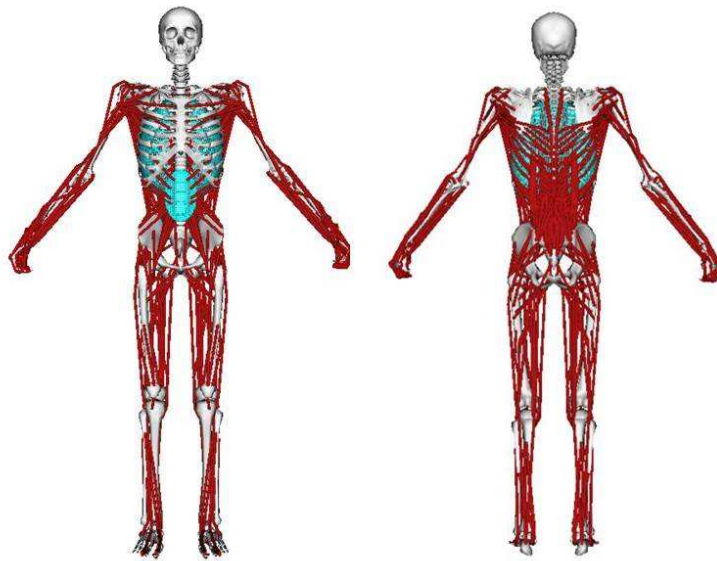


Figure V.11 – The Full-chain model on the OpenSim interface.

### V.3.4 MarkerSet

The markers are used to match the virtual model with a real subject. Locations of the virtual markers are settled in the OpenSim model, referred to which the reflecting markers on the real subject is supposed to placed. With the motion capture system, the spatial location data of the virtual markers can be used to scale the virtual model as well as to re-emerge the posture/motion.

Marker set can be defined and modified according to the configuration of the motion capture system. In Ecole Centrale de Nantes, the *ART-Human* system is used for motion tracking. The human body configuration is identified by the position and orientation of 17 body segments. The tracked subject is supposed to wear a suit which consists 17 plastic modeled parts. Each part corresponds to a body segments, on which three or four reflecting markers are located. With a number of 8 cameras, the spatial location of each marker is identified and the position and configuration of each body segment is settled.

For the connection between the Full-chain model and the *ART-Human* tracking system, we use the generated position data of each body segment as the marker location. Therefore, a total of 17 markers are defined in the Full-chain model.

## V.4 The scaling method of OpenSim models

A simulation of OpenSim is generally started by scaling the generic model specifically to the subject's geometric and mass data. The subject's body geometric data is obtained using a motion capture system, which records the spatial positions of flash reflecting markers that attached to the specific locations of the subject; then the generic OpenSim model is adjusted geometrically with attempts to minimize the position deviations between virtual markers and corresponding real markers. This makes a subject-specific model out of the generic model.

The geometrical adjustment increases the accuracy of posture simulation and kinematic analysis that follow. For accurate dynamic analysis, the body segment inertial parameters, such as segment masses, should also be adjusted specifically to each subject. In OpenSim, this adjustment is carried out by scaling the mass of each segment of the generic model proportionately with respect to the whole body mass of the subject.

This method of determining segment mass is based on the assumption that the mass distribution among body segments is similar among humans, which is not always the case. For example, the mean mass proportion of the thigh has been reported to be 10.27% [129], 14.47% [130], 9.2% [131], and 12.72% [132], which indicates significant individual difference. Therefore, the scaling method used by OpenSim is likely to cause errors in the following dynamic analysis. There is a necessity to estimate the errors.

In this section, errors caused by the scaling method used in OpenSim are estimated. Firstly, subject's segment masses are determined based on the accordingly 3D geometric model constructed with the help of 3D scan. The determined data is taken as an approximation to the true value of the subject's segment mass. Secondly, this set of data, as well as the proportionately scaled segment mass data, is used to specify a generic OpenSim model. Errors caused by proportionately scaling are calculated. Finally, influence of the errors on dynamics analysis is checked on a simulation of a walking task.



**Figure V.12** – Body markers that indicate the location of joint plates.

#### V.4.1 Methodology

##### Approximating segment masses with 3D scan

A whole-body 3D scan was conducted to a male subject (31 years old, 77.0 kg, 1.77 m) with a low-cost 3D scanner (Sense<sup>TM</sup> 3D scanner). Before scanning, reflecting markers were placed on the subject to notify the location of each joint plate as shown in Figure V.12. The locations of the joint plates were set according to Drillis (1966) [133], which meant to facility the dismemberment of the 3D model. During scanning, careful caution was taken to make sure that no extra contact between limbs and the torso. The scanned 3D model was stored in a stl mesh file, as shown in Figure V.13.

Then the 3D model was dismembered into 15 parts in the way that described by Drillis (1969) [133]. Body markers and body parts lengths are referred. An example of the dismembered body part (Pelvis) is shown in Figure V.14. Then, the volume of each body part was calculated.

To analyze the results obtained, the water displacements of eight distal body parts (hands, lower arms, feet, lower legs) were also measured, as described by Drilis (1966) [133].

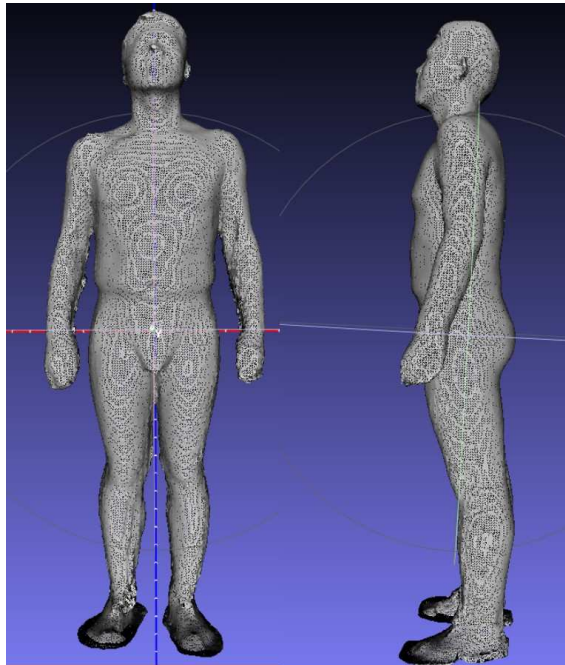


**Figure V.13** – The 3D geometric model of the subject generated by 3D scan.

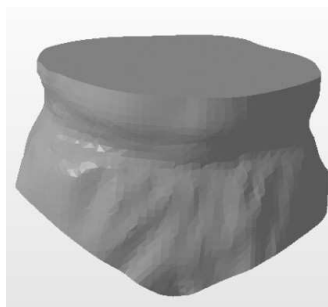


**Figure V.14** – The mesh of pelvis dismembered from the whole-body 3D model.

### Specification of OpenSim models to the subject

In this step, a generic OpenSim model is specified to our subject in aspect of body segment mass. The model is developed by Delp S.L. et al (1990) [134] (<http://simtk-confluence.stanford.edu:8080/display/OpenSim/Gait+2392+and+2354+Models>). It consists of 12 bodies, 23 degrees of freedom, and 52 muscles, as shown in Figure V.15. The unscaled version of the model represents a subject that is about 1.8 m tall and has a mass of 75.16 kg. The approximating body segment mass data obtained from the pro-

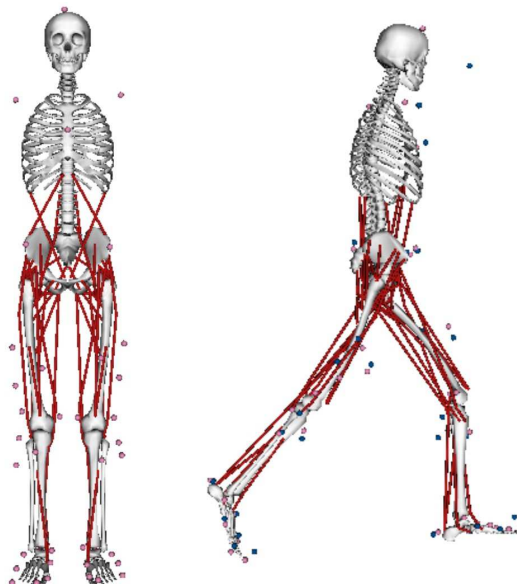


Figure V.15 – The OpenSim model used for error analysis.

cess described in section V.4.1 as well as the proportionately weight-scaled body segment mass data is used to specify the generic model. Thereby, two specific models are generated accordingly.

### Dynamic simulation in OpenSim

An simulation is conducted on the two specific models. The simulation data comes from previous researches [135]. The subject walks two steps in 1.2 s in an ordinary gait. Data of Spatial posture is collected at a frequency of 60 Hz and the and ground reaction forces at a frequency of 600 Hz. Inverse dynamic analysis is conducted on both models. Joint moments are calculated and compared between the two models.

## V.4.2 Results

This section contains the main results of this study.

### The estimation of body segment masses

Significant difference was found between volumes calculated from the 3D scanned geometric model and that measured by water displacement. For lower leg, the difference is as large as 27% (4.5 l vs. 3.3 l). To approximate the real segment masses, assumption is made that the volume distribution of the 3D model merged by 3D scan among head, torso, pelvis, and upper limbs is the same as that of the real subject. Density data of the body parts [136] were used to calculate the whole-body density of the subject, which, as well as body weight, gives estimation of whole-body volume. Then the overall volume was distributed to each segment with respect to the relative volume ratio of the 3D geometric model. In this way, segment volumes and masses are approximated.

Relative data is shown in Table V.3. The whole-body volume calculated from the 3D geometric model is 7.31% larger than the estimated whole-body volume (81.81 l to 76.24 l). The whole body density is estimated to be 1.01 g/ml. Mass proportion of the thigh is about 11.30%, which is between that reported by Clauser et al., (1969) (10.27%) [129], Okada (1996) (9.2%) [131] and by De Leva (1996) (14.47%) [130], Durkin & Dowling (2003) (12.72%) [132].

### Errors analysis of the OpenSim scaled model specific to the subject

Segment masses generated by proportionately scale and 3D modeling are used to specify the OpenSim generic model, which bring about two specific models (noted as scaled model and approximate model). Table V.4 shows the segment mass data of the two models. Errors of the scaled model segment mass are between 4.06% and 47.42%. The most significant error merges from foot data which, however, represents only a small part of the overall body mass.

### Motion simulation and dynamic analysis

Motion simulation is conducted on the two models. The simulated motion includes two steps of walking, lasting for 1.2 s. Since the two models differ in only



segment mass, no difference in kinematic analysis is shown. As an example, the angles, velocity and acceleration of right hip flexion is shown in Figure V.16.

Inverse dynamic analysis on the two models generates different results. Figure V.17 shows the right hip flexion moments calculated from the two models. With the approximate model as yardstick, the error of the calculated right hip flexion moment of the scaled model has a mean of 1.89 Nm, which is 10.11% of its mean absolute value. A total of 18 joint moments was calculated. The means of error percentage vary from 0.65% to 12.68%, with an average of 5.01%. Relative data are shown in Table V.5.

**Table V.3** – Volume, density and mass of the whole body and segments.

	Overall	Pelvis	Head	Torso	Upper arm-l	Upper arm-r	Lower arm-l	Lower arm-r	Upper leg-l	Upper leg-r	Lower leg-l	Lower leg-r	Foot-l	Foot-r	Hand- l	Hand- r
Volume(l)-3D scanned model	81.81	11.29	5.65	29.90	1.63	1.72	1.38	1.34	8.74	8.65	4.42	4.53	1.06	0.89	0.49	0.58
Volume(l)-water dis- placement							1.01	1.12			3.25	3.35	1.00	1.00	0.46	0.46
Volume(l)-estimated	76.24	10.81	5.41	28.64	1.56	1.65	1.01	1.12	8.37	8.29	3.25	3.35	1.00	1.00	0.46	0.46
Density(kg/l)[136]	1.01	1.01	1.07	0.92	1.06	1.06	1.10	1.10	1.04	1.04	1.08	1.08	1.08	1.08	1.11	1.11
Estimated mass(kg)		10.92	5.79	26.35	1.66	1.75	1.11	1.23	8.71	8.62	3.51	3.62	1.08	1.08	0.51	0.51

**Table V.4** – Errors of proportionally scaled segment masses with respect to the approximate masses.

	Pelvis	Torso	Upper leg-l	Upper leg-r	Lower leg-l	Lower leg-r	Talus	Calcaneus
Approximate mass(kg)	10.92	38.91	8.71	8.62	3.51	3.62	0.07	0.87
Proportionally scaled mass (kg)	11.98	34.82	9.46	9.46	3.76	3.76	0.10	1.28
Absolute error (kg)	1.06	-4.08	0.75	0.84	0.25	0.15	0.03	0.41
Percentage of abso- lute error in overall body weight	1.37%	-5.30%	0.98%	1.10%	0.33%	0.19%	0.04%	0.53%
Relate error	9.66%	-10.49%	8.67%	9.80%	7.26%	4.06%	47.42%	47.42%

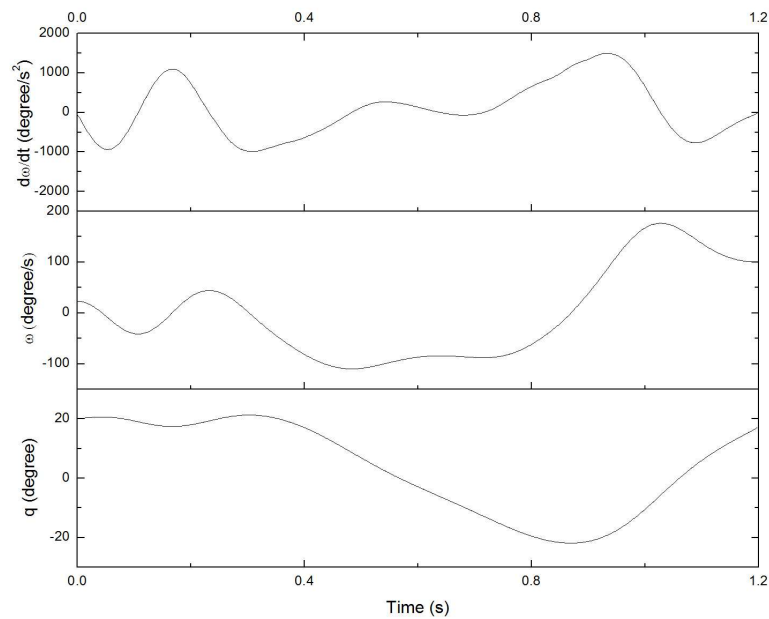


**Figure V.16** – Coordinate ( $q$ ), velocity ( $\omega$ ), acceleration ( $d\omega/dt$ ) of right hip flexion in the motion.

### V.4.3 Discussions on the use of 3D scan in the estimation of body segment masses

In previous researches, the inertial parameters of human body segment are usually determined by two means: (i) Applying predictive equations generated from database [130], (ii) Medical scanning of live subjects [137], and (ii) Segments geometric modelling [138]. The use of the first one, as stated by Durkin & Dowling (2003) [132], is limited by its sample population. Furthermore, the difference in segmentation methods makes it difficult to combine various equations [139]. The second method, medical scanning, such as dual energy X-ray absorptiometry is more accurate in obtaining body segment inertial parameters [140]. But it is more expensive and time-consuming.

In this study, body segment masses are estimated by segment density data and segment volume. 3D scan is used to estimate body segment volume. In this process, errors may merge from two aspects.

First, it is assumed that density data of each segment is constant among humans. This assumption may bring errors. Traditional body composition method defines two distinct body compartments: fat and lean body (fat-free). Fat has a density of 0.90 g/ml, while lean body has a density of 1.10 g/ml [141]. Subject's body fat rate may influence the segment density. However, the range of density variation is smaller than that of the mass distribution. Therefore, the use of density and volume may reduce the estimation error of segment mass.

**Table V.5** – Errors of the joint moments calculated from the scaled model, with respect to that from the approximate model

	Mean of error (Nm)	Mean of instant moment (Nm)	Mean of error percentage
Pelvis tilt	6.73	64.12	10.50%
Pelvis list	4.06	37.78	10.75%
Pelvis rotation	1.02	17.78	5.74%
Right hip flexion	1.89	18.73	10.11 %
Right hip adduction	0.48	18.57	2.60 %
Right hip rotation	0.07	3.47	2.13 %
Right knee angle	0.65	19.21	3.40 %
Right ankle angle	0.31	38.68	0.80 %
Right subtalar angle	0.06	9.02	0.65 %
Left hip flexion	2.27	17.90	12.68 %
Left hip adduction	0.80	24.99	3.18 %
Left hip rotation	0.10	4.28	2.23 %
Left knee angle	0.83	19.37	4.28 %
Left ankle angle	0.36	30.18	1.19 %
Left subtalar angle	0.07	7.65	0.91 %
Lumbar extension	5.47	60.85	9.00 %
Lumbar bending	3.05	37.37	8.17 %
Lumbar rotation	0.33	17.98	1.85 %

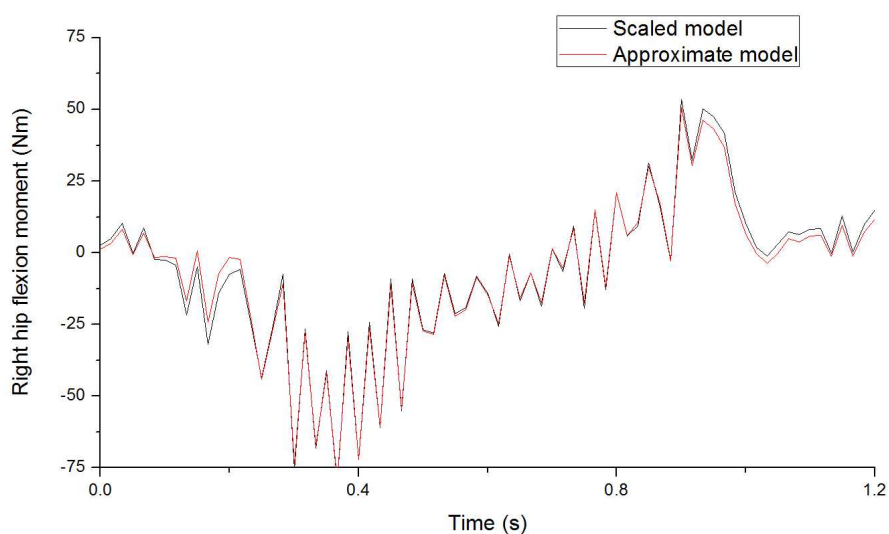


**Figure V.17** – Right hip flexion moments calculated from the two models.

For example, in the current study, the thigh, with a volume of 8.35 l, holds a mass proportion that would vary from 9.74% (all fat, density = 0.90 g/ml) to 11.90% (fat-free, density = 1.10 g/ml). This range is much narrower than that found in previous research (from 9.2% [131] to 14.47% [130]).

Second, 3D scan is used to build up 3D geometric model and calculate segment volumes. Significant difference exists between volumes calculated and volumes measured by water displacement. To approximate the real volume, assumption is made that the 3D geometric model has the same volume distribution with that of the subject, which may bring error.

In summary, as a simple and low-cost method of segment mass determination, the use of density data and 3D geometric model is more likely to reduce the estimation error. 3D scan is an easy way to construct a 3D geometric model, but attention should be paid to the model's volume errors. The method used in this chapter to approximate the real segment volumes with 3D scanned model needs to be examined in future researches.

### **The error and error significance of the proportionately scaled model**

Proportional scaling is efficient to specific a generic model. In this study, relative errors of segment masses of the scaled model are between 4.06% to 47.42%. The error of torso mass is 4.09 kg, which takes up to 5.30% of the overall body weight. In the following motion simulation, these errors bring about difference in the calculated joint moment. Means of the difference of calculated joint moments are

from 3.65% to 12.68%. This suggests that a careful specification of segment masses will increase the accuracy of the dynamic simulation.

#### V.4.4 Conclusions

This study aims at estimating the errors and their influences on dynamic analysis caused by the scaling method used in OpenSim. A 3D scan is used to construct subject's 3D geometric model, according to which segment masses are determined. The determined segment masses data is taken as the yardstick to assess OpenSim proportionately scaled model: errors are calculated, and influence of the errors on dynamics analysis is examined.

As a result, the segment mass error reaches up to 5.31% of the overall body weight (torso). Influence on the dynamic calculation has been found, with a average difference from 3.65% to 12.68% in the joint moments. Conclusions could be drawn that (i) the use of segment volume and density data may be more accurate than mass distribution reference data in the estimation of body segment masses and (ii) a careful specification of segment masses will increase the accuracy of the dynamic simulation significantly. This current work is a study to determine inertial parameters of the human body segment in biomechanical simulation. It explores new, more precise and simpler ways to implement biomechanical analysis. This work is a step towards characterizing muscular capacities for the analysis of work tasks and predicting muscle fatigue.

# VI

---

## The Application of the Full-chain Model on Posture Analysis of an Overhead Drilling Task

### VI.1 Introduction

Overhead work is constantly accused by epidemiologists for its close relationship with shoulder disorders [142, 143]. It is always accompanied by abnormal postures (for example, upper arm flexion or adduction  $\geq 60^\circ$  [142]) and forceful exertions. For some occupations like welder [144] and driller [145], these tasks are sometimes impractical to be avoided. An alternative plan would be to optimize the working posture.

An optimized posture is characterized by lower physical load. When estimating posture loads, attention should be paid to the integrity of human body. There is a possibility that some postures would reduce load from one part of body while bring in extra load to another.

In this study, we use the full-chain OpenSim model to simulate a typical overhead drilling task. Six task postures are analyzed. In each case, joint moments and muscle activations are checked. The sum of activations of all muscles is viewed as the index of posture load. Hypothesis is made that the index varies with different postures.



## VI.2 Simulation setup

Overhead drilling is a common task in industry. Workers hold a driller in hand while applying an force upwards. For a specific task, workers' drilling postures vary with the spatial position of the target point. Postures that vary in the sagittal plane are the main concerns [43]. In this study, we simulate an overhead drilling task about 30 cm higher over head. Six postures are applied, which represents 6 possible combinations of two factors: reach height (with/without stepladder) and reach distance (close reach/middle reach/far reach), shown in Figure VI.1 and in OpenSim in Figure VI.2.

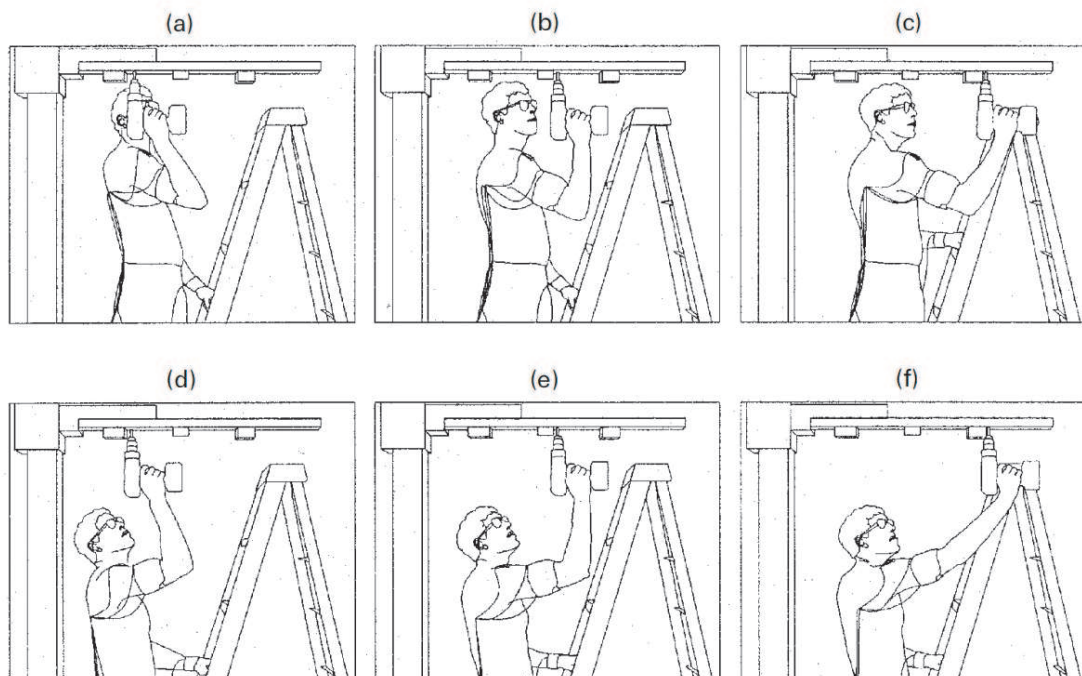


**Figure VI.1** – Six working postures for a drilling task

The “stepladder” is 30 cm high. It enables the “low-reach” postures with the wrist height at eye-level in comparison with the “high-reach” ones. In aspects of the reach distance, “close-reach”, “middle-reach”, “far-reach” are used to denote positions with wrist aligned with the pelvis mass center, aligned with tiptoes, and 15 cm further away from tiptoes, respectively. Settings of the model’s joint space is presented in Table VI.1. The unmentioned joint coordinates are set to 0.

An external force of 44 N is applied downwards on the proximal row of the right hand, which simulates the load of a 2.27 kg portable drill together with a compression force of 22 N [43]. Ground reaction force is applied evenly on the two feet. The left hand is not used to maintain the worker’s balance.

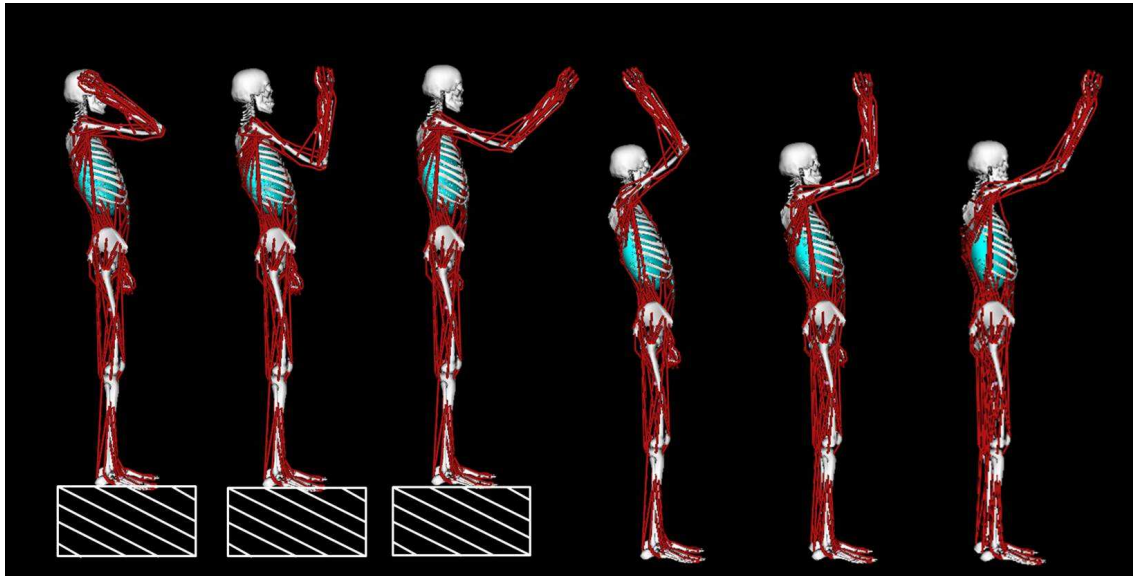


**Figure VI.2** – Simulations of six drilling postures. From left to right: low close reach (L-C); low middle reach (L-M); low far reach (L-F); high close reach (H-C); high middle reach (H-M); high far reach (H-F).

Inverse dynamics are conducted, which computes joint moments. Thus, the muscle forces and activations are estimated on optimizing the sum of total muscle activations.

A study based solely on the arm study shows that the tool must be as close as possible to the axis of the spine to minimize forces in the shoulder [43]. For both working altitudes, shoulder moments are minimal when the tool is close to the shoulder as shown in Figure VI.3.

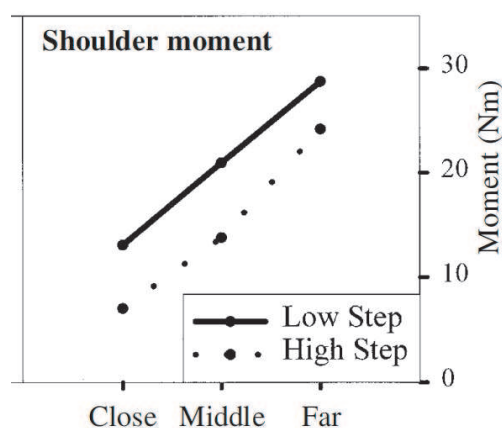


**Figure VI.3** – Shoulder moment according to the worker posture

The objective of a study that includes all the muscles of the body is to show that the optimal posture is different.

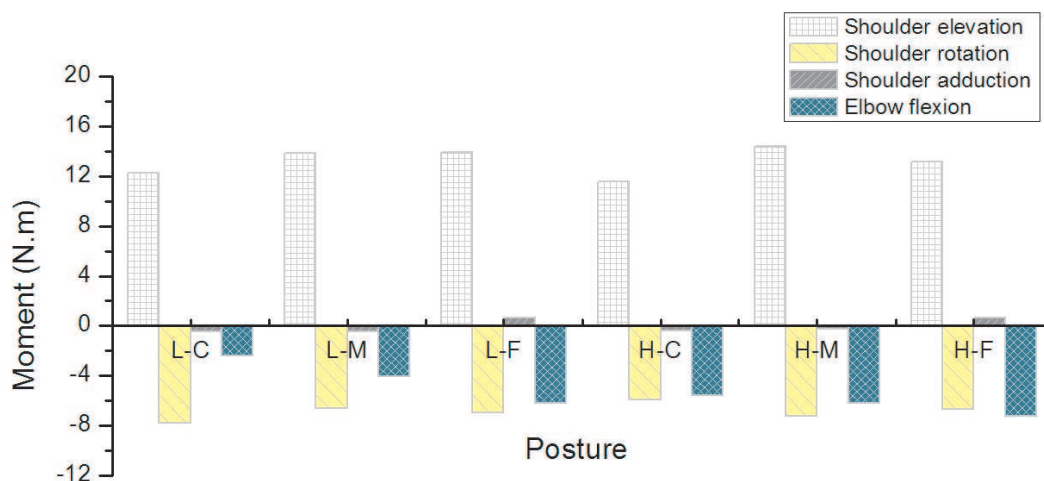
**Table VI.1** – Model joint space settings. Unit: degree.

Coordinate	Permitted joint motion	Posture					
		L-C	L-M	L-F	H-C	H-M	H-F
Flex_extension	Lumbar extension	5	5	0	5	5	0
Elv_angle	Shoulder adduction	80	80	80	80	80	80
Shoulder_elv	Shoulder elevation	75	50	70	120	100	110
Elbow_flexion	Elbow flexion	145	120	60	80	70	40
Flexion	Wrist flexion	-45	-45	-45	-45	-45	-45
Deviation	Wrist deviation	0	-5	-10	0	-5	-10

## VI.3 Simulation results

### VI.3.1 Joint moments

Shoulder moment is the main concern of the overhead work. The simulation with the Whole-body OpenSim model permits not only the estimation of the shoulder elevation moment but a comprehensive overview of joint moments in all coordinates, as shown in Table VI.2 and summarized graphically on the Figure VI.4.

**Figure VI.4** – The shoulder rotation moment is considerable beside of the elevation moment

Results shows that as far as the shoulder, the rotation moment is considerable beside of the elevation moment. The high close reach posture is estimated to lead to the least shoulder moment (17.92 N.m in total), while the high middle reach

**Table VI.2** – Estimated joint moments of six simulations. Unit: *N.m*

Coordinate	Posture					
	L-C	L-M	L-F	H-C	H-M	H-F
Shoulder elevation	12.27	13.87	13.90	11.58	14.39	13.17
Shoulder rotation	-7.78	-6.60	-6.96	-5.95	-7.26	-6.66
Shoulder adduction	-0.48	-0.43	0.65	-0.39	-0.27	0.62
Elbow flexion	-2.40	-4.04	-6.18	-5.57	-6.22	-7.26
Hand flexion	-3.10	-3.92	-2.03	-4.00	-4.25	-3.24
Hand deviation	2.07	9.97	-4.41	-13.40	9.69	-4.64
Hand pronation	6.38	-1.69	-6.27	4.34	0.06	-3.47

posture is related to the most (21.92 N.m in total). The elbow flexion moment varies substantially (from 2.40 N.m to 7.26 N.m). So is the wrist moment, which varies from 11.35 N.m to 21.74 N.m. It is notable that it is the high close reach posture which brings about the least shoulder moment that leads to the largest wrist moment.

### VI.3.2 Muscle activations

Muscle activations are computed on optimizing the sum of total muscle activation while counteracting the joint moments. Table VI.3 presents the sum of activations of some muscle groups and of whole-body muscles in the six simulations. As a whole, the sum of all muscles' activations varies from 11.88 to 29.35, which indicates a variation of average muscle activation from 2.8% to 6.9%. This suggests that the muscles exert efforts of different levels in different postures. Posture optimization would be a efficient way to interfere with muscle-related disorders.

Figure VI.5 summarizes the muscle activation for the six postures for either the right upper arm muscle or the whole body muscles. The upper arm and shoulder muscle group (shown in Figure VI.6(a)) is the primary concern of overhead works. The simulation results show that the average activation of muscles in this group varies from 2.2% (low close reach) to 8.6% (high far reach). It can also be figured out that the muscles of lower arm could be activated in varying degrees as well (averages vary from 1.2% to 8.6%).

The simulation results also highlight the roles played by muscles of latissimus dorsi (shown in Figure VI.6(b)) and hip abductor (shown in Figure VI.6(c)). Sig-

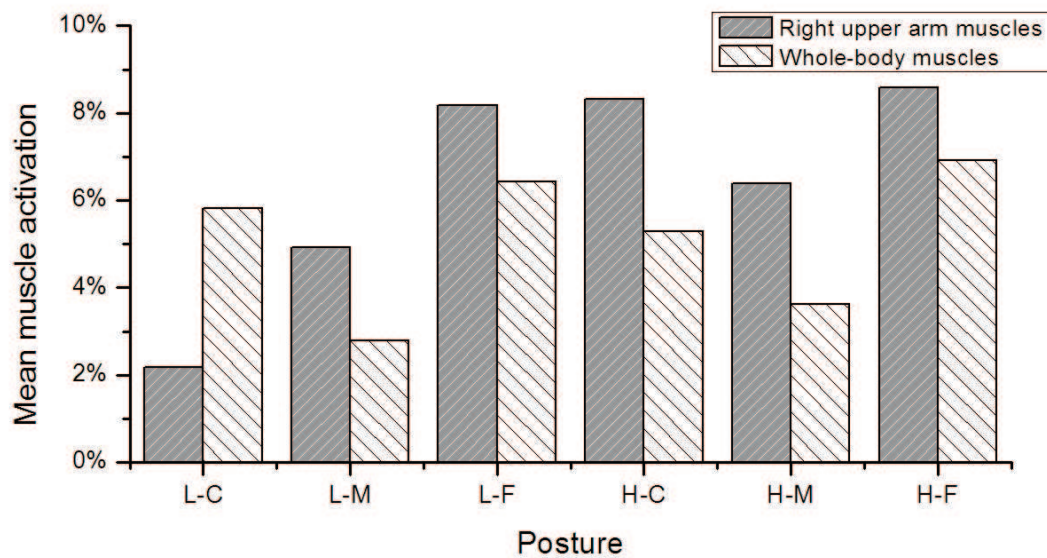


Figure VI.5 – The muscle activations in total for the six postures under studied

nificantly asymmetrical activation levels are shown between left and right side of the two muscle groups. For the latissimus dorsi, muscles of the right side are more activated than that of the left. And for the hip abductor, muscles of the left side are intensively activated (about 16.8% in average in every posture) while that of the right side are almost relaxed (about 0.3% to 0.4% in average). It is also notable that the activations of the right latissimus dorsi muscles vary with postures. For the low middle reach and the high middle reach, right latissimus dorsi shows far less activation than in other postures.

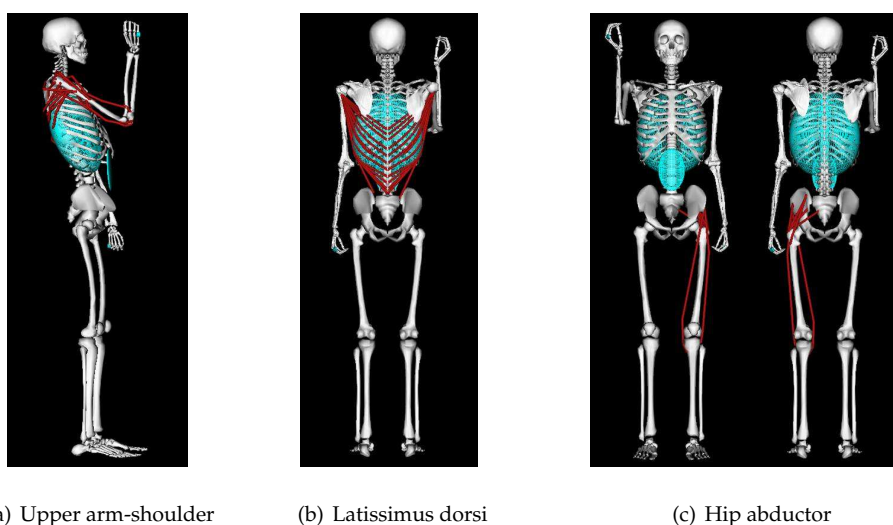


Figure VI.6 – Locations of three muscle groups

**Table VI.3** – Estimated muscle activations

Muscle groups	No. of muscles	Mean muscle activation					
		L-C	L-M	L-F	H-C	H-M	H-F
Right lower arm	18	6.88%	3.96%	1.20%	8.60%	3.18%	1.42%
Right upper arm-shoulder	22	2.18%	4.92%	8.18%	8.31%	6.38%	8.59%
Right Latissimus dorsi	14	82.29%	0.39%	81.64%	40.95%	0.43%	78.97%
Left Latissimus dorsi	14	0.09%	0.06%	0.84%	0.10%	0.06%	0.65%
Right hip abductor	10	0.34%	0.32%	0.41%	0.38%	0.32%	0.37%
Left hip abductor	10	16.77%	16.77%	16.77%	16.77%	16.77%	16.77%
Whole-body	424	5.81%	2.80%	6.43%	5.29%	3.62%	6.92%

As far as overhead works, the activation of some specific muscles such as the biceps, the triceps, the deltoids have concerned researchers. In the current study, the activations of these muscles are estimated, as shown in Table VI.4. The biceps and posterior deltoids are not significantly activated while the anterior deltoids exerts considerable efforts in all the six simulations. The lateral deltoids is activated enormously with high close reach and high far reach posture, whereas makes trivial exertions with low middle reach posture. The long head of triceps does not exert markable effort except with the low middle reach posture; the medial and short head of triceps are most activated with high close posture (about 30%), and least activated with low close reach posture (about 0.4%).

Figure VI.7 represents a graphical interpretation of these results. Significant activations of the right hip adductors go with all the six postures; Intensive activations of the right latissimus dorsi are found in postures with forward or backward arm reach, other than the neutral. This implies the possible relationship between back loads and arm positions.

## VI.4 Discussions

### VI.4.1 The full chain effect

When evaluating work loads of the shoulder joint, ergonomists pay much attention to the moment of shoulder elevation and abduction, rather than the rotation [142, 143]. For example, Anton et.al. [43] studied an overhead drilling task with similar posture configurations with the current simulation, in which the shoulder elevation moments that are calculated from measurements taken on still video frames are used as the only indicators of posture loads, whereas results of the

Table VI.4 – Estimated activations of individual muscles.

Coordinate	Position					
	L-C	L-M	L-F	H-C	H-M	H-F
Biceps long head	0.00%	0.36%	0.00%	0.00%	0.36%	0.00%
Biceps short head	0.39%	0.36%	0.00%	0.00%	0.36%	0.00%
Anterior deltoids	22.06%	18.93%	24.37%	13.37%	36.98%	19.95%
Lateral deltoids	19.69%	0.00%	19.02%	100.00%	7.70%	66.49%
Posterior deltoids	0.39%	0.36%	0.46%	0.43%	0.36%	0.42%
Triceps long head	0.39%	8.98%	0.00%	0.00%	0.00%	0.00%
Triceps medial head	0.39%	5.83%	16.15%	30.54%	13.28%	18.39%
Triceps short head	0.39%	5.72%	15.69%	30.00%	13.01%	17.06%

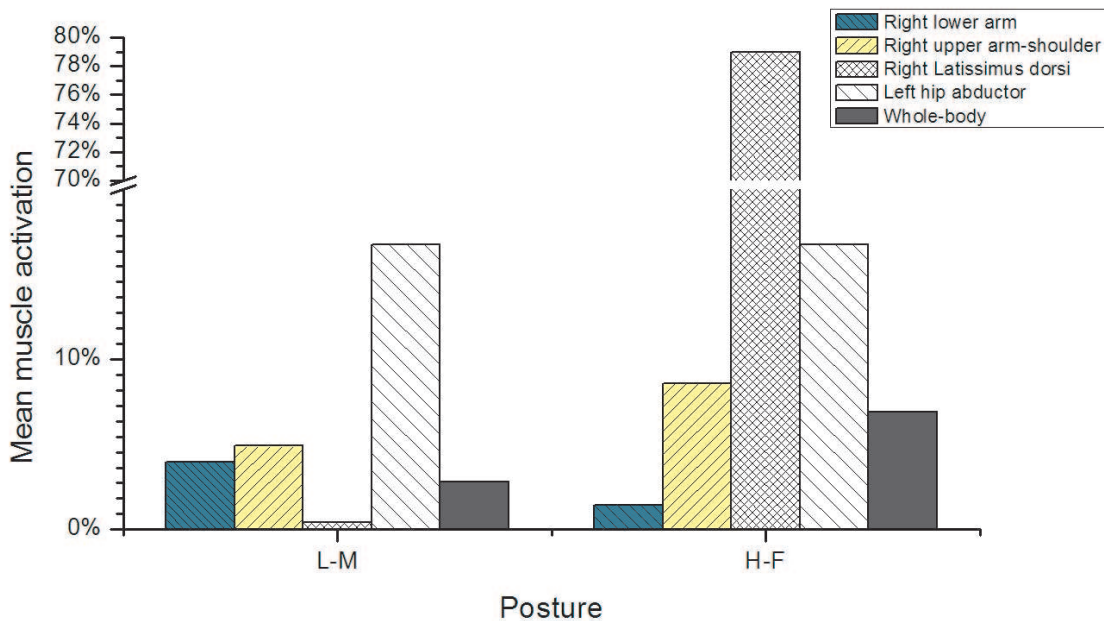


Figure VI.7 – Muscle activations of specific body parts

current simulation imply that shoulder rotation moment is also considerable. To evaluate the moments of multi-degrees-of-freedom joints, the use of refined musculoskeletal models are strongly suggested.

The full-chain effect is underlined by the simulation results. Significant activations of the right hip adductors go with all the six postures, hypothetically because of the asymmetric loads between the left and right arm. Intensive activations of the right latissimus dorsi are found in postures with forward or backward

arm reach, other than the neutral. This result implies the possible relationship between back loads and arm positions.

Low back pain is an important and costly health problem in industry [146, 147]. Among all occupations, the highest recurrence rate is reported in nurses and drivers [148, 149]. Both of the two occupations require lots of forward or backward arm reaches. Among the enormous efforts to study the ergonomic risk factors of low back pain [150, 151, 152], very little has been made on the arms. We suggest more attention to arms with regards to low back pain, and also a synthesized point of view in future ergonomic researches.

#### **VI.4.2 The full-chain model as a way of ergonomic posture analysis**

One of the main findings of the overhead work simulation is that sum of all muscles' activation level varies significantly with different working postures. Here the muscle activations are estimated while solving the muscle-moment redundancy problem. Currently, the commonly used methods for this problem include static optimisation (SO), computed muscle control (CMC) and neuromusculoskeletal tracking (NMT) [153]. These methods are based on optimizations to minimize a given performance criterion. For SO and CMC, the criterion is the sum of squares of muscle activations [154], and for NMT, the criterion is the cumulative muscle efforts expressed in a cost function (see equation 11 in Seth & Pandey, (2007) [155]). The current study takes the SO method, which incorporates time-instant instead of time-dependency cases. It is very computationally efficient, and as concluded by Anderson and Pandey [154], it provides reasonable predictions of muscle forces and is hereby effective. The generated muscle activation could fairly be used as a representation of muscle effort.

The posture analysis benefits also from the whole-body muscle model. As illustrated above, the full-chain effect should be considered in physical assessments. The engagement of the whole-body muscle model would avoid the case that the position reduces efforts on one part while bring in extra efforts on another. The sum of all muscles' activation can be an good indicator of posture load when conducting posture analysis.

#### **VI.4.3 Overhead working**

Simulations of the six working postures indicate that the forward/backward reach (the L-C, L-F, H-C and H-F) postures are much more effort-demanding than the neutral reach (the L-M and H-M) postures (Table VI.3) in the overhead drilling task. This result suggests that the efforts spent on horizontal body balance takes a great portion in total efforts. The study of Maciukiewicz et al. (2016) [156] indi-



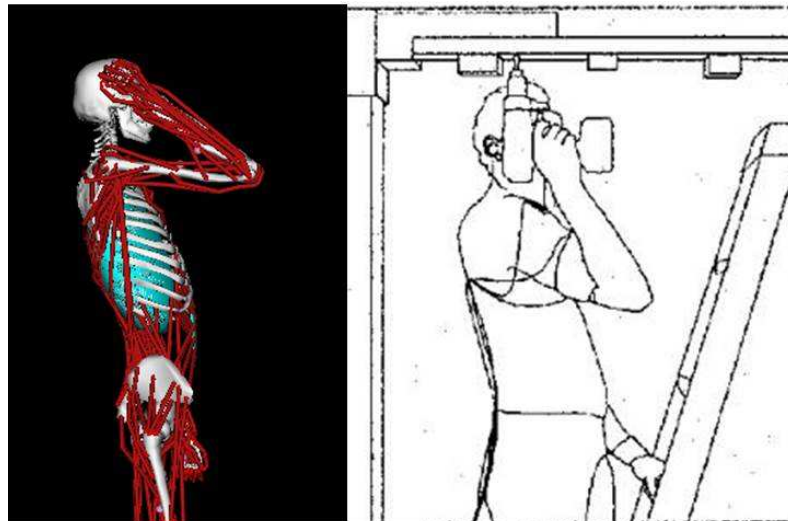


**Figure VI.8** – Backward drilling posture in current simulation (left) and in Anton’s work(right) [43].

cates that for upward overhead drilling, further forward reach distance results in greater muscle demands (measured by EMG of upper extremity muscles). Similar results were reported by Shin & Yoo [157]: overhead work with a forward reach distance of 30cm leads to stronger EMG activities of upper trapezius, lower trapezius, anterior deltoid and serratus anterior than that with the distance of 15cm.

The EMG activity of anterior deltoid was found to be less intensive with backward reach overhead drilling posture than that with neutral reach ones by Anton (2001) [43]. The finding is different from the result of current simulation (Table VI.4). Anton’s work was based on an experimental task simulation with 20 volunteers. One explanation is that in experiments, the subjects would turn their head right and look up towards the drilling point. Whereas in our simulation, no head movement is considered due to model limitation (Figure VI.8). The small difference would probably influence the anterior deltoid, which works to connect the neck and shoulder. Future work should be done to refine the movement of head and neck of the full-chain model.

Most previous researches on overhead drilling postures reported a significant difference in efforts demanded by low reach and by high reach [43, 157]. There are also exceptions. In the study of Maciukiewicz et al.(2016) [156], with the same working height, the standing posture with lower arm reach is found to go with more intensive muscle activities in compare with the sitting posture with higher arm height. In current simulation, the lower reach height is estimated to go with a bit more muscular efforts than the higher reach height in the case of far forward

reach. The diverse results indicate the complexity of posture analysis. No universal principle could apply to all practical cases. Biomachanical analysis based on detailed posture configuration should be conducted for job design.

Besides, the simulation result also reveals significantly different activation states for various head of a muscle branch (Table VI.4), which indicates different roles played by each head of muscles. Therefore, it is suggested that future researches avoid vague terms such as biceps, deltoids, but rather precisely down to the head of muscles.

## VI.5 Conclusions

This research introduces a full-chain OpenSim model. It consists of 45 body segments, 424 muscles and 39 degrees of freedom. This model was used to simulate an overhead drilling task. Results suggest that beside of shoulder elevation moment, shoulder rotation moment is also considerable during overhead drilling; and back muscles play an important role. In addition, the total muscle activations vary markedly with different postures for this task. Conclusions are drawn that the full-chain OpenSim model facilitates biomechanical analysis in three aspects: i) a comprehensive estimation of multi-degree-of-freedom joints' moments; ii) understanding how the muscles across body cooperate in motions; iii) optimizing working posture in view of total muscle efforts.

Future works will be done to optimize working postures under constraint of maximal muscle activity to minimize the worker fatigue or to adjust the behavior of exoskeleton mechanism attached to the worker. Indeed, a local assistant can remove local muscle constraint but increase the muscle activity, for another part body, and yields to new musculoskeleton disorder. Thus, the full-body muscle model with a motion capture system can also predict the dynamic muscle endurance times for complex task where many muscles are activated to produce the motion.

# VII

---

## Conclusions and Perspectives

### VII.1 Contributions

This thesis was devoted to the assessment of the physical risk of work-related MSDs. Work-related MSDs is an overexertion traumas that characterized with the accumulation effect of workload. Therefore, the muscle fatigue and working load analysis are taken as the two primary topics to study in this thesis. The biomechanical digital human modeling technique is identified as one of the most promising tools for ergonomic application in industry.

#### VII.1.1 Muscle fatigue

Muscle fatigue is the main physical manifestation of the workload accumulation. Concerns of the ergonomists interested in this area are how to predict the muscle fatigue before the workbench is fixed, and how to indicate the worker's muscle fatigue when the work is on. In this thesis, the indication of muscle fatigue is studied in chapter III, and the prediction of muscle fatigue is studied in chapter IV.

As the objective reflection of muscle status, the sEMG has long been used to indicate muscle fatigue. However, indicators extracted from sEMG have intrinsic limitations: the amplitude properties such as the RMS are influenced by both the intensity of the current output force and the muscle fatigue level; whereas the frequency properties such as the MPF change insignificantly in the fatiguing process with low efforts. This is a necessity to explore more indicators.

In the chapter III, a new fatigue indicator was conceived based on the sEMG amplitude properties. Two factors have been proven to influence the amplitude RMS of a fatiguing muscle: its fatigue level and its current-exerting force. The idea of the new indicator is to eliminate the force-induced RMS changes, for which two procedures are needed: the sEMG of the fresh muscle exerting the desired force as well as the sEMG of the fatiguing muscle when exerting the same force. The

difference of the RMSs of the two sEMG signals are considered to be represent the intensity of fatigue. The new indicator has been shown to increase with the fatigue intensifies. It could be used as a supplement of the current ones, especially for operations involving non-constant work loads.

In the chapter IV methods for the prior predictions of muscle fatigue is studied. A plug-in to OpenSim was written, which enables the estimation of the remaining muscle force capability in any fatiguing process. The plug-in benefits from the dynamic analysis process of the OpenSim: the inverse kinematics that generate the subject's body configurations, the inverse dynamics that calculate his joint moments, and the optimization algorithm that further distribute the joint moments down to individual muscle forces. Hence the force output history of each muscle is available. The plug-in applies the Force-load muscle fatigue model, so that the remaining force of each muscle could be estimated with considerations of its force history, its maximal voluntary contraction forces, and the subject's fatigability. The advantage of this plug-in is that the muscle capacity at each moment could be estimated and there is no limitation for the type of task. The muscle capacity current would work as the criterion to assess the worker's risk of overexertion.

### VII.1.2 Working posture analysis

It might be debatable whether muscle fatigue is avoidable or not. But enormous ergonomic researches have proven that the muscle fatigue is amendable to work postures. The hypothesis of this thesis is that for a given operation, there is an 'optimal' work posture accompanied with the least posture load. To examine this hypothesis, it is necessary to find out a indicator for the evaluation of posture load.

Two prerequisites are to be met for the indicator:

- for a certain posture, the loads on the whole body should be included into consideration, other than the loads merely on some body parts. This is to preclude the possibility that a posture that is considered as 'better' reduces load on one body parts while increases that on the other.
- the unit of the indicator should be normalized. This is because the capacity of body parts (muscles or joints) varies in a large scale. A load of 50 *N.m* means different for the elbow joint and the knee joint. There is a necessity to organize the weights of different body parts properly.

For the first request, a Full-chain musculoskeletal model is built up in chapter V. The model is based on the protocol of OpenSim. It consists of 45 body segments,

39 DoFs and 424 muscles that covers the main dynamic chain of human body. Its inertial parameters represent those of a male with 1.77 m height, 75 kg weight.

In OpenSim, when we want to adapt a general musculoskeletal model to a new worker, the inertial parameters are 'scaled' with the ratio of weight between the new worker and the general model. For example, the mass of the thigh of a subject of 75 kg is assumed to be 1.5 times larger than that of someone who is 50 kg, which is not always the truth. In this chapter, an experiment was conducted to evaluate the errors caused by this scaling method. A subject's body segment masses are determined with the help of 3D scan. The determined mass data as well as the proportionately scaled mass data is used to specify an OpenSim generic model to the subject model. Dynamic analysis on the two specific models are conducted with the same set of kinematic data separately. In a 1.2 s normal walking, the average computation difference of 18 joint moments between the two specific models are as large as 5.01%.

For the second request, the idea of indicating work load with the muscle activation level is proposed in the chapter VI. The muscle activation level is a normalized parameter (varies from 0 to 1) input to muscle contraction dynamics and determines the output muscle contraction force. It reflects the effort level made by the muscle. The average of the activation of all muscles can be the comprehensive indicator of posture load.

This proposition is tested with the developed Full-chain OpenSim model. Six postures to conducted a specific overhead drilling operation are simulated. The average activations of the 424 muscles varies markedly with the six posture: the 'worse' posture is marked with the average muscle activation level 2.47 times larger than that of the 'best' posture (6.92% to 2.80%). It is promising to optimize the posture with respect to the indicator.

Other benefits of the Full-chain model to the physical risk assessment of the MSDs include:

- A comprehensive estimation of multi-degree-of-freedom joints' moments, such as the shoulder joint. As suggested in the current simulation, the shoulder rotation moment of the overhead drilling operators is as considerable as the shoulder elevation moment, but is usually neglected in ergonomic analysis.
- Understanding how the muscles across body cooperate for a motion or posture, noted in this thesis as the 'full chain effect'. In the current simulation, intensive activations of the right latissimus dorsi are found in postures with forward or backward arm reach, other than the neutral. This implies the possible relationship between back loads and arm positions.

### VII.1.3 The framework of the MSDs physical risk assessment

This thesis seeks to develop the biomechanical methods of the MSDs physical risk assessment for the purpose of enabling efficient intervention at the stage of work design. The framework of the MSDs physical risk assessment is proposed based on the Full-chain musculoskeletal model, the Muscle fatigue analysis plugin, and the proposed fatigue sEMG indicator. The framework includes a sequence of 3 steps.

The first step means to minimize the load of single work unit. The virtual working environment with tools and operating platform as well as the digital operator is supposed to be constructed. The Full-chain musculoskeletal model is used as the generic model based on which the anthropometric data and fatigability of the operator is specified. For the working simulation, the task 'units', such as the static working postures and the repeated dynamic operating sequences are to be identified and simulated in the virtual environment. Then posture/motion optimization is conducted with respect to the average muscle activation level, while the risky body parts, i.e., the muscle groups simulated with high activation levels, are to be identified.

The second step means to properly arrange the time sequence of the task units with respect to the muscle capacity. The time sequence includes the frequency of the task units, the work/rest cycle, and the duration of the operation. The plugin described in chapter IV is to be applied on the determined time sequence to make sure that the remaining muscle force is above the operation demand. Attention should be paid to the high-risk muscle groups. Fatigability data should be specified according to the traits of the operator population.

After the design of task units and time sequence, a pilot trial is supposed to be conducted with prototype working platform. The sEMG indicator developed in chapter III could be used to assist the risk assessment in this step. The sEMG of the risk muscles should be collected both before and during the trial operation. The difference of the RMS of EMG signal when the muscles are fresh and when the muscle are fatiguing could indicate the intensity of muscle fatigue.

## VII.2 Further investigations and perspectives

The framework proposed above aims to involve the physical risk assessment of MSDs into work design. However, the effective application of the framework requires some more investigations.

Firstly, the build up of the virtual working environment is not yet planted into OpenSim. The normal simulation procedure of OpenSim is from the realistic

motion to the simulated motion: the motion capture system is used to identify the kinematic data. There is no module for the working platform easily-available like that in traditional digital human modeling softwares such as the DELMIA. This would reduce the effectiveness and efficiency of the industrial application of the proposed framework.

Key point of this problem is to identify the spatial location of the digital worker's reach point, i.e., the workspace configuration. OpenSim is an open-source platform. It is suggested here that more work should be done to contribute to the database of virtual environment and to the algorithms to specify the digital worker's workspace configuration.

Second, the posture is evaluated by its resulting average muscle activation level, which reflects the load on individual muscles. The muscle loads are computed by re-distributing the joint moments generated from inverse dynamics down to individual muscles. This is a redundant problem. The algorithm used here in OpenSim is by minimizing the sum of squared activation level of all muscles. Another example of optimization algorithm for this problem is the one that developed by Pontonnier & Dumont [158], which aims to minimize the relative muscle stress (the objective function see Equation VII.1,  $F_i$ : the force of muscle  $i$ ;  $F_{max}$ : the maximal force of muscle  $i$ ). Both the two algorithms arise from the belief that there is a certain control strategy of brain to conduct motions. In view that human is capable to repeat a motion with high accuracy, this belief is well accepted.

$$\min \quad f(F) = \sum_m \left( \frac{F_i}{(F_{max})_i} \right)^2 \quad (\text{VII.1})$$

However, there are still much space for improvement. For example, as Pontonnier & Dumont [159] have put it, the muscle co-contraction should be taken into account. Without the information on muscular antagonism, the computed activation of many muscles do not present as that they are in reality. Extra constraints are to be added to improve the algorithm.

Third, with the indicator proposed in chapter VI, we are able to appraise a working posture or motion. But for industrial application, the posture/motion optimization is expected. It is suggested here that future investigation should be taken to finalize the posture optimization algorithm, with the objective function as Equation VII.2 ( $a_i$ : the activation level of muscle  $i$ ).

$$\min \quad f(a) = m^{-1} \sum_m (a_i) \quad (\text{VII.2})$$

Fourth, with the plug-in developed in chapter IV, we estimate the real-time muscle capacity influenced by the effect of fatigue for the arrangement of time se-



quence of the optimized task unit. However, in reality the fatigued muscle would enter into a recovering process during the rest cycle. Future investigation should include muscle recovery into account.

Fifth, the database of population muscle fatigability is required for the muscle fatigue analysis. As stated in section II.7, more researches on the muscle fatigability is needed for predicting the fatiguing process of different populations. This also holds true for the proper arrangement of the working sequence for different worker populations.

Finally, the sEMG indicator proposed in chapter III shows qualitative relationship with muscle fatigue. But to assess the physical risk of MSDs posteriorly, further investigation is needed to build up quantitative relationship between the proposed indicator and muscle fatigue intensity.

# VIII

---

## Jing CHANG's publications

- Jing Chang, Damien Chablat, Liang Ma, and Bennis Fouad. Using 3D Scan to Determine Human Body Segment Mass in OpenSim Model. In 20th International Conference on Computer Interaction HCI, Las Vegas, United States, July 2018. URL <https://hal.archives-ouvertes.fr/hal-01771866>.
- Jing Chang, Damien Chablat, Fouad Bennis, and Liang Ma. Muscle Fatigue Analysis Using OpenSim. In 19th International Conference on Human-Computer Interaction, Vancouver, Canada, July 2017.  
URL <https://hal.archives-ouvertes.fr/hal-01521854>.
- Jing Chang, Damien Chablat, Fouad Bennis, and Liang Ma. Estimating the EMG response exclusively to fatigue during sustained static maximum voluntary contraction. In 7th International Conference on Applied Human Factors and Ergonomics, Orlando, United States, July 2016.  
URL <https://hal.archives-ouvertes.fr/hal-01319907>.
- Tsao L, Chang J, Ma L. Fatigue of Chinese railway employees and its influential factors: structural equation modelling[J]. Applied ergonomics, 2017, 62: 131-141.  
URL <https://doi.org/10.1016/j.apergo.2017.02.021>
- Tao Y, Chang J, Rau P L P. When China Encounters Smart TV: Exploring Factors Influencing the User Adoption in China[C]//International Conference on Cross-Cultural Design. Springer, Cham, 2014: 696-706.  
URL [https://doi.org/10.1007/978-3-319-07308-8\\_67](https://doi.org/10.1007/978-3-319-07308-8_67)



# Bibliography

- [1] Victor Hirsch Frankel and Margareta Nordin. *Basic biomechanics of the skeletal system*. Lea & Febiger, 1980. 5
- [2] Julian A Waller. Injury: conceptual shifts and preventive implications. *Annual review of public health*, 8(1):21–49, 1987. 5
- [3] Samuel R Hamner, Ajay Seth, and Scott L Delp. Muscle contributions to propulsion and support during running. *Journal of biomechanics*, 43(14):2709–2716, 2010. 11
- [4] Margaret E Raabe and Ajit MW Chaudhari. An investigation of jogging biomechanics using the full-body lumbar spine model: Model development and validation. *Journal of biomechanics*, 49(7):1238–1243, 2016. vii, 12, 85, 86
- [5] Katherine R Saul, Xiao Hu, Craig M Goehler, Meghan E Vidt, Melissa Daly, Anca Velisar, and Wendy M Murray. Benchmarking of dynamic simula-

- tion predictions in two software platforms using an upper limb musculoskeletal model. *Computer methods in biomechanics and biomedical engineering*, 18(13):1445–1458, 2015. vii, 12, 86, 88
- [6] Health and Safety at Work Act UK. Musculoskeletal disorders in great britain 2016/17, 2018. 19
- [7] EuropGip. Reporting of occupational diseases: Issues and good practices in five european countries, 2015. 19
- [8] M Maier and J Ross-Mota. Work related musculoskeletal disorders, oregon, 1990-2000, 2001. 19
- [9] Laura Punnett and David H Wegman. Work-related musculoskeletal disorders: the epidemiologic evidence and the debate. *Journal of electromyography and kinesiology*, 14(1):13–23, 2004. 19
- [10] William D. McKinney. Occupational injuries & illnesses report. Technical report, Commonwealth of Massachusetts, 2017. ix, 19, 20
- [11] Jason Devereux et al. *Work-related neck and upper limb: musculoskeletal disorders*. European Agency for Safety and Health at work, 1999. 19
- [12] Alex Burdorf. Exposure assessment of risk factors for disorders of the back in occupational epidemiology. *Scandinavian journal of work, environment & health*, pages 1–9, 1992. 20
- [13] Thomas J Armstrong, Peter Buckle, Lawrence J Fine, Mats Hagberg, Bengt Jonsson, Asa Kilbom, Ilkka AA Kuorinka, Barbara A Silverstein, Gisela Sjo-gaard, and Eira RA Viikari-Juntura. A conceptual model for work-related neck and upper-limb musculoskeletal disorders. *Scandinavian Journal of Work, Environment & Health*, pages 73–84, 1993. 20, 21

- 
- [14] Angelika Hauke, Julia Flintrop, Emmanuelle Brun, and Reiner Rugulies. The impact of work-related psychosocial stressors on the onset of musculoskeletal disorders in specific body regions: A review and meta-analysis of 54 longitudinal studies. *Work & Stress*, 25(3):243–256, 2011. 21
- [15] Sue Hignett and Lynn McAtamney. Rapid entire body assessment. In *Handbook of Human Factors and Ergonomics Methods*, pages 97–108. CRC Press, 2004. v, 23
- [16] Victor Z Priel. A numerical definition of posture. *Human Factors*, 16(6):576–584, 1974. 22
- [17] Osmo Karhu, Pekka Kansi, and Iikka Kuorinka. Correcting working postures in industry: a practical method for analysis. *Applied ergonomics*, 8(4):199–201, 1977. 22
- [18] EN Corlett, ? SJ MADELEY, and I Manenica. Posture targeting: a technique for recording working postures. *Ergonomics*, 22(3):357–366, 1979. 22
- [19] G Li. The development of practical tool for musculoskeletal risk assessment. *Contemporary ergonomics*, 1997. 22
- [20] Lynn McAtamney and E Nigel Corlett. Rula: a survey method for the investigation of work-related upper limb disorders. *Applied ergonomics*, 24(2):91–99, 1993. 23
- [21] M Christmansson. The hama-method: a new method for analysis of upper limb movements and risk for work-related musculoskeletal disorders. In *Proceedings of the 12th Triennial Congress of the International Ergonomics Association/Human Factors Association of Canada, August, Toronto*, pages 173–175, 1994. 23

- [22] Kristina Kemmlert. A method assigned for the identification of ergonomic hazards–plibel. *Applied Ergonomics*, 26(3):199–211, 1995. 23
- [23] Guangyan Li and Peter Buckle. Current techniques for assessing physical exposure to work-related musculoskeletal risks, with emphasis on posture-based methods. *Ergonomics*, 42(5):674–695, 1999. ix, 23, 24
- [24] Danuta Roman-Liu. Comparison of concepts in easy-to-use methods for msd risk assessment. *Applied ergonomics*, 45(3):420–427, 2014. ix, 26
- [25] Dohyung Kee and Waldemar Karwowski. Luba: an assessment technique for postural loading on the upper body based on joint motion discomfort and maximum holding time. *Applied Ergonomics*, 32(4):357–366, 2001. 25, 26
- [26] NJ Delleman, M Boocock, and B Kapitaniak. Evaluation of working postures in relation to machinery. In *Proc. of the XIVth Triennial Congress of the INT. Ergonomics Ass. and the 44th annual Meeting of the Human Factors and Ergonomics Society*, 444-445, 2000. 26
- [27] Alison M Trinkoff, Jane A Lipscomb, Jeanne Geiger-Brown, Carla L Storr, and Barbara A Brady. Perceived physical demands and reported musculoskeletal problems in registered nurses. *American journal of preventive medicine*, 24(3):270–275, 2003. 27
- [28] Alireza Choobineh, Abdolreza Rajaeefard, and Masoud Neghab. Association between perceived demands and musculoskeletal disorders among hospital nurses of shiraz university of medical sciences: a questionnaire survey. *International Journal of Occupational Safety and Ergonomics*, 12(4):409–416, 2006. 27
- [29] Il-Ho Kim, Jeanne Geiger-Brown, Alison Trinkoff, and Carles Muntaner. Physically demanding workloads and the risks of musculoskeletal disor-

- 
- ders in homecare workers in the usa. *Health & social care in the community*, 18(5):445–455, 2010. 27
- [30] Alireza Choobineh, Mehrnoosh Movahed, Sayed Hamidreza Tabatabaie, and Masaharu Kumashiro. Perceived demands and musculoskeletal disorders in operating room nurses of shiraz city hospitals. *Industrial health*, 48(1):74–84, 2010. 27
- [31] Robert Karasek. Job content questionnaire user’s guide. *Department of Work Environemnt*, 1985. 27
- [32] E Nigel Corlett and RP Bishop. A technique for assessing postural discomfort. *Ergonomics*, 19(2):175–182, 1976. 27
- [33] Gunnar Borg. *Borg’s perceived exertion and pain scales*. Human kinetics, 1998. 27
- [34] Elizabeth Åhsberg, Francesco Garnberale, and Anders Kjellberg. Perceived quality of fatigue during different occupational tasks development of a questionnaire. *International journal of industrial ergonomics*, 20(2):121–135, 1997. 27
- [35] Tove Østensvik, Kaj Bo Veiersted, and Petter Nilsen. Association between numbers of long periods with sustained low-level trapezius muscle activity and neck pain. *Ergonomics*, 52(12):1556–1567, 2009. 29
- [36] Göran M Hägg and Annika Åström. Load pattern and pressure pain threshold in the upper trapezius muscle and psychosocial factors in medical secretaries with and without shoulder/neck disorders. *International archives of occupational and environmental health*, 69(6):423–432, 1997. 29
- [37] Kaj B Veiersted, Rolf H Westgaard, and Per Andersen. Electromyographic evaluation of muscular work pattern as a predictor of trapezius myalgia.



- Scandinavian journal of work, environment & health*, pages 284–290, 1993. 29
- [38] Corinne Nicoletti, Christina M Spengler, and Thomas Läubli. Physical workload, trapezius muscle activity, and neck pain in nurses' night and day shifts: A physiological evaluation. *Applied ergonomics*, 45(3):741–746, 2014. 29
- [39] Ingrid Åkesson, Istvan Balogh, and G-Å Hansson. Physical workload in neck, shoulders and wrists/hands in dental hygienists during a work-day. *Applied ergonomics*, 43(4):803–811, 2012. 29
- [40] Etienne Grandjean and Karl HE Kroemer. *Fitting the task to the human: a textbook of occupational ergonomics*. CRC press, 1997. 29
- [41] Jeannette Unge Byström, Gert-Åke Hansson, Lars Rylander, Kerstina Ohlsson, Gabriella Källrot, and Staffan Skerfving. Physical workload on neck and upper limb using two cad applications. *Applied ergonomics*, 33(1):63–74, 2002. 29
- [42] Liang Ma, Wei Zhang, Damien Chablat, Fouad Bennis, and François Guillaume. Multi-objective optimisation method for posture prediction and analysis with consideration of fatigue effect and its application case. *Computers & Industrial Engineering*, 57(4):1235–1246, 2009. v, 30, 79
- [43] Dan Anton, Lee D Shibley, Nathan B Fethke, Jennifer Hess, Thomas M Cook, and John Rosecrance. The effect of overhead drilling position on shoulder moment and electromyography. *Ergonomics*, 44(5):489–501, 2001. vii, 30, 108, 109, 113, 116
- [44] D.B. Chaffin, G.B.J. Andersson, and B.J. Martin. *Occupational Biomechanics*. Wiley, 1999. v, 30, 31, 38, 47

- 
- [45] Kai-Nan An, Edmund YS Chao, Bernard F Morrey, et al. Hand position affects elbow joint load during push-up exercise. *Journal of biomechanics*, 26(6):625–632, 1993. 31
- [46] Felix E Zajac. Muscle and tendon properties models scaling and application to biomechanics and motor. *Critical reviews in biomedical engineering*, 17(4):359–411, 1989. vi, 32, 33, 34, 74
- [47] RE Burke et al. Motor units: anatomy, physiology, and functional organization. *Handbook of physiology. The nervous system. Motor control*, 3:345–422, 1981. 32
- [48] Archibald Vivian Hill. The heat of shortening and the dynamic constants of muscle. *Proc. R. Soc. Lond. B*, 126(843):136–195, 1938. 34
- [49] DR Wilkie. The mechanical properties of muscle. *British medical bulletin*, 12(3):177–182, 1956. 34
- [50] JM Ritchie and DR Wilkie. The dynamics of muscular contraction. *The Journal of physiology*, 143(1):104–113, 1958. 34
- [51] Darryl G Thelen et al. Adjustment of muscle mechanics model parameters to simulate dynamic contractions in older adults. *Transactions-American Society Of Mechanical Engineers Journal Of Biomechanical Engineering*, 125(1):70–77, 2003. vi, 34, 35
- [52] S Ebashi and Mi Endo. Calcium and muscle contraction. *Progress in biophysics and molecular biology*, 18:123–183, 1968. 35
- [53] Jack M Winters. An improved muscle-reflex actuator for use in large-scale neuromusculoskeletal models. *Annals of biomedical engineering*, 23(4):359–374, 1995. 35

- [54] Jan Karlsson and Bengt Saltin. Lactate, atp, and cp in working muscles during exhaustive exercise in man. *Journal of Applied Physiology*, 29(5):598–602, 1970. 39
- [55] J Karlsson, CULLIE F Funderburk, BIRGITTA Essen, and ALEXANDER R Lind. Constituents of human muscle in isometric fatigue. *Journal of Applied Physiology*, 38(2):208–211, 1975. 39
- [56] Jerrold Scott Petrofsky, Roger M Glaser, Chandler A Phillips, Alexander R. Lind, and Carole Williams. Evaluation of the amplitude and frequency components of the surface emg as an index of muscle fatigue. *Ergonomics*, 25(3):213–223, 1982. 39, 40, 69
- [57] TOSHIO Moritani, MASUO Muro, and AKIRA Nagata. Intramuscular and surface electromyogram changes during muscle fatigue. *Journal of Applied Physiology*, 60(4):1179–1185, 1986. 39, 42, 63
- [58] Toshio Moritani, Akira Nagata, and Masuo Muro. Electromyographic manifestations of muscular fatigue. *Medicine and Science in Sports and Exercise*, 14(3):198–202, 1981. 39
- [59] TOMMY Öberg, LEIF SANDSJÖ, and Roland Kadefors. Subjective and objective evaluation of shoulder muscle fatigue. *Ergonomics*, 37(8):1323–1333, 1994. 39, 41, 62
- [60] Lee S Caldwell, Don B Chaffin, Francis N Dukes-Dobos, KHE Kroemer, Lloyd L Laubach, Stover H Snook, and Donald E Wasserman. A proposed standard procedure for static muscle strength testing. *American industrial hygiene association journal*, 35(4):201–206, 1974. 39
- [61] Maury A Nussbaum et al. Effects of age, gender, and task parameters on fatigue development during intermittent isokinetic torso extensions. *Interna-*

- 
- tional journal of industrial ergonomics*, 39(1):185–191, 2009. 40
- [62] H Iridiastadi and MA Nussbaum. Muscle fatigue and endurance during repetitive intermittent static efforts: development of prediction models. *Ergonomics*, 49(4):344–360, 2006. 40, 62, 63, 69
- [63] Maury A Nussbaum. Static and dynamic myoelectric measures of shoulder muscle fatigue during intermittent dynamic exertions of low to moderate intensity. *European journal of applied physiology*, 85(3):299–309, 2001. 40, 41, 62
- [64] Keijo Häkkinen and Paavo V Komi. Effects of fatigue and recovery on electromyographic and isometric force-and relaxation-time characteristics of human skeletal muscle. *European journal of applied physiology and occupational physiology*, 55(6):588–596, 1986. 40
- [65] Olivier Maisetti, Arnaud Guével, Patrick Legros, and Jean-Yves Hogrel. Prediction of endurance capacity of quadriceps muscles in humans using surface electromyogram spectrum analysis during submaximal voluntary isometric contractions. *European journal of applied physiology*, 87(6):509–519, 2002. 40
- [66] W West, A Hicks, L Clements, and J Dowling. The relationship between voluntary electromyogram, endurance time and intensity of effort in isometric handgrip exercise. *European journal of applied physiology and occupational physiology*, 71(4):301–305, 1995. 40
- [67] Claes Krogh-Lund and Kurt Jørgensen. Changes in conduction velocity, median frequency, and root mean square-amplitude of the electromyogram during 25% maximal voluntary contraction of the triceps brachii muscle, to limit of endurance. *European journal of applied physiology and occupational physiology*, 63(1):60–69, 1991. 40

- [68] Deepti Sood, Maury A Nussbaum, and Kris Hager. Fatigue during prolonged intermittent overhead work: reliability of measures and effects of working height. *Ergonomics*, 50(4):497–513, 2007. 40
- [69] Carlo J De Luca. Physiology and mathematics of myoelectric signals. *IEEE Transactions on Biomedical Engineering*, 26(6):313–325, 1979. 41, 62, 71
- [70] Mario Cifrek, Vladimir Medved, Stanko Tonković, and Saša Ostojić. Surface emg based muscle fatigue evaluation in biomechanics. *Clinical Biomechanics*, 24(4):327–340, 2009. 41, 62
- [71] Carlo J De Luca. Spectral compression of the emg signal as an index of muscle fatigue. In *Neuromuscular fatigue. Proceedings of the symposium*, pages 44–51. Royal Netherlands Academy of Art and Sciences, 1992. 41, 62
- [72] John V Basmajian and CJ De Luca. *Muscles alive*. Williams & Wilkins, 1985. 41, 62
- [73] LR Brody, MARK T Pollock, SERGE H Roy, CJ De Luca, and B Celli. ph-induced effects on median frequency and conduction velocity of the myoelectric signal. *Journal of Applied Physiology*, 71(5):1878–1885, 1991. 41, 62
- [74] B Bigland-Ritchie, F Furbush, and JJ Woods. Fatigue of intermittent submaximal voluntary contractions: central and peripheral factors. *Journal of Applied Physiology*, 61(2):421–429, 1986. 41, 62, 69
- [75] Åsa Dederig, Gunnar Németh, and Karin Harms-Ringdahl. Correlation between electromyographic spectral changes and subjective assessment of lumbar muscle fatigue in subjects without pain from the lower back. *Clinical Biomechanics*, 14(2):103–111, 1999. 41, 62

- 
- [76] Carlo J De Luca. The use of surface electromyography in biomechanics. *Journal of applied biomechanics*, 13(2):135–163, 1997. 42, 62
- [77] Jane A Kent-Braun. Central and peripheral contributions to muscle fatigue in humans during sustained maximal effort. *European journal of applied physiology and occupational physiology*, 80(1):57–63, 1999. 42, 63, 70
- [78] Anthony S Wexler, Jun Ding, and Stuart A Binder-Macleod. A mathematical model that predicts skeletal muscle force. *IEEE transactions on biomedical engineering*, 44(5):337–348, 1997. 42
- [79] Yohanan Giat, Joseph Mizrahi, and Mark Levy. A musculotendon model of the fatigue profiles of paralyzed quadriceps muscle under fes. *IEEE transactions on biomedical engineering*, 40(7):664–674, 1993. 42
- [80] Inmaculada Rodríguez, Ronan Boulic, and Daniel Meziat. A model to assess fatigue at joint-level using the half-joint concept. In *Proceedings of Humanoids 2003*, pages 97–105, 2003. 42
- [81] Jing Z Liu, Robert W Brown, and Guang H Yue. A dynamical model of muscle activation, fatigue, and recovery. *Biophysical journal*, 82(5):2344–2359, 2002. 42
- [82] Liang Ma, Damien Chablat, Fouad Bennis, and Wei Zhang. A new simple dynamic muscle fatigue model and its validation. *International Journal of Industrial Ergonomics*, 39(1):211–220, 2009. 42, 62
- [83] Liang Ma, Damien Chablat, Fouad Bennis, Wei Zhang, Bo Hu, and François Guillaume. A novel approach for determining fatigue resistances of different muscle groups in static cases. *International Journal of Industrial Ergonomics*, 41(1):10–18, 2011. ix, 43, 47, 48, 62

- [84] Walter Rohmert. Ermittlung von erholungspausen für statische arbeit des menschen. *Internationale Zeitschrift fuer Angewandte Physiologie einschliesslich Arbeitsphysiologie*, 18(2):123–164, 1960. 43, 47
- [85] Ruina Ma, Damien Chablat, Fouad Bennis, and Liang Ma. Human muscle fatigue model in dynamic motions. In *Latest Advances in Robot Kinematics*, pages 349–356. Springer, 2012. 43
- [86] Deep Seth, Damien Chablat, Fouad Bennis, Sophie Sakka, Marc Jubeau, and Antoine Nordez. New dynamic muscle fatigue model to limit musculo-skeletal disorder. In *Proceedings of the 2016 Virtual Reality International Conference*, page 26. ACM, 2016. vi, 44, 45
- [87] Liang Ma and Jing Chang. Measurement of subject-specific local muscle fatigability. *Advances in Physical Ergonomics and Human Factors: Part II.*, 15:215–220, 2014. 46
- [88] Tejin Yoon, Ryan Doyel, Claire Widule, and Sandra K Hunter. Sex differences with aging in the fatigability of dynamic contractions. *Experimental gerontology*, 70:1–10, 2015. 46, 47
- [89] Jane A Kent-Braun, Alexander V Ng, Julie W Doyle, and Theodore F Towse. Human skeletal muscle responses vary with age and gender during fatigue due to incremental isometric exercise. *Journal of Applied Physiology*, 93(5):1813–1823, 2002. 46, 47
- [90] Liang Ma, Wei Zhang, Bo Hu, Damien Chablat, Fouad Bennis, and François Guillaume. Determination of subject-specific muscle fatigue rates under static fatiguing operations. *Ergonomics*, 56(12):1889–1900, 2013. 48, 62
- [91] C Godin and J Chiang. The use of digital human models for advanced industrial applications. *Handbook of DIGITAL HUMAN MODELING, USA: Taylor*

- 
- and Francis*, pages 39–1, 2009. 49
- [92] PW Ryan and WE Springer. Cockpit geometry evaluation final report. *Vol. V, JANAIR Report*, 69105, 1969. 49
- [93] Don B Chaffin, Kerry E Kilpatrick, and Walton M Hancock. A computer-assisted manual work-design model. *AIIE Transactions*, 2(4):348–354, 1970. 50
- [94] EC Kingsley, NA Schofield, and K Case. A computer aid for man machine modelling. *ACM SIGGRAPH Computer Graphics*, 15(3):163–169, 1981. 50
- [95] MC Bonney, CaA Blunsdon, K Case, and JM Porter. Man-machine interaction in work systems. *International Journal of Production Research*, 17(6):619–629, 1979. 50
- [96] SM Evans and DB Chaffin. A method for integrating ergonomic operator information within the manufacturing design process. In *Proceedings of the HE Conference, Chicago, IL*, 1985. 50
- [97] A Coblenz, R Mollard And, and C Renaud. Ergoman: 3-d representation of human operator and man-machine systems. *International Journal of Human Factors in Manufacturing*, 1(2):167–178, 1991. 50
- [98] Norman I Badler, Cary B Phillips, and Bonnie Lynn Webber. *Simulating humans: computer graphics animation and control*. Oxford University Press, 1993. 50
- [99] Heiner Bubb and F Fritzsche. A scientific perspective of digital human models: past, present, and future. *Handbook of Digital Human Modeling: Research for Applied Ergonomics and Human Factors Engineering*, 3, 2009. 51



- [100] John Rasmussen, Michael Damsgaard, Egidijus Surma, Søren T Christensen, Mark de Zee, and Vit Vondrak. Anybody-a software system for ergonomic optimization. In *Fifth World Congress on Structural and Multidisciplinary Optimization*, volume 4. Citeseer, 2003. 54
- [101] Michael Damsgaard, John Rasmussen, Søren Tørholm Christensen, Egidijus Surma, and Mark De Zee. Analysis of musculoskeletal systems in the anybody modeling system. *Simulation Modelling Practice and Theory*, 14(8):1100–1111, 2006. 54
- [102] Scott L Delp, Frank C Anderson, Allison S Arnold, Peter Loan, Ayman Habib, Chand T John, Eran Guendelman, and Darryl G Thelen. Opensim: open-source software to create and analyze dynamic simulations of movement. *IEEE transactions on biomedical engineering*, 54(11):1940–1950, 2007. 54
- [103] Scott L Delp, Frank C Anderson, Allison S Arnold, Peter Loan, Ayman Habib, Chand T John, Eran Guendelman, and Darryl G Thelen. Opensim: open-source software to create and analyze dynamic simulations of movement. *IEEE transactions on biomedical engineering*, 54(11):1940–1950, 2007. 56
- [104] Dan Lämkkull, Lars Hanson, and Roland Örtengren. The influence of virtual human model appearance on visual ergonomics posture evaluation. *Applied Ergonomics*, 38(6):713–722, 2007. 56
- [105] Jingzhou Yang, Esteban Pena Pitarch, Joo Kim, and Karim Abdel-Malek. Posture prediction and force/torque analysis for human hands. Technical report, SAE Technical Paper, 2006. 56
- [106] Patrick Chedmail, Damien Chablat, and Christophe Le Roy. A distributed approach for access and visibility task with a manikin and a robot in a virtual

- 
- reality environment. *IEEE Transactions on Industrial Electronics*, 50(4):692–698, 2003. 56
- [107] Heiner Bubb, Florian Engstler, Florian Fritzsche, Christian Mergl, Olaf Sabbah, Peter Schaefer, and Iris Zacher. The development of ramsis in past and future as an example for the cooperation between industry and university. *International Journal of Human Factors Modelling and Simulation*, 1(1):140–157, 2006. 56
- [108] Sc C Gandevia. Spinal and supraspinal factors in human muscle fatigue. *Physiological reviews*, 81(4):1725–1789, 2001. 63
- [109] B Bigland-Ritchie, R Johansson, OC Lippold, and JJ Woods. Contractile speed and emg changes during fatigue of sustained maximal voluntary contractions. *Journal of neurophysiology*, 50(1):313–324, 1983. 63
- [110] JJ Woods and B Bigland-Ritchie. Linear and non-linear surface emg/force relationships in human muscles. an anatomical/functional argument for the existence of both. *American journal of physical medicine*, 62(6):287–299, 1983. 68
- [111] Emer P Doheny, Madeleine M Lowery, David P FitzPatrick, and Mark J O’Malley. Effect of elbow joint angle on force–emg relationships in human elbow flexor and extensor muscles. *Journal of Electromyography and Kinesiology*, 18(5):760–770, 2008. 68
- [112] Amedeo Troiano, Francesco Naddeo, Erik Sosso, Gianfranco Camarota, Roberto Merletti, and Luca Mesin. Assessment of force and fatigue in isometric contractions of the upper trapezius muscle by surface emg signal and perceived exertion scale. *Gait & posture*, 28(2):179–186, 2008. 68

- [113] JA Stephens and A Taylor. Fatigue of maintained voluntary muscle contraction in man. *The Journal of physiology*, 220(1):1–18, 1972. 70
- [114] B Bigland-Ritchie, R Johansson, OC Lippold, and JJ Woods. Contractile speed and emg changes during fatigue of sustained maximal voluntary contractions. *Journal of neurophysiology*, 50(1):313–324, 1983. 70
- [115] B Bigland-Ritchie. Emg and fatigue of human voluntary and stimulated contractions. *Human muscle fatigue: physiological mechanisms*, pages 130–156, 1981. 70
- [116] TOSHIO Moritani, MASUO Muro, and AKIRA Nagata. Intramuscular and surface electromyogram changes during muscle fatigue. *Journal of Applied Physiology*, 60(4):1179–1185, 1986. 69, 70
- [117] H Peter Clamann. Activity of single motor units during isometric tension. *Neurology*, 20(3):254–254, 1970. 71
- [118] LENNART Grimby and J Hannerz. Firing rate and recruitment order of toe extensor motor units in different modes of voluntary contraction. *The Journal of physiology*, 264(3):865–879, 1977. 71
- [119] Alexander Gydikov and Dimiter Kosarov. Some features of different motor units in human biceps brachii. *Pflügers Archiv*, 347(1):75–88, 1974. 71
- [120] Samuel R Hamner, Ajay Seth, and Scott L Delp. Muscle contributions to propulsion and support during running. *Journal of biomechanics*, 43(14):2709–2716, 2010. 75, 79, 85
- [121] Ruina Ma. *Modélisation de la fatigue musculaire dynamique et son application pour lâŽžanalyse ergonomique*. PhD thesis, Ecole Centrale de Nantes (ECN), 2012. 79

- 
- [122] Jason R Fuller, Karen V Lomond, Joyce Fung, and Julie N Côté. Posture-movement changes following repetitive motion-induced shoulder muscle fatigue. *Journal of Electromyography and Kinesiology*, 19(6):1043–1052, 2009. 79
- [123] Herman Pontzer, John H Holloway, David A Raichlen, and Daniel E Lieberman. Control and function of arm swing in human walking and running. *Journal of Experimental Biology*, 212(4):523–534, 2009. 85
- [124] Richard N Hinrichs, Peter R Cavanagh, and Keith R Williams. Upper extremity function in running. i: center of mass and propulsion considerations. *International Journal of Sport Biomechanics*, 3(3):222–241, 1987. 85
- [125] Christopher J Arellano and Rodger Kram. The effects of step width and arm swing on energetic cost and lateral balance during running. *Journal of biomechanics*, 44(7):1291–1295, 2011. 85
- [126] T Robert, L Chèze, R Dumas, and J-P Verriest. Validation of net joint loads calculated by inverse dynamics in case of complex movements: application to balance recovery movements. *Journal of biomechanics*, 40(11):2450–2456, 2007. 85
- [127] Miguel Christophy, Nur Adila Faruk Senan, Jeffrey C Lotz, and Oliver M O’Reilly. A musculoskeletal model for the lumbar spine. *Biomechanics and modeling in mechanobiology*, 11(1-2):19–34, 2012. 85
- [128] Edith M Arnold, Samuel R Ward, Richard L Lieber, and Scott L Delp. A model of the lower limb for analysis of human movement. *Annals of biomedical engineering*, 38(2):269–279, 2010. 85
- [129] Charles E Clauser, John T McConville, and John W Young. Weight, volume, and center of mass of segments of the human body. Technical report, Antioch Coll Yellow Springs OH, 1969. 95, 99

- [130] Paolo De Leva. Adjustments to zatsiorsky-seluyanov's segment inertia parameters. *Journal of biomechanics*, 29(9):1223–1230, 1996. 95, 99, 102, 104
- [131] Hidetaka Okada. Body segment inertia properties of japanese elderly. *Biomechinsm*, 13:125–138, 1996. 95, 99, 104
- [132] Jennifer L Durkin, James J Dowling, et al. Analysis of body segment parameter differences between four human populations and the estimation errors of four popular mathematical models. *Transactions-American Society of Mechanical Engineers Journal of Biomechanical Engineering*, 125(4):515–522, 2003. 95, 99, 102
- [133] Rudolfs Drillis, Renato Contini, and Maurice Bluestein. *Body segment parameters*. New York University, School of Engineering and Science Research Division, NY, 1966. 96
- [134] Scott L Delp, J Peter Loan, Melissa G Hoy, Felix E Zajac, Eric L Topp, and Joseph M Rosen. An interactive graphics-based model of the lower extremity to study orthopaedic surgical procedures. *IEEE Transactions on Biomedical engineering*, 37(8):757–767, 1990. 98
- [135] Chand T John, Ajay Seth, Michael H Schwartz, and Scott L Delp. Contributions of muscles to mediolateral ground reaction force over a range of walking speeds. *Journal of biomechanics*, 45(14):2438–2443, 2012. 98
- [136] Chen Wei and Robert K Jensen. The application of segment axial density profiles to a human body inertia model. *Journal of biomechanics*, 28(1):103–108, 1995. 99, 101
- [137] Mei Kay Lee, Ngoc Sang Le, Anthony C Fang, and Michael TH Koh. Measurement of body segment parameters using dual energy x-ray absorptiome-

- 
- try and three-dimensional geometry: An application in gait analysis. *Journal of Biomechanics*, 42(3):217–222, 2009. 102
- [138] Peter L Davidson, Suzanne J Wilson, Barry D Wilson, and David J Chalmers. Estimating subject-specific body segment parameters using a 3-dimensional modeller program. *Journal of biomechanics*, 41(16):3506–3510, 2008. 102
- [139] David J Pearsall and Gavin Reid. The study of human body segment parameters in biomechanics. *Sports Medicine*, 18(2):126–140, 1994. 102
- [140] Jennifer L Durkin, James J Dowling, and David M Andrews. The measurement of body segment inertial parameters using dual energy x-ray absorptiometry. *Journal of biomechanics*, 35(12):1575–1580, 2002. 102
- [141] Henry C Lukaski. Methods for the assessment of human body composition: traditional and new. *The American journal of clinical nutrition*, 46(4):537–556, 1987. 102
- [142] Rogier M Van Rijn, Bionka MA Huisstede, Bart W Koes, and Alex Burdorf. Associations between work-related factors and specific disorders of the shoulder? a systematic review of the literature. *Scandinavian journal of work, environment & health*, pages 189–201, 2010. 107, 113
- [143] Bruce P Bernard et al. Musculoskeletal disorders and workplace factors: a critical review of epidemiologic evidence for work-related musculoskeletal disorders of the neck, upper extremity, and low back. In *Musculoskeletal disorders and workplace factors: a critical review of epidemiologic evidence for work-related musculoskeletal disorders of the neck, upper extremity, and low back*. NIOSH, 1997. 107, 113
- [144] Peter Herberts, Roland Kadefors, Gun Andersson, and Ingemar Petersén. Shoulder pain in industry: an epidemiological study on welders. *Acta Or-*

- thopaedica Scandinavica*, 52(3):299–306, 1981. 107
- [145] David Rempel, Demetra Star, Alan Barr, Marco Mendoza Blanco, and Ira Janowitz. Field evaluation of a modified intervention for overhead drilling. *Journal of Occupational and Environmental Hygiene*, 7(4):194–202, 2010. 107
- [146] Bruce F Walker. The prevalence of low back pain: a systematic review of the literature from 1966 to 1998. *Clinical Spine Surgery*, 13(3):205–217, 2000. 115
- [147] Simon Dagenais, Jaime Caro, and Scott Haldeman. A systematic review of low back pain cost of illness studies in the united states and internationally. *The spine journal*, 8(1):8–20, 2008. 115
- [148] Gunnar BJ Andersson. Epidemiological features of chronic low-back pain. *The lancet*, 354(9178):581–585, 1999. 115
- [149] Kyung Ja June and Sung-Hyun Cho. Low back pain and work-related factors among nurses in intensive care units. *Journal of Clinical Nursing*, 20(3-4):479–487, 2011. 115
- [150] France Tissot, Karen Messing, and S Stock. Studying the relationship between low back pain and working postures among those who stand and those who sit most of the working day. *Ergonomics*, 52(11):1402–1418, 2009. 115
- [151] Wilhelmina E Hoogendoorn, Paulien M Bongers, Henrica CW de Vet, Marjolein Douwes, Bart W Koes, Mathilde C Miedema, Geertje AM Ariëns, and Lex M Bouter. Flexion and rotation of the trunk and lifting at work are risk factors for low back pain: results of a prospective cohort study. *Spine*, 25(23):3087–3092, 2000. 115

- 
- [152] R. Wells, Norman R., Neuman P., Andrews D., Frank J., Shannon H., and Kerr M. Assessment of physical work load in epidemiologic studies: common measurement metrics for exposure assessment. *Ergonomics*, 40(1):51–61, 1997. PMID: 8995047. 115
- [153] Yi-Chung Lin, Tim W Dorn, Anthony G Schache, and Marcus G Pandy. Comparison of different methods for estimating muscle forces in human movement. *Proceedings of the Institution of Mechanical Engineers, Part H: Journal of Engineering in Medicine*, 226(2):103–112, 2012. 115
- [154] Frank C Anderson and Marcus G Pandy. Dynamic optimization of human walking. *Journal of biomechanical engineering*, 123(5):381–390, 2001. 115
- [155] Ajay Seth and Marcus G Pandy. A neuromusculoskeletal tracking method for estimating individual muscle forces in human movement. *Journal of biomechanics*, 40(2):356–366, 2007. 115
- [156] Jacquelyn M Maciukiewicz, Alan C Cudlip, Jaclyn N Chopp-Hurley, and Clark R Dickerson. Effects of overhead work configuration on muscle activity during a simulated drilling task. *Applied ergonomics*, 53:10–16, 2016. 115, 116
- [157] Seung-Je Shin and Won-Gyu Yoo. Effects of overhead work involving different heights and distances on neck and shoulder muscle activity. *Work*, 51(2):321–326, 2015. 116
- [158] Charles Pontonnier and Georges Dumont. From motion capture to muscle forces in the human elbow aimed at improving the ergonomics of workstations. *Virtual and Physical prototyping*, 5(3):113–122, 2010. 123
- [159] Charles Pontonnier and Georges Dumont. Inverse dynamics method using optimization techniques for the estimation of muscles forces involved in the



elbow motion. *International Journal on Interactive Design and Manufacturing (IJIDeM)*, 3(4):227, 2009. 123

---

**Title :** The Risk Assessment of Work-related Musculoskeletal Disorders based on OpenSim

**Keywords :** Musculoskeletal model, muscle fatigue, work design, work load, posture, load analysis, OpenSim

Les troubles musculo-squelettiques liés au travail causent des maladies physiques et mentales chez les travailleurs, réduisent leur productivité et causent de grandes pertes aux industries et à la société. Cette thèse porte sur l'évaluation du risque physique de troubles musculo-squelettiques liés au travail, pour laquelle quatre points clés sont identifiés : la mesure de la charge de travail, l'évaluation de l'effet de l'accumulation de la charge de travail, la quantification des caractéristiques individuelles et l'intégration de l'évaluation des risques dans les outils de modélisation numérique humaine. Dans l'état de l'art, les études épidémiologiques des désordres musculo-squelettiques et les méthodes actuelles utilisées pour l'évaluation des risques physiques sont présentées, ainsi que les études concernant les quatre points clés. La deuxième partie présente une étude expérimentale portant sur 17 sujets afin d'explorer un nouvel indicateur de la fatigue musculaire avec EMG de surface. Dans la partie suivante, des développements sont faits pour intégrer

un modèle de fatigue musculaire dans OpenSim, un logiciel de modélisation humaine numérique, avec lequel la diminution de capacité de chaque muscle est prévisible pour une tâche donnée. Les valeurs prévues peuvent s'appliquer à l'évaluation des risques physiques. La quatrième partie présente le travail de construction d'un modèle musculo-squelettique à chaîne complète dans OpenSim, étant donné qu'aucun modèle actuel ne couvre les muscles du torse et tous les membres. Une attention particulière est portée à la méthode utilisée par OpenSim pour adapter les propriétés inertielles du modèle aux individus. Les erreurs de la méthode sont évaluées à l'aide des données de référence provenant du scanner 3D du corps entier. Dans la dernière partie, le nouveau modèle de la chaîne complète est appliqué à l'analyse de la posture d'une tâche de perçage en hauteur. L'activité musculaire varie en fonction des postures, ce qui est suggéré comme indicateur des charges posturales.

---

**Title :** The Risk Assessment of Work-related Musculoskeletal Disorders based on OpenSim

**Keywords :** Musculoskeletal model, muscle fatigue, work design, work load, posture, load analysis, OpenSim model

Work-related musculoskeletal disorders cause physical and mental illnesses in workers, reduce their productivity and cause great losses to industries and society. This thesis focuses on the assessment of the physical risk of work-related musculoskeletal disorders in industry, for which four key points are identified: measuring workloads, assessing the effect of workload accumulation, quantifying individual characteristics and integrating the risk assessment into digital human modeling tools. In the state of the art, the epidemiologic studies of musculoskeletal disorders and the current methods used for its physical risk assessment are reviewed, as well as the studies concerning the four key points. The second part presents an experimental study involving 17 subjects to explore a new indicator to muscle fatigue with surface EMG. In the next part, efforts are made

to integrate a muscle fatigue model into OpenSim, a digital human modeling software, with which the capacity decrease of each muscle is predictable for a given task. The predicted values could be applicable to the physical risk assessment. The fourth part introduce the work to build up a Full-chain musculoskeletal model in OpenSim in view that no current model covers muscles of the torso and all the limbs. Special attention is paid to the method used by OpenSim to adapt the model inertial properties to individuals. Errors of the method is evaluated with reference data coming from the whole-body 3D scan. In the last part, the newly built Full-chain model is applied on the posture analysis of an overhead drilling task. The muscle activation varies as a function of postures, which is suggested as the indicator of posture loads.